Biochemical and structural studies of multistep posttranslational modification system for a quinone cofactor-containing enzyme subunit

キノン補酵素含有サブユニットの多段階翻訳後修飾機構の生化学的・構造生物学的研究

Department of Biomolecular Science and Reaction

The Institute of Scientific and Industrial Research, Osaka university

大阪大学産業科学研究所 生体分子反応科学研究分野

Department of Biologiacl Science, Graduate School of Science, Osaka University

大阪大学大学院理学研究科　生物科学専攻

Toshinori Oozeki

大関　俊範

Abstract

Quinoheme protein amine dehydrogenase (QHNDH) is a heterotrimeric enzyme that catalyzes the oxidative deamination of primary amines in a variety of Gram-negative bacteria. The smallest 9-kDa subunit QhpC, which forms the active center, contains two unique post-translational modification structures: the quinone cofactor cysteine tryptophylquinone (CTQ) and an intramolecular thioether bond. Previous studies have shown that a radical SAM enzyme QhpD first forms three intramolecular thioether bridges between Asp/Glu and Cys residues of QhpC in the cytoplasm. Next, it is postulated that the FAD-dependent monooxygenase QhpG is involved in modification of the precursor Trp residue as an initial reaction for CTQ formation. Subtilisin-like serine peptidase QhpE then remove the leader peptide of the N-terminal 28 residues of QhpC. For QhpE and QhpG, their characteristics have not been elucidated, and three-dimensional structures have been also unknown. This study focused on the roles of QhpG and QhpE in the post-translational modification of QhpC to clarify the detailed reaction mechanisms of the individual enzymes.

First, to identify the catalytic reaction of QhpG, I expressed and purified all related proteins QhpC, QhpD, QhpE, and QhpG from *Ps putida* using the *E. coli* expression system. In vitro reaction system was constructed, and the product QhpC was analyzed by mass spectrometry. The obtained results demonstrated that QhpG catalyzed the single-turnover dihydroxylation of the CTQ-precursor, Trp43, in the protein substrate QhpC containing triple intra-peptidyl crosslinks that were pre-formed by QhpD. Interestingly, it is found that QhpCDG ternary complex formation is essential for the both reactions of QhpD and QhpG. Crystal structure of this peptidyl tryptophan dihydroxylase QhpG revealed a large pocket that can dock the crosslinked QhpC with

the bound FAD situated close to the precursor tryptophan. Based on the enzyme-protein substrate docking model, the peptidyl tryptophan dihydroxylation is predicted to be catalyzed by repetition of mono hydroxylation reaction that is done by the flavoprotein monooxygenase.

As for the serine proteinase QhpE from *Ps. putida*, kinetic analysis of removal of the leader peptide from QhpC showed that the QhpE reacts the structure of QhpC by about 50-fold faster than the linear QhpC without crosslinks. Probably the conformational change of QhpC due to crosslink formation affects the activity of QhpE. As shown above, the QhpC still keeps the QhpC/QhpD/QhpG ternary complex even after modification reactions by QhpD and QhpG. The results exhibited that QhpE can efficiently remove the leader peptide of the crosslinked QhpC from the ternary complex, not for the linear QhpC. In addtion, the X-ray crystal structure of QhpE was determined at 1.80 Å resolution. In the active center of QhpE, there was a large pocket where the QhpC is thought to be bound. Probably the compact structure of crosslinked QhpC is recognized by this pocket. The high reactivity of QhpE toward the crosslinked QhpC is predicted to prevent the cleavage of the newly translated and uncrosslinked QhpC, facilitating the progress of QhpC biosynthesis through complex formation.

Thus, I demonstrated that multiple enzyme system regulates the biosynthesis of mature QhpC through complex formation and reactivity of each enzyme. These efficient and rational mechanisms seem essential for rapid production of the active QHNDH to assimilate primary amines under starvation conditions without carbon sources. It is expected that the posttranslational mechanism of QhpC including crosslinking and processing of peptides is applicable for developing bioactive cyclic peptides.

Index

Chapter I

General Introduction

Most enzymes utilize low molecular weight organic cofactors as catalysts. It was generally thought that the cofactors in enzymes that catalyze redox reactions are dissociable elements such as flavins, NAD^+, and $NADP^+$. However, in the 1990s, cofactors called "built-in" cofactors, which are generated from amino acid residues of proteins and covalently bound to the enzyme's polypeptide backbone, were discovered. These cofactors rely on post-translational processing of the encoded amino acid residues to form novel structural motifs in the active site of the enzyme protein. The following prosthetic groups are known as "built-in" cofactors (Figure 1): The pyruvoyl group in histidine decarboxylase or *S*-adenosylmethionine decarboxylase is formed when a precursor Ser residue is nucleophilically attacked by the hydroxyl group of an adjacent Ser residue[1] (Fig. 1A). The tyrosine-cysteine crosslink cofactor in galactose oxidase (GO)[2] is generated by autocatalytic thioether bond formation between Tyr and Cys residues in the presence of copper ions[3] (Fig. 1B). The tyrosine-cysteine crosslinking cofactor and the copper ion are located in the active site of the mature enzyme and catalyze the oxidation of primary alcohols to the corresponding aldehydes and the reduction of O_2 to hydrogen peroxide. 2-oxoalanine (formylglycine, FGly) in sulfatase[4] is located in the active site and produced by post-translational modification of Ser or Cys residues of the precursor protein (Fig. 1C). This modification is catalyzed by another protein molecule (Asl B protein)[5]. Sulfatase hydrolyzes sulfate esters to the corresponding phenols and inorganic sulfates. Cysteine-sulfinic acid in nitrile hydratase[6] is formed by the post-translational modification of two iron-coordinated Cys residues,

Cys112 and Cys114, to Cys sulfonic acid and sulfenic acid, respectively (Fig. 1D). This modification requires another protein molecule (*nha3* product) encoded downstream of the subunit gene[7], whose amino acid sequence is similar to that of the magA iron transporter gene from *Magnetospirillum sp*. AMB-1[8] and the cobalt transporter gene of nhlF from *Rhodococcus rhodochrous J1*[9] show significant similarity. 2,4,5-Trihydroxyphenylalanine quinone (TPQ)[10] in copper amine oxidases distributed from bacteria to higher animals is derived from a specific Tyr residue and produced autocatalytically by a copper-dependent process[11, 12] (Fig. 1E). Lysine tyrosyl quinone (LTQ)[13] in lysyl oxidase is produced by a copper-mediated post-translational crosslinking reaction between the -amino group of a Lys residue and the side chain of a Tyr residue at position 2[14] (Fig. 1F). Tryptophantriptylquinone (TTQ) in methylamine dehydrogenase (MADH) or aromatic amine dehydrogenase[15, 16], which is produced by post-translational crosslinking between C2 of the Trp residue and C4 of the modified Trp residue, tryptophylquinone (Fig. 1G). In addition, in the 2000s, cysteine tryptophylquinone (CTQ) was found in the active centers of several enzymes, including quinohemoprotein amine dehydrogenase (QHNDH) (Fig. 1H). It has been speculated that CTQ is formed from specific Cys and Trp residues by enzyme-catalyzed post-translational modifications. These protein-derived cofactors are examples of functional extensions of the basic 20 amino acids that make up proteins and are thought to have developed through molecular evolution in nature.

QHNDH is an inducible enzyme produced in the periplasm of Gram-negative bacteria such as *Paracoccus denitrificans* and *Ps. putida*, and catalyzes the oxidation of primary amines such as *n*-butylamine and benzylamine to the corresponding aldehydes [17, 18, 19] (Equation 1). This enzyme is responsible for assimilating the primary amines as

an energy and carbon/nitrogen sources *in vivo*. Electrons generated in the substrate reduction reaction are transferred from the reduced quinone cofactor to the electron acceptor such as cytochrome c_{550} via two heme molecules in the enzyme molecule and are finally used by the terminal oxidase for the reduction of molecular oxygen to water.

$$RCH_2NH_3^+ + H_2O \rightarrow RCHO + NH_4^+ + 2H^+ + 2e^- \quad \text{(Equation 1)}$$

In previous studies, the X-ray crystal structure of QHNDH has been already determined and is composed of αβγ heterotrimeric structures (Fig. 2)[20, 21]. In QHNDH from *Pa. denitrificans*, the α-subunit (QhpA) with the highest molecular weight (approximately 60 kDa) consists of a 489-residue peptide chain and is divided into four domains with independent folding. Among them, a domain I (1-167 residues) consists of two subdomains (αd1a: 3α-70α residues, αd1b: 95α-162α residues) with bi-rotationally symmetrical axes, and binds two *c*-type heme molecules (heme 1: proximity to CTQ, heme 2: molecular surface). These hemes are covalently bound to the peptide chain via cysteine residues and are thought to play an important role in catalyzing the transfer of substrate amine-derived electrons to the electron acceptors. Domains II-IV all have a β-barrel structure consisting of multiple anti-parallel β-strands. The β-subunit (QhpB), with a molecular weight of approximately 40 kDa, is composed of a 337-residue peptide chain and has a seven-bladed β-propeller structure characteristic of many quinoprotein dehydrogenases, such as methylamine dehydrogenase and methanol dehydrogenase (Fig. 2). Furthermore, the smallest γ-subunit (QhpC) (9 kDa) of the 82 residues is bound between QhpA and QhpB and contains two unique post-translational modification structures (Fig. 3A). The first is the peptide-derived redox cofactor, CTQ (Fig. 3B), which is formed from side chains of specific cysteine and tryptophan residues as

described above (Fig. 1H). The second is three thioether intramolecular crosslinks formed between the sulfur atom of the cysteine residue and the methylene carbon atom of the aspartate/glutamate residue side chain[22] (Fig. 3). In QHNDH from *Pa. denitrificans*, CTQ is genetically encoded as a cysteine residue (Cys37) and a tryptophan residue (Trp43). The precursor residues are connected by a thioether bridge between the S atom of Cys37 and the C4 atom of the Trp43 side chain indole ring, and the indole ring is ortho-quinonated at C6 and C7 positions. The complex structure of mature QhpC clearly indicates that multiple posttranslational modification system is involved in these modifications.

To elucidate the mechanism of post-translational modification of QhpC, the QHNDH gene region was analyzed and the genes were found to be encoded by a *qhp* operon consisting of multiple open reading frames (ORFs) (Fig. 4)[23]. *QhpA*, *qhpB*, and *qhpC* encode the α, β, and γ subunits, respectively. In addition to these three structural genes, the QHNDH operon contains five ORFs (*qhpD*, *qhpE, qhpF*, *qhpR*, and *qhpG*), suggesting that they may be involved in the post-translational modification because they are non-structural genes. *QhpD* encodes a radical SAM superfamily protein, *qhpE* encodes a sub subtilisin-like serine protease, *qhpF* encodes an ABC transporter, *qhpR* encodes a transcriptional regulator, and *qhpG* encodes an FAD-dependent monooxygenase (Fig. 4). Analysis of the disrupted strains and in vitro crosslink formation experiments showed that QhpC is first translated as a linear peptide with an N-terminal leader peptide that is eventually removed, and that the radical SAM enzyme QhpD forms three thioether crosslinks, starting from the N-terminal side of QhpC[24, 25] (Fig. 4). Furthermore, after the serine protease QhpE cleaves the N-terminal leader peptide of crosslinked QhpC[26], QhpC is thought to be transported from the cytosol to

the periplasm by the ABC transporter QhpF (Fig. 4). Among the two unique post-translational modifications present in QhpC, the thioether crosslink formation has been elucidated in detail and shown to be generated by the radical SAM enzyme QhpD. QhpG is found to be essential for the generation of the active form QHNDH[23], and the coded protein (FAD-dependent monooxygenase) suggests to be involved in the modification of the CTQ precursor Trp as several FAD-dependent monooxygenases catalyze the oxygenation reaction including hydroxylation of various compounds. However, the mechanism of CTQ formation is still poorly understood. For QhpG, the characteristics at the protein level have not been elucidated in detail. No enough experimental information has been obtained for QhpE-catalyzed reaction. In addition, X-ray crystal structures of Qhp proteins including QhpE and QhpG, except QHNDH subunits (QhpA, QhpB, and QhpC), remained unsolved yet.

A peptide-linked quinone cofactor similar to CTQ is tryptophan-tryptophylquinone (TTQ) (Fig. 1G), which is derived from two Trp residues. CTQ and TTQ are similar in that specific Trp residues are ortho-quinonated and crosslinked with the other residues. The formation of TTQ in MADH was previously well elucidated in comparison with the mechanism of CTQ formation[27, 28, 29]. MADH has $\alpha_2\beta_2$ four subunit structures and TTQ resides in the two β subunits (Fig. 5A). The initial reaction for TTQ formation is monohydroxylation of position 7 of the βTrp57 residue side-chain indole ring. Subsequently, it has been shown that MauG leads to ortho-quinonation through the formation of crosslinks with βTrp108 residues (Fig. 5B). However, the enzyme responsible for hydroxylation at position 7 in the Trp residue side chain indole ring has not been identified. Recently, the mechanism of CTQ formation has attracted much attention because it was found that CTQ is included as a redox cofactor in lysine

oxidase LodA and glycine oxidase GoxA, which have completely different characteristics from QHNDH[30, 31, 32]. LodA and GoxA were isolated from the melanogenic marine bacterium *Marinomonas mediterranea*. Interestingly, the gene clusters containing *lodA* and *goxA*, respectively, contained only one gene of *lodB* or *goxB*, which are required for the expression of the active forms of LodA or GoxA, respectively. Moreover, LodB and GoxB are predicted to be FAD-dependent monooxygenase that shows low but apparent sequence similarity with QhpG. A progenitor protein with monohydroxylated Trp residues forming CTQ was isolated when expressed under gene-disrupted conditions[33]. Although LodA or GoxA shows no homology to the QHNDH subunits, the idea that CTQ is generated by similar posttranslational mechanism with FAD-dependent monooxygenase.

Therefore, in this study, I will elucidate the roles of several enzymes involved in the post-translational modification of QhpC. In particular, I focused on the FAD enzyme QhpG and the serine peptidase QhpE. The detailed reaction mechanisms and the substrate recognition mechanism of two enzymes are investigated on the basis of the x-ray crystal structures. Furthermore, I will clarify how the overall biosynthetic reaction of QhpC is regulated in this multi-step process.

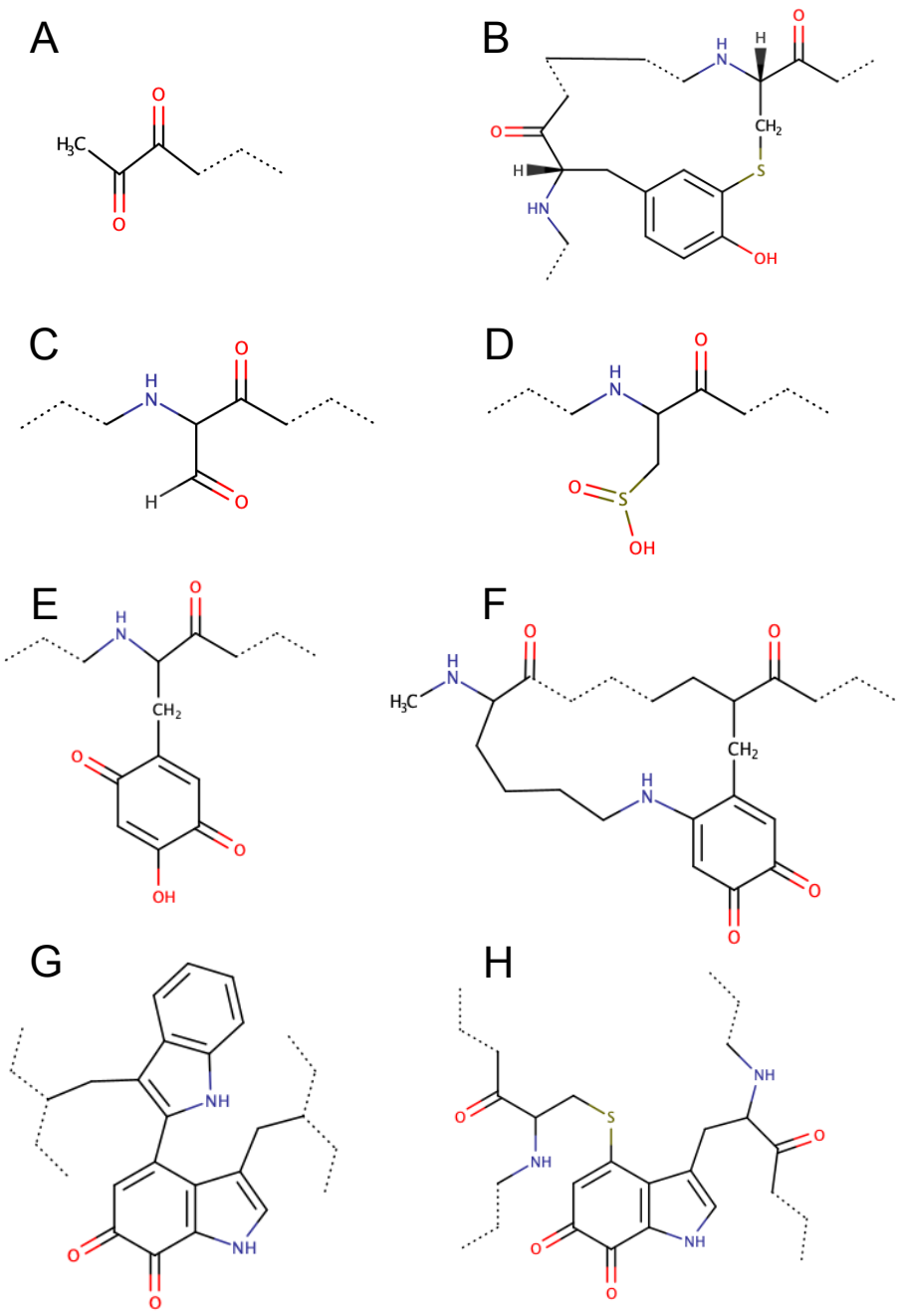

Figure 1. Chemical structures of 'built-in' cofactors. ***A***, pyruvoyl group; ***B***, Tyr-Cys crosslinking cofactor; ***C***, formylglycine (FGly); ***D***, Cys-sulfinic acid; ***E***, 2,4,5-trihydroxyphenylalanine quinone (TPQ); ***F***, lysine tyrosylquinone (LTQ); ***G***, tryptophan tryptophylquinone (TTQ) and ***H***, cysteine tryptophylquinone (CTQ).

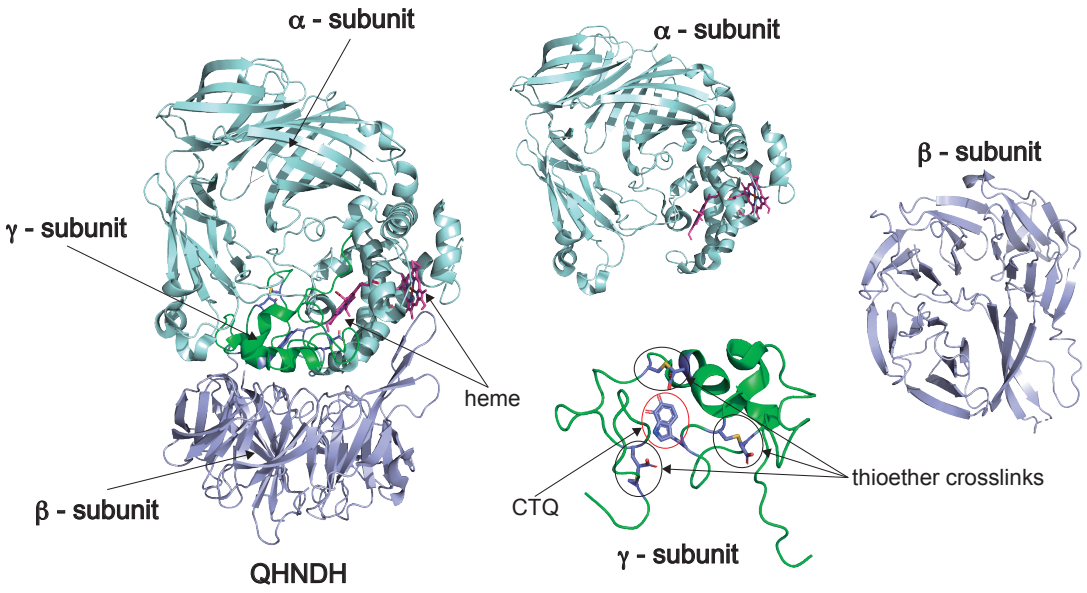

Figure 2. Crystal structure of QHNDH. The α-subunit (60 kDa) has two heme molecules at the N-terminus domains. The β-subunit (40 kDa) has a seven-winged propeller structure characteristic of quinone protein dehydrogenases. The γ-subunit (9 kDa) has three thioether bridges and a CTQ.

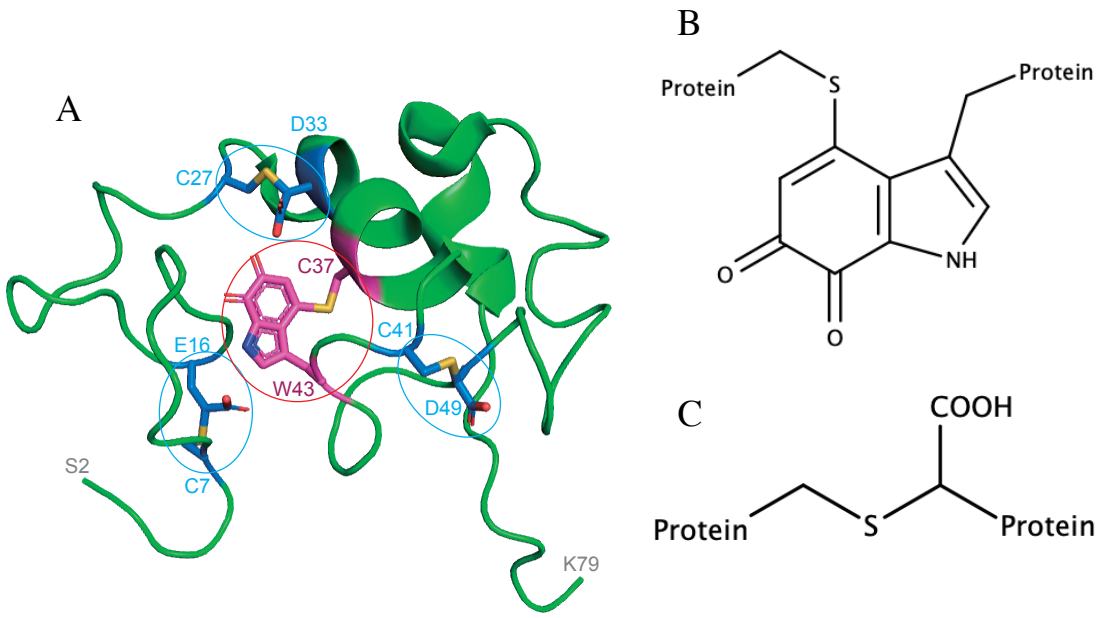

Figure 3. Three-dimensional structure and translation-modification structure of QhpC. ***A***, the overall structure of *Ps. putida* QhpC. ***B***, the CTQ structure formed from a Cys residue side chain and a Trp residue side chain. ***C***, the thioether bridge structure formed from an Asp or Glu residue side chain and a Cys residue side chain.

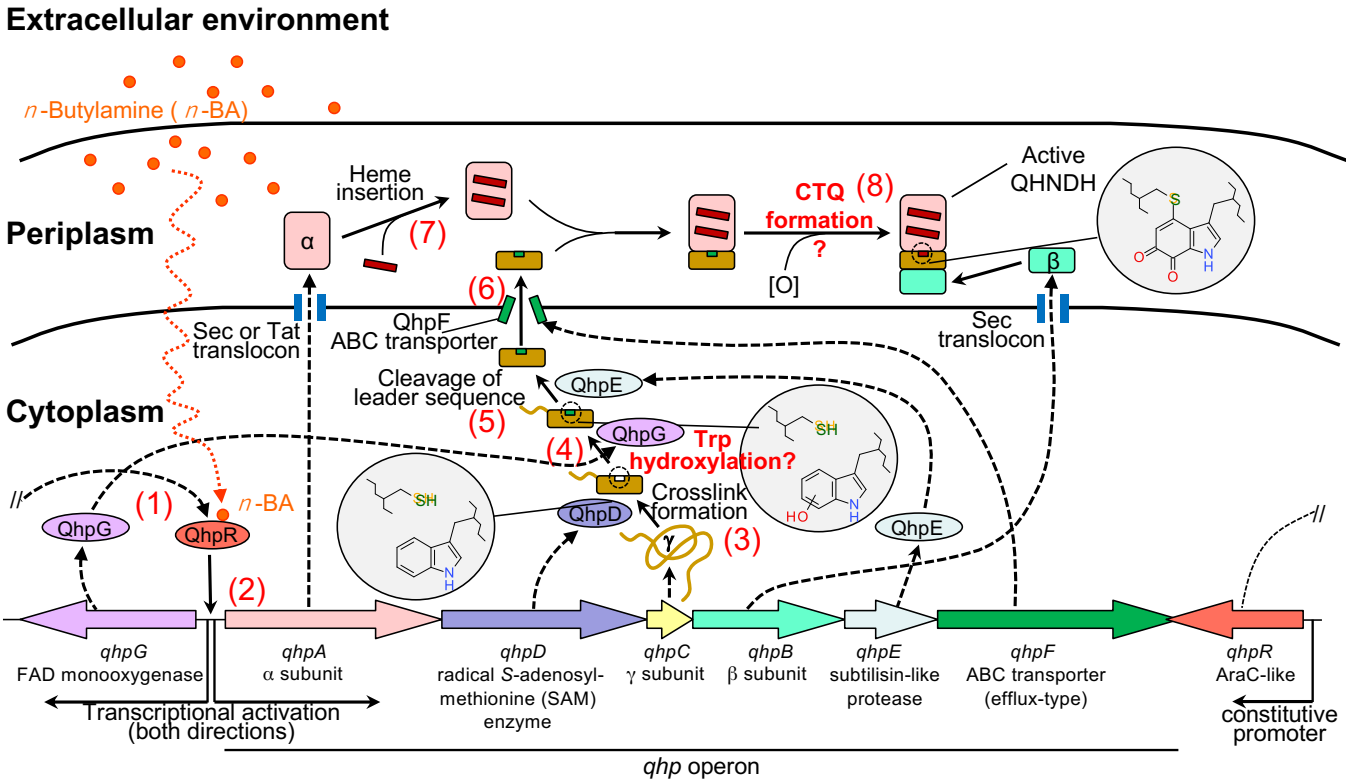

Figure 4. Predicted QHNDH biosynthetic pathway diagram. When long-chain primary amines such as *n*-butylamine bind to QhpR, transcription of the *qhp* gene is activated. Translated QhpA and QhpB are transported to the periplasm. QhpC is first translated and is triply crosslinked through thioether bonds by the radical SAM enzyme QhpD. QhpG, a FAD-dependent monooxygenase, hydroxylates the indole ring on the side chain of the Trp residue of the CTQ precursor in the crosslinked QhpC. The leader peptide is then cleaved by QhpE, a serine protease, and the thus modified QhpC is transported to the periplasm by QhpF, an ABC transporter. At the periplasm, QhpA, in which hemes are inserted, is bound to the QhpC. It is postulated that CTQ is finally generated in QhpC by QhpA. The binary complex of QhpA and QhpC is bound with QhpB to form the mature hetero trimeric enzyme. This figure is adapted from previous study of our laboratory[23] and is modified.

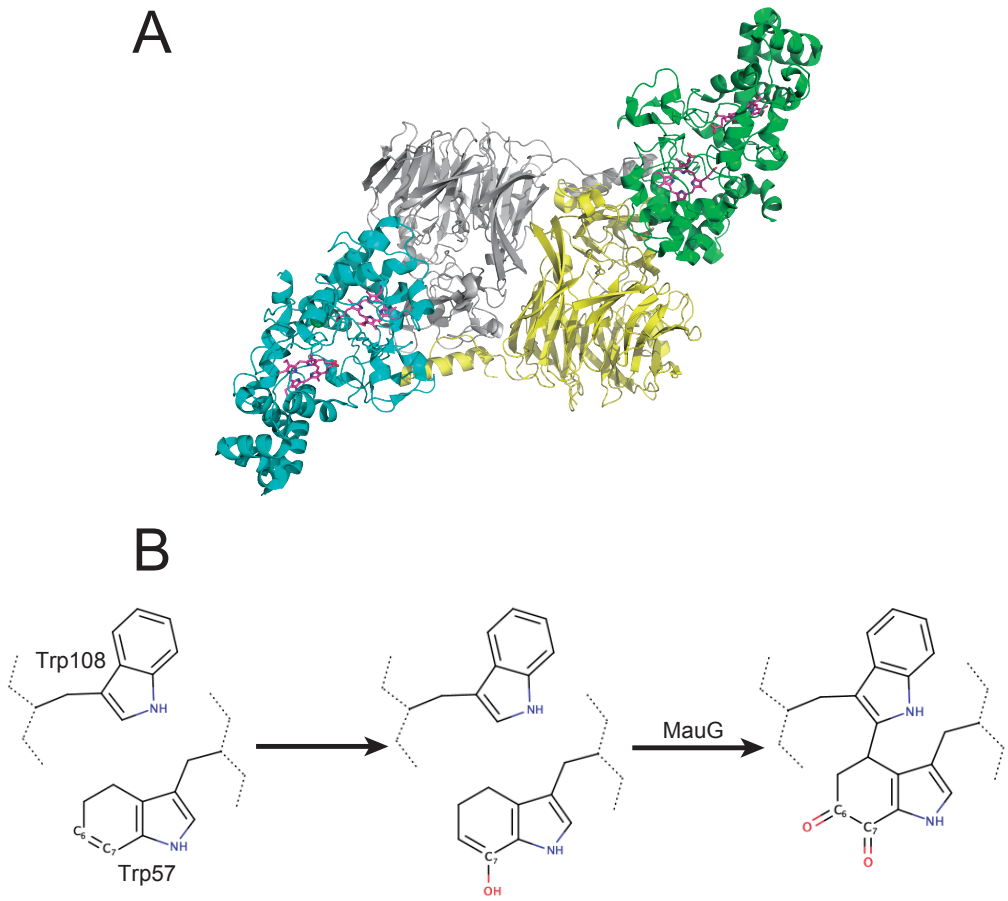

Figure 5. Structure of MauG/MADH complex and formation mechanisms of TTQ. **A**, The three-dimensional structure of the MauG/MADH complex during the biosynthesis of TTQ is shown. **B**, The biosynthetic mechanism of the cofactor TTQ of MADH, which has a structure similar to that of the cofactor CTQ formed in the γ-subunit of QHNDH. Cofactor TTQ is biosynthesized by the covalent connecting of two Trp residues. The initial reaction for TTQ formation is monohydroxylation at position 7 of the βTrp57 residue side chain indole ring, followed by MauG leading to crosslink formation (TTQ formation) via hydroxylation and ortho-quinonation of the βTrp108 residue.

References

1. van Poelje, P. D. and Snell, E. E. (1990) *Annu. Rev. Biochem.* **59**, 29–59
2. Ito, N., Phillips, S. E. V., Stevens, C., Ogel, Z. B., McPhason, M. J., Keen, J. N., Yadav, K. D. S., and Knowles, P. F. (1991) *Nature* **350**, 87–90
3. Rogers, M. S., Baron, J., McPhason, M. J., Knowles, P. F., and Dooley, D. M. (2000) *J. Am. Chem. Soc.* **122**, 990–991
4. Schmidt, B., Selmer, T., Ingendoh, A., and von Figura, K. (1995) *Cell* **82**, 271–278
5. Szameit, C., Miech, C., Balleininger, M., Schmidt, B., von Figura, K., and Dierks, T. (1999) *J. Biol. Chem.* **274**, 15375–15381
6. Tsujimura M., Dohmae, N., Odaka, M., Chijimatsu, M., Takio, K., Yohda, M., Hoshino, M., Nahashima, S., and Endo I. (1997) *J. Biol. Chem.* 272, 29455–29459
7. Nojiri, M., Yohda, M., Odaka, M., Matsushita, Y., Tsujimura, M, Yoshida, T., Dohmae, T., Takio, K., and Endo, I. (1999) *J. Biochem.* **125**, 696–704
8. Nakamura, C., Burgess, J. G., Sode, K., and Matsunaga, T. (1995) *J. Biol. Chem.* **270**, 28392–28396
9. Komeda, H., Kobayashi, M., and Shimizu, S. (1997) *Proc. Natl. Acad. Sci. USA* **94**, 36–41
10. Janes, S. M., Mu, D., Wemmer, D., Smith, A. J., Kaur, S., Maltby, D., Burlingame, A. L., and Klinman, J. P. (1990) *Science* **248**, 981–987
11. Matsuzaki, R., Fukui, T., Sato, H., Ozaki,Y., and Tanizawa, K. (1994) *FEBS Letter* **351**, 360-364
12. Ruggieno, C. E., Smith, J. A., Tanizawa, K., and Dooley, D. M. (1997) *Biochemistry* **36**, 1953-1959

13. Wang, S. X., Mure, M., Medzihradszky, K. F., Burlingame, A. L., Brown, D. E., Dooley, D. M., Smith, A. J., Kagan, H. M., and Klinman, J. P. (1996) *Science* **273**, 1078–1084
14. Rucker, R. B., Kosonen, T., Clegg, M. S., Mitchell, A. E., Rucker, B. R., Uriu-Hare, J. Y., and Keen, C. L. (1998) *Am. J. Clin. Nutr.* **67**, 996S-1002S
15. McIntire, W. S., Wemmer, D. E., Chistoserdov, A., and Lidstrom, M. E. (1991) *Science* **252**, 817–824
16. Govindaraj, S., Eisenstein, E., Johns, L. H., Sanders-Loehr, J., Chistoserdov, A. Y., Davidson, V. L., and Edwards, S. L. (1994) *J. Bactriol.* **176**, 2922–2929
17. Durham, D. R., and Perry, J. J., (1978) *J. Bacteriol.* **134,** 837-843.
18. Takagi, K., Torimura, M., Kawaguchi, K., Kano, K., and Ikeda, T. (1999) *Biochemistry* **38**, 6935–6942
19. Shinagawa, E., Matsushita, K., Nakashima, K., Adachi, O., and Ameyama, M., (1988) *Agric. Biol. Chem.* **52,** 2255-2263.
20. Datta, S., Mori, Y., Takagi, K., Kawaguchi, K., Chen, Z. W., Okajima, T., Kuroda, S., Ikeda, T., Kano, K., Tanizawa, K., and Mathews, F. S. (2001) *Proc. Natl. Acad. Sci. U.S.A.* **98**, 14268–14273
21. Satoh, A., Kim, J. K., Miyahara, I., Devreese, B., Vandenberghe, I., Hacisalihoglu, A., Okajima, T., Kuroda, S., Adachi, O., Duine, J. A., Van Beeumen, J., Tanizawa, K., and Hirotsu, K. (2002) *J. Biol. Chem.* 277, 2830–2834
22. Vandenberghe, I., Kim, J. K., Devreese, B., Hacisalihoglu, A., Iwabuki, H., Okajima, T., Kuroda, S., Adachi, O., Jongejan, J. A., Duine, J. A., Tanizawa, K., and Van Beeumen, J. (2001) *J. Biol. Chem.* 276, 42923–42931

23. Nakai, T., Deguchi, T., Frébort, I., Tanizawa, K., and Okazima, T., (2014) *Biochemistry* 53, 895–907.

24. Ono, K., Okajima, T., Tani, M., Kuroda, S., Sun, D., Davidson, V. L., and Tanizawa, K., (2006) *J. Biol. Chem.* 281, 13672–13684.

25. Nakai, T., Ito, H., Kobayashi, K., Takahashi, Y., Hori, H., Tsubaki, M., Tanizawa, K., and Okajima, T., (2015) *J. Biol. Chem.* 290, 11144–11166.

26. Nakai, T., Ono, K., Kuroda, S., Tanizawa, K., and Okazima, T., (2012) *J. Biol. Chem.* 287, 6530–6538.

27. Pearson, A. R., Mora-Rey, T. D. L., Graichen, M. E., Wang, Y., Jones, L. H., Marimanikkupam, S., Agger, S. A., Grimsrud, P. A., Davidson, V. L., and Wilmot, C. M., (2004) *Biochemistry* 43, 5494–5502

28. Wang, Y. T., Li, X. H., Jones, L. H., Pearson, A. R., Wilmot, C. M., and Davidson, V. L., (2005) *J. Am. Chem. Soc.* **127**, 8258-8259.

29. Jensen, L.M., Sanishvili, R., Davidson, V. L., and Wilmot, C. M., (2010) *Science*, **327**, 1392-1394.

30. Okazaki, S., Nakano, S., Matsui, D., Akaji, S., Inagaki, K., & Asano, Y., (2013) *J. Biochem.* 154, 233-236.

31. Gomez, D., Lucas-Elío, P., Sánchez-Amat, A. and Solano, F., (2006) *Biochim. Biophys. Acta* 1764, 1577-1585.

32. Campillo-Brocal, J.C., Lucas-Elio, P., & Sanchez-Amat, A., (2013) *MicrobiologyOpen* 2, 684-694.

33. Chacón-Verdú, M.D., Campillo-Brocal, J.C., Lucas-Elío, P., Davidson, V.L., & Sánchez-Amat, A., (2015) *Biochim. Biophys. Acta.* **1854**, 1123-1131.

Chapter 2

Functional and structural characterization of a flavoprotein monooxygenase essential for biogenesis of tryptophylquinone cofactor

2.1. Introduction

Post-translational protein modifications expand the chemical repertoire of amino acid residues defined by genetic codons. A variety of protein-derived cofactors have so far been identified at the active sites of many enzymes, and their biosynthesis from one or more amino acid residues is recognized as an important category of post-translational modification[1–3]. Among them, the quinone cofactors produced from aromatic amino acid residues, Tyr or Trp, attached covalently to another residue in some cases, play redox catalytic roles[4–6]. These cofactors are produced either by an autocatalytic process, assisted only by the proper protein fold and occasionally a metal ion, or by the participation of one or more modifying enzymes[1–3].

Cysteine tryptophylquinone (CTQ) is a protein-derived quinone cofactor initially identified in quinohemoprotein amine dehydrogenase (QHNDH), a bacterial enzyme that catalyzes oxidative deamination of various aliphatic primary amines for use as energy, carbon, and nitrogen sources[7,8]. The crystal structures of QHNDH, determined for the enzymes from two different Gram-negative bacteria[9,10], revealed the common heterotrimeric subunit structure (Fig. 1), consisting of the ~60-kDa α-subunit that contains two *c*-type hemes, the ~37-kDa β-subunit, and the ~9-kDa γ-subunit that

contains CTQ in an uncommon protein structure with four intra-peptidyl thioether bonds (three Cys-to-Asp/Glu crosslinks, and one in CTQ) (Fig. 1). The intricate structure of the γ-subunit as well as the presence of CTQ indicates that multiple steps of post-translational modification are required for the generation of CTQ in the mature γ-subunit.

Structural genes encoding QHNDH constitute an operon, termed "*qhp*", along with several nearby genes (*qhpABCDEFGR*; the arrangement, order, and coding strands of the genes are variable), all of which are necessary for the amine-induced expression of the enzyme in the periplasm of bacterial cells[11]. The *qhp* operon is distributed in more than 1300 bacterial species, currently identified by the Position-Specific Iterated (PSI) BLAST search (https://blast.ncbi.nlm.nih.gov/Blast.cgi)[12]. The *qhpA*, *qhpB*, and *qhpC* genes encode the α-, β-, and γ-subunits of QHNDH, respectively. The *qhpD* gene encodes an unusual radical *S*-adenosylmethionine (SAM) enzyme (QhpD) that catalyzes sequential formation of three Cys-to-Asp/Glu thioether bonds within a single polypeptide of QhpC (γ-subunit)[13,14]. The *qhpE* gene encodes a subtilisin-like serine protease (QhpE) that cleaves the N-terminal 28-residue leader peptide from the crosslinked QhpC[15] (Fig. 1) before periplasmic translocation through an efflux ABC transporter, encoded by the *qhpF* gene[11]. The QhpE protease is also unusual in that it serves as a single-turnover processing enzyme acting in a suicidal manner. This chapter shed light on the *qhpG* gene, which has been predicted to encode a flavoprotein monooxygenase, directly involved in CTQ biogenesis[11]. Biochemical evidence reported herein proves that QhpG is an atypical single-component monooxygenase, catalyzing dihydroxylation of an unmodified Trp residue in the protein substrate.

2.2. Methods

2.2.1. Plasmid construction

Expression plasmids for QhpG, QhpC, and QhpD from *Ps. putida* IFO 15366 (NBRC 15366) were constructed using either an *E. coli* expression vector pET-15b or a broad-host-range vector pBBR1, mostly according to the standard molecular genetic protocols (Fig. 20. Coding regions of these proteins were amplified by PCR using a sense primer containing an NdeI site at the 5′-terminus and an antisense primer containing a BamHI or NheI site at the 3′-terminus (Table 3) with *Ps. putida* genome DNA. For plasmid construction of QhpG, the C-terminal Ala430 was replaced by Val in response to the designed primer sequence. A His_6-tag and a Tobacco Etch Virus (TEV) protease digestion site (GSSHHHHHHDYDIPTTENLYFQG) were appended to the N-terminus of QhpG (pET-His_6-TEV-QhpG) by inserting a DNA fragment obtained from annealed synthetic oligonucleotides (His_6-TEV; Table 3). A His_6-tag and a St_2-tag were also appended to the N-terminus of QhpD and the C-terminus of QhpC in the constructs (pET-His_6-QhpD and pBBR-QhpC-St_2), respectively, as reported previously for expression of the QhpCD complex from *Pa. denitrificans*[14]. The expression plasmid for QhpD from *Pa. denitrificans* Pd1222 was constructed in the previous work[14]. The expression plasmid for QhpA from *Pa. denitrificans* (pRK-His_6-QhpA) was constructed by PCR amplification with synthetic oligonucleotides (pdQhpA; Table 3) as described previously[11]. A His_6-tag (GSSHHHHHHSSG) was appended at the C-terminus of the signal peptide in the construct by PCR amplification using synthetic oligonucleotides (His_6-pdQhpA; Table 3). The plasmids for site-directed mutagenesis of QhpG and QhpC (Fig. 20) were prepared by the PCR-based method using primers listed in Table

3. The absence of PCR-derived errors in all constructs was confirmed by sequencing the entire coding regions.

2.2.2. Protein expression and purification

The inactive QHNDH produced in the periplasm of the Δ*qhpG* mutant strain of *Pa. denitrificans* was purified from the cells transformed with pRK-His_6-QhpA (Fig. 20) as described previously[11,13]. Briefly, the periplasmic fractions of the cells were added with 0.375 mM $MgCl_2$, 500 mM NaCl, and 10 mM imidazole and centrifuged at 20,000*g* for 30 min. The supernatant solution was loaded at 1 ml min^{-1} onto a 5-ml HisTrap HP column (GE Healthcare) pre-equilibrated with 20 mM Tris-HCl, pH 7.4, and 500 mM NaCl (buffer A) containing 10 mM imidazole. The column was washed with buffer A containing 10 mM imidazole and the protein was eluted with a linear gradient of 10–250 mM imidazole in buffer A. Fractions containing QHNDH was pooled and stored at 4 °C until use.

The QhpCD binary complex was expressed in *E. coli* C41 (DE3) cells carrying expression plasmids pBBR-QhpC-St_2 and pET-His_6-QhpD (either from *Pa. denitrificans* or *Ps. putida*) and purified as described previously[14]. After chemical reconstitution of the [Fe-S] clusters of QhpD in the as-purified QhpCD binary complex[14], the complex (~180 μM) dissolved in 25 mM Tris-HCl, pH 8.0, containing 150 mM NaCl and 10% (w/v) glycerol was anaerobically incubated at ~20 °C for ~15 h with 1 mM sodium dithionite and 1 mM SAM, in the absence or presence of ~180 μM purified QhpG (with QhpD derived from *Pa. denitirificans* or *Ps. putida*, respectively), for the QhpD-catalyzed intra-peptidyl thioether bond formation in QhpC. The free linear and crosslinked QhpC proteins were prepared before and after the QhpD-

catalyzed reaction, respectively, by removing the QhpD protein by heat denaturation at 60 ºC for 20 min and following centrifugation.

To prepare the wild-type or mutant protein of QhpG, *E. coli* C41 (DE3) cells carrying a relevant expression plasmid were grown at 37 °C for 3 h by reciprocal shaking at 160 r.p.m. and further at 25 °C and 180 r.p.m. for 20 h in an Overnight Express™ Instant TB Medium (Novagen) supplemented with ampicillin (50 μg ml^{-1}). The cells were harvested by centrifugation at 5,000*g* for 10 min and stored at −80 °C until use. For purification of QhpG, the frozen cells were suspended in 50 mM sodium phosphate buffer, pH 8.0, containing 300 mM NaCl and 10% glycerol (v/v) (buffer B) plus 5 mM imidazole, 1 mM FAD, and cOmplete Protease Inhibitor (Roche) (1 tablet per 50 ml of cell suspension), and disrupted by ultrasonic oscillation. The cell-free extract was obtained by centrifugation at 20,000*g* for 20 min, and was applied to a Ni-Sepharose FF column (5-ml bed volume, GE Healthcare) preequilibrated with buffer B. After washing the column with 100 ml of buffer B containing 5 mM imidazole, QhpG was eluted in a stepwise manner with buffer B containing 10 mM, 20 mM, 50 mM, 100 mM, and 200 mM imidazole. The fractions colored yellow (eluted by 50–100 mM imidazole) were collected, and 1 mM FAD was supplemented. After twice repeated dialysis against buffer B, the protein solution was further applied to a HisTrap HP column (5-ml bed volume, GE Healthcare) preequilibrated with buffer B containing 5 mM imidazole. After extensive washing with buffer B containing 5 mM imidazole, QhpG was eluted with a linear gradient of 5–100 mM imidazole in buffer B. The fractions containing QhpG were pooled, added with 1 mM FAD, dialyzed against buffer B, and concentrated to about 10 mg ml^{-1}. To remove the N-terminal His_6-tag, the concentrated protein was digested with a His_6-tagged TEV protease[16] (added at 1%

protein weight) for 48 h at 6 °C. The His_6-tagged TEV protease was produced by an *E. coli* expression system with plasmid pRK793 which was a gift from David Waugh (Addgene plasmid #8827; http://n2t.net/addgene:8827; RRID:Addgene_8827) and purified according to the Addgene protocol. After the digestion, the protease and released His_6-tag were removed by repeating the HisTrap HP purification, and the tag-less QhpG was collected from fractions containing 40–50 mM imidazole based on its weak affinity for the column. After addition of 1 mM FAD, the protein solution was dialyzed against buffer B. Finally, the purified QhpG was concentrated to >10 mg ml^{-1} and stored at −80 °C in the presence of 1 mM FAD. Excess FAD was removed by a PD-10 column (GE Healthcare) before use.

2.2.3. Characterization of QhpG

Protein concentration of purified QhpG was determined with a molecular extinction coefficient at 280 nm (ε_{280} = 71,960 M^{-1} cm^{-1}) calculated from the amino acid sequence of QhpG with a program ProtParam[17], by subtracting the contribution of FAD absorption (ε_{280} = 2340 M^{-1} cm^{-1}) measured in the same buffer. The FAD content was determined spectrophotometrically in buffer B containing 8 M urea with a molecular extinction coefficient at 450 nm (ε_{450} = 11,300 M^{-1} cm^{-1})[18]. Approximate molecular size of QhpG in solution was determined by a gel-filtration method with the purified QhpG (6 mg ml^{-1}) applied onto a Superdex 10/300 GL column (1.0 × 30 cm) using 50 mM sodium phosphate, pH 7.0, containing 150 mM NaCl as an eluent at a flow rate of 0.5 ml min^{-1}. Chymotrypsinogen A (MW, 25,000), ovalbumin (43,000), albumin (67,000), aldolase (158,000), catalase (232,000), and ferritin (440,000) were used for standards.

2.2.4. MALDI-TOF mass spectrometric analysis

The purified QHNDH from the *ΔqhpG* mutant strain of *Pa. denitrificans* was denatured by addition of 10% (w/v) trichloroacetic acid (TCA) and washed twice with cold acetone. The precipitates collected by centrifugation were thoroughly dried, then dissolved in 50 µl of 6 M urea in 50 mM potassium phosphate, pH 7.5, containing 1 mM *tris*(2-carboxyethyl)phosphine (TCEP), and incubated at 37 °C for 1 h, as described previously[11,14]. For chemical modification of the free sulfhydryl groups, a 10-µl aliquot of the solution was mixed with 1 µl of 500 mM IAA in 50 mM potassium phosphate, pH 7.5, and the mixture was kept at room temperature for 1 h. The mixture was acidified with 2% (v/v) formic acid, adsorbed in a desalting C_{18} ZipTip pipette tip (Millipore), and eluted with 10 µl of 0.1% (v/v) trifluoroacetic acid (TFA) in 50% (v/v) acetonitrile. A 1-µl aliquot of the eluate was analyzed with a Bruker Ultraflex III MALDI-TOF mass spectrometer using 1 mg ml^{-1} sinapic acid (Bruker) dissolved in 90% (v/v) acetonitrile containing 0.1% (v/v) TFA as a matrix, which was co-crystallized with the protein by the drying-droplet method. Before each mass spectrometric analysis, mass calibration was done using Protein Calibration Standard I (Bruker).

For identification of the bound cofactor in QhpG, the purified protein (~0.125 mg in 10 µl distilled water) was incubated at 50 °C for 10 min and the precipitated protein was removed by centrifugation at 4 °C. A 1 µl aliquot of the supernatant was subjected to MALDI-TOF mass spectrometric analysis using a nearly saturated concentration of 2,5-dihydroxy benzoic acid dissolved in 50% (v/v) acetonitrile and 2.5% (v/v) formic acid as a matrix. FAD standard was dissolved at 1 mg ml^{-1} in distilled water. The mass spectrometer was calibrated with a combination of peptide standard II (Bruker).

2.2.5. Mobility shift assay on native PAGE

Protein samples dissolved in 8 μl of 25 mM Tris-HCl, pH 8.0, containing 150 mM NaCl and 12.5% (w/v) glycerol were analyzed by native PAGE using an Any kD Mini-protean TGX precast gel (Bio-Rad) according to the manufacturer's protocol. Pre-running at a constant electric current of 34 mA was done for 15 min. After applying the samples, electrophoresis (10 mA, 40 V) was run at 4 °C for ~3 h. In the analysis of the QhpCDG ternary complex formation, 1 mM sodium dithionite was added to the electrophoresis buffer to remove dissolved dioxygen in the gel during the pre-running, and all procedures were done under anaerobic conditions maintained in a glovebox filled with 99.999% (v/v) nitrogen gas; oxygen concentration was routinely maintained below 0.1% (v/v) by monitoring with an oxygen sensor.

2.2.6. BLI assay

Protein-protein interaction was analyzed quantitatively by BLI assays conducted in 10 mM Tris-HCl, pH 7.4, containing 150 mM NaCl, 0.1% (w/v) bovine serum albumin, and 0.02% (v/v) Tween 20 (kinetics buffer) at 25 °C using a BLItz system (Molecular Devices, LLC., CA). Streptavidin (SA)-coated biosensors were hydrolyzed for 30 min in 250-μl kinetics buffer. A baseline was measured with a ligand-free biosensor in the kinetics buffer for 30 s prior to the immobilization step. A 4-μl aliquot of 0.5 μM protein solution (linear or crosslinked QhpC) was applied for immobilization through the St_2-tag to the surface of biosensor tips for 4 min and the baseline was measured again with the ligand-attached biosensor in the kinetics buffer for 6.5 min. An association step was monitored by applying an analyte solution (4 μl of 0.06–0.5 μM QhpG) to the biosensors for 4 min. Subsequently, a dissociation step was monitored by

pouring the kinetics buffer (250 μl) for 4 min. To correct for the non-specific binding, reference data with the same concentrations of analyte were also measured with a ligand-free biosensor. To determine the dissociation constant (K_D), association rate constant (k_a), and dissociation rate constant (k_d), the binding data obtained were analyzed by a BLItz Pro1.2 software (Molecular Devices, LLC., CA) using a global analysis mode with corrections for association and dissociation steps.

2.2.7. Assay of QhpG activity

After conducting the QhpD-catalyzed thioether bond formation as described above, a 250 μl reaction mixture of the QhpCDG ternary complex (52 μM) in 25 mM Tris-HCl, pH 8.0, containing 150 mM NaCl and 10% (w/v) glycerol (buffer C) was incubated with 3 mM sodium dithionite for 1 h at room temperature in the glovebox. The reduced mixture was taken out from the glovebox, added with twice volumes of O_2-satureated buffer C, and further incubated for 1 h at room temperature under atmospheric conditions. For the reaction in the absence of QhpD, the free crosslinked QhpC (18 μM) in buffer C was mixed with 22.5 μM QhpG, reduced with 1 mM sodium dithionite in the glovebox, and further incubated with twice volumes of O_2-satureated buffer C, as described above. The reaction product was precipitated by addition of cold acetone and was subjected to sodium dodecyl sulfate PAGE followed by blotting onto a polyvinylidene difluoride membrane and quinone staining as described previously[13]. Another portion of the precipitated reaction product was used for digestion with endoproteinase Asp-N (Sigma-Aldrich) (added at 1% protein weight) according to the manufacturer's protocol. The Asp-N digests were desalted with a C_{18} ZipTip pipette tip and subjected to the MALDI-TOF mass spectrometric analysis as described above using

2,5-dihydroxy benzoic acid dissolved in 90% acetonitrile and 0.01% TFA as a matrix. A collision-induced dissociation method with Ar gas was used for peptide fragmentation in the MS/MS analysis. For the reaction in $H_2{}^{18}O$, buffer C dissolving QhpG and the QhpCD binary complex was exchanged with $H_2{}^{18}O$ (≥ 98atom% ^{18}O; Taiyo Nissan Co., Tokyo, Japan) by repeating concentration and dilution three times using an Amicon 10K concentrator. The $^{16}O_2$-saturated buffer C was also prepared from the $H_2{}^{18}O$-buffer C. The QhpG reaction and MS analysis of the product were conducted as described above.

2.2.8. Crystallization and data collection

The buffer used for the storage of purified QhpG was exchanged with a freshly prepared buffer consisting of 10 mM Tris-HCl, pH 8.0, 0.1 M NaCl, and 0.1 mM DTT using a PD-10 column. The protein solution was concentrated to 12.5 mg ml^{-1}, filtrated through a 0.22-μm centrifugal filter (Millipore), and used for crystallization screening. Initial crystallization conditions were screened with commercially available screening kits by the sitting-drop vapor diffusion method. After optimization, the crystals used for data collection were obtained by the sitting-drop method at 4 ºC in the reservoir solution consisting of 100 mM HEPES (pH 7.0), 20 mM $MgCl_2$, 17% (v/v) Poly(acrylic acid sodium salt) 5,100, 1.8% (w/v) 1,6-hexanediol, and 34 mM cyclohexyl-methyl-β-D-maltoside. Thin platy crystals (ca. 0.2–0.3 mm size) appeared within 1–2 months. After cryoprotection with the crystallization buffer containing 30% (v/v) glycerol, the crystals were mounted on thin nylon loops (ϕ, 0.2–0.3 mm) and frozen by flash cooling at 100K in a cold N_2 gas stream or in liquid nitrogen. Hg derivatives were prepared by soaking the native crystals in the crystallization buffer containing 30% (v/v) glycerol and a saturated concentration (ca. 5 mM) of carbon tetra(acetoxymercuride) for overnight.

Diffraction data sets were collected with a synchrotron X-radiation at SPring-8 (Hyogo, Japan) at 100 K in the beam-line station BL44XU using a CCD detector EIGER X 16M (Dectris) at λ = 0.900 Å for a native crystal and using a CCD detector MX300HE (Rayonix) at λ = 1.0070 Å for an Hg-derivatized crystal. The collected data were processed, merged, and scaled using the program XDS[19] or HKL2000[20]. The space group was $P2_1$ with the unit cell dimensions of a = 88.5 Å, b = 51.8 Å, and c = 101.8 Å, β = 99.8° in the native crystal. The cell content analysis suggested that two molecules are in the asymmetric unit. The details and statistics of the data collection are summarized in Table 2.

2.2.9. Structure determination and refinement

The structure of QhpG was solved by single isomorphous replacement with anomalous scattering (SIRAS) of the Hg-derivatized crystal. The positions of 2 mercury sites were determined by calculating anomalous peaks with the programs SHELXC/D[21] within the program suite autoSHARP[22]. Initial phases were calculated using the program SHARP[23], and subsequent cycles of density modification and automatic model building with autoSHARP[23] gave an initial model containing 55% of the peptide backbone in the asymmetric unit. Non-crystallographic symmetry (NCS) relating two QhpG molecules in the asymmetric unit was manually determined by analyzing the electron density along with the positions of the two Hg sites and their neighboring identical α-helices in the initial model. The resulting NCS matrices together with the phases and coordinates of the autoSHARP output was subsequently input to the program PHENIX AutoBuild[24] for further cycles of density modification and automatic model building, which gave an overall figure of merit of 0.70 and built 70% of the

peptide backbone in the asymmetric unit including 58% of the side chains. The resulting map was of good quality and clearly exhibited electron density corresponding to two FAD molecules. The remaining model was built manually into the map using the program Coot[25]. Refinement using the program PHENIX[24], and manual model rebuilding cycles produced the final model. Analysis of the stereochemistry showed that the model was of good quality, with more than 99.8% of the residues falling in the allowed regions. One proline residue (Pro342) in each QhpG monomer was found in the *cis*-conformation. PyMOL version 1.8 or 2.4 (Schrödinger Inc. New York, USA) was used for figure drawings. The refinement statistics are summarized in Table 2, and the coordinates and structure factors have been deposited in the Protein Data Bank (PDB entry ID: 7CTQ).

2.2.10. Construction of docking models

The initial docking model of the QhpCG binary complex was built with the ZDOCK software and server[26] using the crystal structure of γ-subunit in *Ps. putida* QHNDH (PDB entry ID: 1JMX)[10] as ligand and the monomer structure (chain A) of QhpG as the receptor. Starting from this initial model, Coot[25]-based manual modeling was carried out as follows: The thioether bond of CTQ was cleaved and the Trp42–Trp43 dipeptide portion was separately placed at the bottom of the *re*-face channel of QhpG so that the indole ring of Trp43 overlaps with the phenyl ring of L-kynurenine modeled in the active site of kynurenine 3-monooxygenase[27]. The Asp39–Met51 loop lacking Trp42–Trp43 was moved into the *re*-face channel and re-connected to the Trp42–Trp43 portion. The docking model of the QhpCG binary complex thus constructed was energy-minimized with a Schrödinger program suit (Schrödinger Inc. New York, USA).

For model building of the QhpCDG ternary complex, a structure model of QhpD was first generated using the SWISS-MODEL homology-modelling server (https://swissmodel.expasy.org)[28]. Template molecules for modeling were searched with BLAST[29] and HHblits[30] against the SWISS-MODEL template library which includes the PDB. Finally, the model of the QhpCDG ternary complex was built with the ZDOCK software and server[31] using the modeled QhpD structure as ligand and the QhpCG binary complex as the receptor.

2.3. Results

2.3.1. Analysis of quinone-less γ-subunit in inactive QHNDH

My laboratory previously demonstrated that inactive QHNDH, produced in the *qhpG* gene-disrupted mutant strain (Δ*qhpG*) of *Pa. denitrificans*, contains no quinone group in the γ-subunit (fully processed QhpC)[11]. To elucidate the modification state of the CTQ-precursor Trp residue in the quinone-less QhpC, the QhpC polypeptide in the inactive QHNDH complex was isolated from the periplasm of the Δ*qhpG* mutant by Ni affinity chromatography utilizing N-terminally hexa-His (His_6)-tagged γ -subunit (QhpA), and analyzed it by MALDI-TOF mass spectrometry. The observed mass (*m*/*z*, 8829.3) was smaller by about 28-mass unit than the calculated mass of the γ -subunit (*m*/*z*, 8857.6)[13], and corresponded well to that of the QhpC polypeptide (*m*/*z*, 8828.6) containing three intra-peptidyl thioether bonds formed between Cys and Asp or Glu residues, and each one of the unmodified Cys and Trp residues (without 2 oxygen atoms and a Cys–Trp crosslink contained in CTQ of γ-subunit) (Fig. 2). In addition, treatment of the QhpC sample with 2-iodoacetamide (IAA) shifted the mass spectrum peak to a higher *m*/*z* value (*m*/*z*, 8887.7), the increase (Δ = ~58) corresponding to acetamidation

of a single free Cys residue. Although the mass spectrometric analysis of the whole peptide is insufficient for identification of the unmodified residues, Cys37 and Trp43 that form CTQ most likely remain intact in the quinone-less QhpC (Fig. 2). Thus, it is strongly suggested that QhpG is an enzyme that acts on the quinone-less QhpC with three intra-peptidyl thioether bonds as the protein substrate, and converts it into a mature form (γ-subunit) containing CTQ, or its immediate precursor, such as mono- or di-hydroxylated Trp.

2.3.2 Purification and characterization of QhpG

My initial attempt at purifying QhpG from *Pa. denitrificans* was unsuccessful due to the formation of inclusion bodies during expression in recombinant *E. coli* cells. Therefore, an ortholog of QhpG was cloned from *Ps. putida*, which also produces QHNDH[7,10]. The *Ps. putida* QhpG expressed in recombinant *E. coli* cells was purified to homogeneity in a soluble form (Fig. 3a). It behaved as a monomeric protein of molecular weight (MW) of about 40,000 in a gel-filtration chromatographic analysis (calculated MW, 47,194), and exhibited a UV-visible spectrum characteristic of an FAD-containing protein, which was readily reduced with sodium dithionite under anaerobic conditions (Fig. 3b). Addition of O_2-saturated buffer to the dithionite-reduced QhpG resulted in rapid re-oxidation of the bound FAD (Fig. 3b). FAD was found to be tightly, but non-covalently bound to QhpG in a molar ratio of nearly 1:1 (determined spectrophotometrically), as it was extractable by heat treatment at 50 ºC for 10 min (Fig. 3c). For studying the QhpG reaction in vitro, *QhpC* and *QhpD* genes of *Ps. putida*, were cloned and expressed as a stable QhpCD binary complex in *E. coli* cells, as described previously for *Pa. denitrificans* proteins[14]. In the following experiments, the

QhpCD complex derived from *Ps. putida*, in which QhpC is the nascent polypeptide carrying the 28-residue leader peptide that is necessary for the interaction with QhpD and a C-terminal Twin-Strep (St_2)-tag (hereafter designated 'linear QhpC'; calculated MW, 14,875.5), was used after chemical reconstitution of [4Fe-4S] clusters contained in QhpD[14].

2.3.3. Preparation of substrate for QhpG

During preparation of the protein substrate for QhpG, i.e., the quinone-less QhpC containing three intra-peptidyl thioether bonds, 28-residue leader peptide, and one each of free Cys and Trp residues (Cys37 and Trp43) (hereafter designated as 'crosslinked QhpC'; calculated MW, 14,869.4), the mass analysis showed that the QhpD-catalyzed thioether bond formation in QhpC was significantly promoted by QhpG. Thus, in the presence of an equimolar amount of QhpG, the crosslinked QhpC was formed almost completely (Fig. 5a, *top* panel), whereas in the absence of QhpG, the linear QhpC underwent only partial formation of thioether bonds with 1–4 Cys residues, which remained modifiable with IAA (Fig. 5a, *bottom*). These results suggest that QhpG interacts with the QhpCD binary complex. Indeed, as shown in Fig. 5b, mobility shift assays by native polyacrylamide gel electrophoresis (PAGE) performed under an anaerobic condition revealed the formation of a QhpCDG ternary complex (*middle* band) between the bands of the QhpCD binary complex (*lower*) and QhpG (*upper*), depending on the increasing amounts of QhpCD in combination with a constant amount of QhpG. Moreover, formation of the ternary complex was more prominent with the crosslinked QhpC (*lanes* 7–10) than with the linear QhpC (*lanes* 2–5). These results show that QhpG binds the QhpCD complex more preferentially through the crosslinked

QhpC, than the linear one lacking internal thioether bonds. Presumably, the QhpD-catalyzed thioether bond formation in QhpC is facilitated by QhpG that captures the partially crosslinked QhpC, which is structurally more stable than the linear one.

2.3.4. Analysis of QhpG–QhpC interaction

The interaction of QhpG with QhpC was further analyzed quantitatively by bio-layer interferometry (BLI) assays, using QhpC polypeptide immobilized on the biosensor surface (Fig. 5c). Linear and crosslinked QhpC polypeptides were isolated from the QhpCD binary complex by removing the QhpD protein by heat denaturation, before and after conducting the crosslinking reaction, respectively. QhpG showed a 100-fold higher affinity for the crosslinked QhpC than the linear one in terms of estimated K_D values (Table 1), which agreed with the mobility shift assays (Fig. 5b). Comparison of association (k_a) and dissociation (k_d) rate constants also indicated faster association and slower dissociation of QhpG for the crosslinked QhpC, explaining the high affinity. Comparable results were obtained in the mobility shift assay on native PAGE, where the interaction of QhpG with the linear QhpC was almost unobservable, in contrast to the significant interaction with the crosslinked QhpC forming a QhpCG binary complex (Fig. 5d). Collectively, it may be concluded that QhpG interacts with the crosslinked QhpC, which serves as the protein substrate.

2.3.5. Determination of catalytic activity of QhpG

Assuming that QhpG is an FAD-dependent oxygenase, the purified QhpG was first anaerobically incubated with several reducing reagents: NADPH, NADH, $FADH_2$, and sodium dithionite. Two other small biomolecules, dihydrolipoate and reduced

glutathione with lower reduction potentials than FAD, were also tested. Beside the artificial reductant (sodium dithionite) (Fig. 4b), none of the physiological reagents reduced the QhpG-bound FAD without affecting its absorption spectrum (Fig. 4b - f). Free $FADH_2$ neither reduced nor replaced the bound FAD. Therefore, after reducing the reaction mixture containing the QhpCDG ternary complex with excess sodium dithionite (~3 mM), the single-turnover reaction of QhpG was initiated by the addition of O_2-saturated buffer, and continued for 1 h under an atmospheric condition until the initially added dithionite was mostly consumed by air (Fig. 6). The reaction product was then precipitated by treatment with cold acetone and digested with Asp-N proteinase, followed by MALDI-TOF mass spectrometric analysis (Fig. 7). Among the peptide fragments produced by Asp-N digestion, the peak labeled **d** was assigned to the peptide starting at Asp39 and ending at Gln55 in the triply crosslinked QhpD polypeptide, including the CTQ-precursor Trp43 and an internal thioether bond formed between Cys41 and Asp49. Averaged mass (*m*/*z*, 2054.7 ± 0.2; *n* = 10) of peak **d** (monoprotonated form) before the QhpG reaction agreed well with the calculated molecular mass (*m*/*z*, 2054.3) of this peptide (Fig. 8a, *top* panel). After the QhpG reaction, relative intensity of peak **d** decreased significantly, and simultaneously the intensity of a new peak having *m*/*z*, 2086.7 ± 0.3 (*n* = 10) increased (Fig. 8a, *middle* panel). The mass increase (Δ = 32.0 ± 0.3; *n* = 10) was reproducibly observed in QhpG reactions performed with different preparations of the QhpCDG ternary complex, and was consistent with the incorporation of two oxygen atoms into the peak **d** peptide by the QhpG reaction. Furthermore, when the initial anaerobic reduction with dithionite was done in the $H_2{}^{18}O$-buffer and then the QhpG reaction was started by the addition of $^{16}O_2$-saturated $H_2{}^{18}O$-buffer, the reaction product contained two ^{16}O atoms but no ^{18}O

atom (Fig. 8b), supporting that the oxygen atoms inserted into the CTQ-precursor Trp are not derived from solvent H_2O. Interestingly, this **d**+32 peak was not formed in the QhpG reaction with the crosslinked QhpC alone (Fig. 8b, *bottom* panel), showing that the QhpG-catalyzed oxygen incorporation proceeds in the QhpCDG ternary complex as efficiently as the QhpD-catalyzed formation of intra-peptidyl thioether bonds described previously. A minor peak of about 16-mass unit higher than peak **d** was often observed, suggesting the formation of a reaction intermediate with a single oxygen atom being incorporated into this peptide. However, relative intensities of the **d**+16 peak did not change before or after the QhpG reaction; it may have been derived from partial oxidation of Met residues contained in this peptide, which could occur during Asp-N digestion and sample handling for mass spectrometric analysis. It is noticeable that the CTQ-forming Cys37 is outside peptide **d**, indicating that the thioether bond of CTQ was not formed in the peak **d** peptide. The absence of a dye-stainable quinone group in the product of QhpG reaction (Fig. 10) also indicates that tryptophylquinone was not formed. Hence, the 32-mass unit increase may be attributed to the insertion of two oxygen atoms in the form of two hydroxyl groups.

MS/MS analysis of the peptides before (peak **d**) and after the QhpG reaction (peak **d**+32) revealed that the incorporation of two oxygen atoms occurred within the circular peptide (Cys41–Asp49), resistant to fragmentation in MS/MS analysis[32] (Fig. 9). Moreover, the **d**+32 peak was not present in the reaction with a QhpC mutant, in which Trp43 was replaced by Phe (Fig. 11a). Based on these results, I concluded that the CTQ-precursor Trp43 is doubly hydroxylated, most likely at 6- and 7-positions of the indole ring, by the QhpG reaction. Taken together, QhpG was identified as an unusual

flavoprotein that catalyzes dihydroxylation of a peptidyl tryptophan in the single-turnover reaction, though belonging to a monooxygenase as proposed previously[11].

2.3.6. Crystal structure of QhpG

QhpG was crystallized as yellowish thin plates (Fig. 3d), and the crystal structure was determined at 1.98-Å resolution by single isomorphous replacement with anomalous scattering of an Hg-derivatized crystal (PDB entry ID: 7CTQ, Table 2). In the crystal, each asymmetric unit contained two monomers that are related by a non-crystallographic two-fold axis and packed compactly (Fig. 13a). However, PISA analysis (https://www.ebi.ac.uk/pdbe/pisa/)[33] indicated that there are no strong interactions enough to form a stable dimer in the protein interface. Additionally, molecular weight determination by a gel-filtration method suggested that QhpG is a monomer protein in solution, as described above. Thus, the dimerization is assumed to be a crystallographic artifact. Each monomer consists of a large N-terminal catalytic domain (residues 1–344) and a small C-terminal winged-helix (WH) domain (residues 349–429), with a large pocket between the two domains (Fig. 12a).

The overall structure of QhpG resembled FAD-dependent halogenases[34–36] and monooxygenases[37,38], with the highest structural similarity to *Streptomyces venezuelae* alkylhalidase SvCmlS[36] (PDB entry ID, 3I3L; root mean squared deviation, 3.2 Å over 337 superposed residues; sequence identity, 19%; *Z*-score, 34.1, in Dali server search[39]). The catalytic domain of QhpG contains a glutathione reductase-type Rossmann-fold for FAD binding, in which FAD is bound between two lobes of the catalytic domain (Fig. 13b), showing a clear $F_o - F_c$ omit map for the entire FAD molecule (Fig. 12b). Briefly, the isoalloxazine ring of FAD is sandwiched by the side chains of Pro267 and

Glu42/Arg240 from the *re*- and *si*-faces, respectively (Fig. 12b). The di-phosphate moiety interacts with the side chains of Arg36 and Arg89, and the main chain NH groups of Ala14 and Asp260. The adenine ring and ribose moieties are packed with Glu34, Arg36, Arg111, Arg140, Gln143, and Val112 with its carbonyl group hydrogen-bonding to the N6 amino group of the ring. Several residues involved in binding of FAD, and those found in its vicinity are comparable to those of FAD-dependent halogenases[34–36]. In comparison with the SvCmlS structure, Ala14, Glu42, Arg89, Arg111, Asp260, and Pro267 of QhpG are fully conserved or conservatively replaced (Fig. 14). In marked contrast to the well conserved FAD-binding site, QhpG has considerably different secondary structural motifs in the region corresponding to the NAD(P)H-binding region of other flavin monooxygenases (FMOs). For example, an FMO from *Schizosaccharomyces pombe* (PDB ID: 2GV8)[40] has the NADPH-binding region consisting of a parallel five-stranded β-sheet, an antiparallel three-stranded β-sheet, and four α-helices, with a consensus sequence for the nucleotide-binding loop (GXSXXA), whereas the corresponding region of QhpG consists of an antiparallel five-stranded β-sheet and two α-helices without the consensus sequence (Fig. 15). The small WH domain of QhpG resembles the domain often found in the core components of transcription systems as a DNA binding motif[41]. The WH domain is mounted over the catalytic domain that is linked by a random loop.

Two channels connecting the molecular surfaces to the *re*- and *si*-faces of the isoalloxazine ring of FAD have been identified. The narrow and deep *re*-face channel is open at the bottom of the large pocket between the two domains and composed of the main chains of Gly43–Val44 and Ser269–Asn271, and several hydrophobic residues (Val72, Trp74, Val174, Trp181, Trp183, Leu268, and Phe322) (Fig. 12c), most of

which are conserved in SvCmlS and QhpG orthologs (Fig. 14). In addition, several charged residues such as Arg70 and Glu84, also highly conserved in QhpG orthologs, are located at the rim of the channel. This channel corresponds to the substrate-binding site of flavoprotein monooxygenases[37,38], and the HOCl tunnel conserved in FAD-dependent halogenases[34–36]. It is most likely that the *re*-face channel plays as the binding site for the CTQ-precursor Trp43 in the substrate polypeptide (crosslinked QhpC) as described in the following section. The *si*-face channel connected to FAD is composed of a conserved residues (Glu42) and seven less conserved residues (Arg36, Phe38, Ala40, Arg89, Arg142, Gln143, and Arg240) (Fig. 12d, Fig. 14). More hydrophilic residues than those of the *re*-face channel constitute the wide and shallow channel. On the *si*-face of FAD, in addition to Arg240, a loop of Glu34–Glu42 covers the bound FAD, and exhibits higher thermal factors than other regions. The side chains of Glu42 and Arg240 are apart by about 4.5 Å from each other, suggesting a weak electrostatic interaction, and are located over the middle of the isoalloxazine ring (Fig. 12d). It is possible that Glu42 and Arg240 act as a lid for the *si*-face channel, through which dissolved dioxygen is able to access to the isoalloxazine ring.

2.3.7. Construction of docking models of binary and ternary complexes

Based on the biochemical evidence showing the significant interaction between QhpG and crosslinked QhpC described above, survey of the surface area of QhpG that may interact with the crosslinked QhpC showed a cluster of positively charged residues (Arg47, Arg70, Arg307, and Arg314) located near the entrance of the *re*-face channel (Fig. 16a); the molecular surface of the γ-subunit of QHNDH is rich in acidic residues (Asp12, Asp33, Asp39, Asp56, Glu66, and Glu67)[9,10] (Fig. 16b). Therefore, the

crosslinked QhpC (substrate for QhpG) is assumed to interact electrostatically with the entrance of the *re*-face channel of QhpG. To validate this assumption, a docking model was first built using the crystal structure of γ-subunit in *Ps. putida* QHNDH[10] and the monomer structure (chain A) of QhpG. Among the top 10 complexes generated by the ZDOCK software and server[42], the one was selected, showing the best fit with the above-described electrostatic interaction of γ-subunit with the large pocket between the two domains of QhpG (Fig. 17a). Then a structure model of crosslinked QhpC (without CTQ and the leader peptide) was manually built in the docking model of the QhpCG binary complex (Fig. 17a). In this docking model, the Asp39–Met51 loop of QhpC fit well into the deep *re*-face channel of QhpG, with Trp43 being placed close to the isoalloxazine ring of FAD (Fig. 17b), in a manner similar to the modeled substrate L-kynurenine bound to kynurenine 3-monooxygenase[38]. Also, the side chain of the neighboring Trp42 was accommodated in a hydrophobic pocket formed by the conserved residues (Trp74, Leu268, and Phe322) of QhpG (Fig. 17b). This docking model was further corroborated by site-directed mutagenesis of the residues located in the vicinity of the isoalloxazine ring of FAD (Glu42 and Trp183), or at the *re*-face channel entrance (Arg47, Arg70, and Arg314), which resulted in the nearly complete loss of the single-turnover activity of QhpG (Fig. 11b), and/or significant decreases in the affinity for the crosslinked QhpC (Table 1).

For construction of the docking model of the QhpCDG ternary complex, a structure model of QhpD had to be first generated using the SWISS-MODEL homology-modelling server (https://swissmodel.expasy.org)[43], because of the absence of its crystal structure. In the modeling, a radical SAM enzyme, a sactionine bond-forming enzyme CteB from *Clostridium thermocellum* (PDB ID: 5WGG)[44] was auto-selected as the

template based on sequence homology. Subsequently, a possible model of the QhpCDG ternary complex was obtained with ZDOCK by docking the above QhpD model structure to the model of the QhpCG binary complex (Fig. 18). As reported previously for QhpD from *Pa. denitrificans*[14], the structure model of *Ps. putida* enzyme also has a large groove with sufficient space to accommodate the core QhpC polypeptide containing several negatively charged residues. The structure model of the ternary complex shows that QhpD binds the crosslinked QhpC at the large groove and from the opposite side of QhpC involved in the interaction with QhpG. Altogether, the crosslinked QhpC may be sandwiched by QhpD and QhpG and serves as the common protein substrate for these two enzymes, to undergo efficient and successive Cys–Asp/Glu crosslinking and Trp-dihydroxylation reactions.

2.4. Discussion

The results described above reveal that QhpG is an atypical FAD-dependent oxygenase, catalyzing dihydroxylation of a peptidyl tryptophan. Such enzymes that regio- and stereo-specifically insert two or more hydroxyl groups into a single substrate have been reported for several cytochrome P450 monooxygenases[45]; 5-epiaristolochene 1,3-dihydroxylase (EAH) involved in capsidiol biosynthesis in plant[46] (2× hydroxylation), DoxA[45] involved in doxorubicin biosynthesis (2× hydroxylation), Sky32[47] involved in biosynthesis of a cyclic depsipeptide skyllamycin A (3× hydroxylation), Taml[45] involved in tirandamycin B biosynthesis (2× hydroxylation, 1 epoxidation), and MycG[45] involved in mycinamycin biosynthesis (1 hydroxylation, 1 epoxidation). A microbial nonheme Fe^{II} α-ketoglutarate-dependent oxygenase (named OrfP) involved in antibiotic (streptothricin-F) biosynthesis[48] also inserts two hydroxyl

groups into a single substrate. However, within the flavoprotein monooxygenase (FMO) family, there is no precedent for the enzyme that catalyzes dihydroxylation, although there is a related enzyme brominase (Bmp5)[49], which performs two successive regiospecific bromination reactions.

Referring to the mechanisms of EAH and OrfP, both accomplishing two independent and successive hydroxylation reactions within a single catalytic cycle, it is most likely that QhpG also catalyzes dihydroxylation in a successive manner. In the first hydroxylation step of the predicted reaction mechanism of QhpG (Fig. 19), the bound FAD is reduced to $FADH_2$ that reacts with dioxygen to form C4a-hydroperoxy-FAD, by analogy to another FAD-dependent monooxygenases[50,51] (step **1**→**2**), which would then perform electrophilic substitution with the indole ring of Trp43 in QhpC (step **3**), positioned nearly perpendicularly, close to the isoalloxazine ring of FAD (Fig. 17b). it is speculated that the indole ring C7 position is the first hydroxylation site because of elevated nucleophilicity of this position induced by the formation of a hydrogen bond between the indole ring N1 and FAD O4 atoms. Following the release of a water molecule, the 7-hydroxy-Trp residue is produced in QhpC, and the oxidized FAD is regenerated in QhpG (step **4**→**5**). In the second hydroxylation step, formation of a new hydrogen bond between the 7-hydroxyl group of Trp43 and FAD O4 may bring a slight positional shift of the indole ring relative to FAD (step **6**). A small conformational change of the Asp39–Met51 loop of QhpC (Fig. 17b) may also be induced after the first hydroxylation. The remaining dithionite again reduces FAD to $FADH_2$, which then reacts with dioxygen to form C4a-hydroperoxy-FAD again, for insertion of the second hydroxyl group at the C6 position of 7-hydroxy-Trp, finally yielding the 6,7-dihydroxy-Trp43 (steps **6**→**7**→**8**). The predicted reaction mechanism is consistent with those

proposed for EAH[46] and OrfP[48] in that the first mono-hydroxylated intermediate re-engages in the reaction without being released from the catalytic center. The observation that the crosslinked QhpC with two oxygen atoms incorporated was the major product of the QhpG reaction (Fig. 8a), suggesting the faster reaction rate of QhpG for the mono-hydroxylated intermediate (7-hydroxy-Trp) than for the initial substrate (crosslinked QhpC), is in agreement with the reaction catalyzed by EAH[30].

The positive effect of the QhpCDG ternary complex formation exerted on both of the QhpD-catalyzed thioether bond formation (Fig. 5a) and the QhpG-catalyzed dihydroxylation of the Trp residue (Fig. 8a) may be attributed to structural stabilization of the common substrate, i.e., the QhpC polypeptide chain, composed mostly of random coils with only two short α-helices (Fig. 17a). It is assumed that the QhpG protein facilitates the QhpD reaction by capturing the partially crosslinked QhpC, and vice versa, the QhpD protein helps the QhpG reaction by stably holding the protein substrate (crosslinked QhpC) through the N-terminal leader peptide[14]. Supporting the structural significance, the QhpG reaction does not occur in the absence of QhpD (Fig. 8a), even though the bound FAD is reduced by sodium dithionite in the presence of crosslinked QhpC (Fig. 3b). The physiological electron donor for the QhpG reaction is unknown at present. An electron-transfer protein existing in bacterial cells (e.g., ferredoxin, flavodoxin, and thioredoxin) may directly supply electrons for QhpG. Another possibility is that electrons supplied by an electron-transfer protein may be transferred to QhpG via QhpD that contains [4Fe-4S] clusters (one RS and two auxiliary clusters)[13,14] within the QhpCDG ternary complex. These possibilities remain to be examined in future studies.

The role played by QhpG in the quinone cofactor biogenesis is worth comparing with those of the modifying enzymes involved in other tryptophylquinone-generating systems[6], such as MauG[4,52,53], a di-heme protein participating in the biosynthesis of tryptophan tryptophylquinone (TTQ), the first tryptophylquinone cofactor discovered in methylamine dehydrogenase (MADH)[54], and LodB[55] and GoxB[56–58], flavoproteins required for the formation of CTQ identified in L-lysine ε-oxidase (LodA)[59] and glycine oxidase (GoxA)[60], respectively. Most importantly, the target Trp residue in the substrate proteins for MauG, LodB, and GoxB is a mono-(7-)hydroxy-Trp[4,52,53], whereas that for QhpG is an unmodified Trp. Thus, QhpG inserts both oxygens into the Trp of CTQ, whereas in the biogenesis of TTQ in MADH and CTQ in LodA and GoxA, the substrate for the modifying enzyme has the first hydroxyl present and only the second is added along with the formation of the Trp–Trp or Trp–Cys crosslink. Formation of the initial mono-hydroxy-Trp intermediate in MADH and LodA/GoxA is thought to be an autocatalytic process[36,45], which appears to be copper-ion dependent in LodA[61], with the participation of an Asp residue[56,62,63] located close to the cofactor, and strictly conserved in all tryptophylquinone enzymes. However, a recent study on GoxA has shown that mutation of the corresponding Asp678 does not abolish CTQ formation[64]. In addition, the corresponding Asp33 in QhpC may be placed in the equivalent position only after the formation of the CTQ thioether bond (Fig. 17b), apparently excluding its role in CTQ biogenesis, although a catalytic role in amine oxidation has been suggested[65]. Both QhpG (crystal) and GoxB (model)[58] show the highest structural similarity to alkylhalidase CmlS[20] with FAD bound to a nearly equivalent position and in an almost identical conformation (Fig. 13c). However, FAD is bound loosely in GoxB[58], but very tightly in QhpG, suggesting that QhpG belongs to the category of single-component

monooxygenases[50], but without bound $NADP^+$ or using NADPH as a co-substrate. The crystal or modeled structure of MauG-preMADH[63] and GoxB-GoxA[58] complexes shows the catalytic centers (di-heme in MauG, FAD in GoxB model) being far away from the target Trp residue in their partner protein substrates, indicating long-range electron transfer for remote Trp modification. In clear contrast, the CTQ-precursor Trp in the crosslinked QhpC substrate can be placed close to the bound FAD of QhpG, as shown in the docking model (Fig. 17a), and may directly undergo hydroxylation by C4a-hydroperoxy-FAD (Fig. 19). The γ -subunit (mature QhpC) of QHNDH contains three Cys-to-Asp/Glu thioether bonds, instead of six disulfide bonds contained in the TTQ-bearing β -subunit of MADH[4,63].

In conclusion, the γ-subunit intermediate of QHNDH containing the 6,7-dihydroxy-Trp and triple thioether crosslinks is produced in vitro from the nascent linear polypeptide of QhpC by the collaborative activities of two unusual modifying enzymes, QhpD and QhpG. The single-turnover feature of the reactions of QhpD[14], QhpE[15], and QhpG (this paper) is consistent with the fact that the genes for these proteins are encoded within the same operon (*qhp*) as their substrate (QhpC) and they are expressed altogether under the control of the *n*-butylamine inducible transcriptional regulator[11]. Thus, a single-use of each modifying enzyme is allowed in processing a single molecule of the substrate polypeptide, as reported for the ribosomally-synthesized and post-translationally-modified peptides (RiPPs) with various biological activities[64].

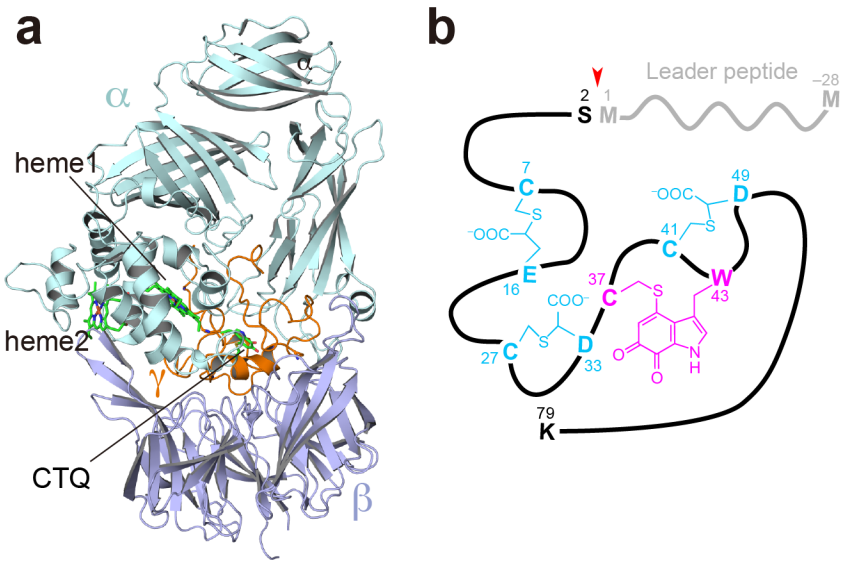

Fig. 1. Crystal structure of QHNDH and schematic representation of γ-subunit. a, Overall structure of QHNDH from *Ps. putida*. The α-subunit (QhpA, pale cyan), β-subunit (QhpB, purple), and γ-subunit (QhpC, orange) are depicted by a cartoon model with two hemes and CTQ shown in green stick model. **b**, Schematic presentation of γ-subunit polypeptide with a 28-residue leader peptide (light gray). Chemical structures of thioether crosslinks and CTQ are shown in cyan and magenta, respectively. The QhpE-cleavage site is indicated by a red arrowhead.

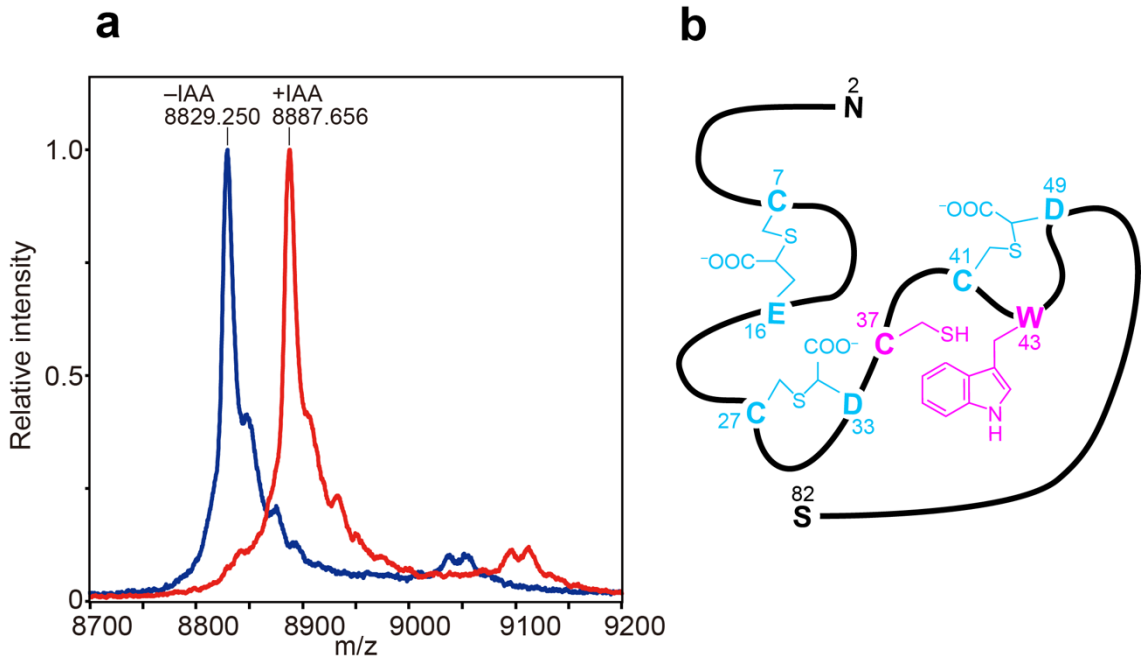

Fig. 2. Structural analysis of quinone-less γ-subunit. a, MALDI-TOF mass spectra of the quinone-less γ-subunit (fully processed QhpC) isolated from the *ΔqhpG* strain. −IAA and +IAA indicate before (blue) and after (red) treatment with IAA, respectively. Numbers indicate *m/z* for the peaks. Intensity is expressed in a relative value. **b**, Schematic drawing of the quinone-less γ-subunit with triple intra-peptidyl sulfur-to-methylene carbon thioether bonds. The CTQ-precursor residues, Trp43 and Cys37, and thioether crosslinks are shown in magenta and cyan, respectively.

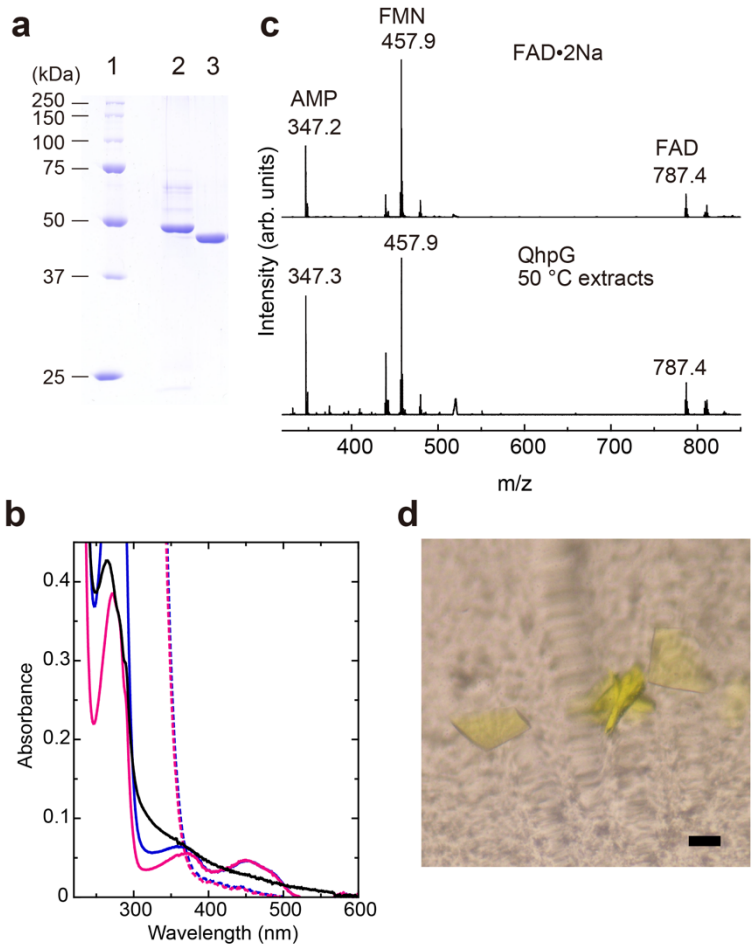

Fig. 3. Purification and characterization of QhpG. a, Purification steps monitored by sodium dodecyl sulfate PAGE. About 2-μg protein was applied in each lane. Protein bands were stained with Coomassie Brilliant Blue R-250. Lane 1, precision plus protein dual color standard (Bio-Rad); lane 2, after the first HisTrap HP purification; lane 3, after the TEV proteinase digestion and the second HisTrap HP purification. Sodium dodecyl sulfate PAGE performed in every purification (n > 10) showed a similar level of the protein purity. **b**, UV-visible absorption spectra. Magenta curve, purified QhpG (5 μM); blue curve, purified QhpG (5 μM) plus crosslinked QhpC (5 μM); magenta and blue dotted curves, after anaerobic addition of 25 μM dithionite to each sample; black curve, reduced QhpG after removing excess dithionite with a desalting spin column in an anaerobic chamber and adjusted to the same protein concentration with the oxidized

QhpG. **c**, MALDI-TOF mass spectrometric analysis of FAD standard (upper panel), and QhpG extract (lower panel). A 1-μl aliquot of the heated extract of QhpG (50 ºC, 10 min) was used for mass spectrometric analysis. Mass number (*m/z*) and assignments of fragmented FAD are indicated. Intensity is expressed in arbitrary units (arb. units). **d**, A photo of QhpG crystals (scale bar, 100 μm) ($n > 10$).

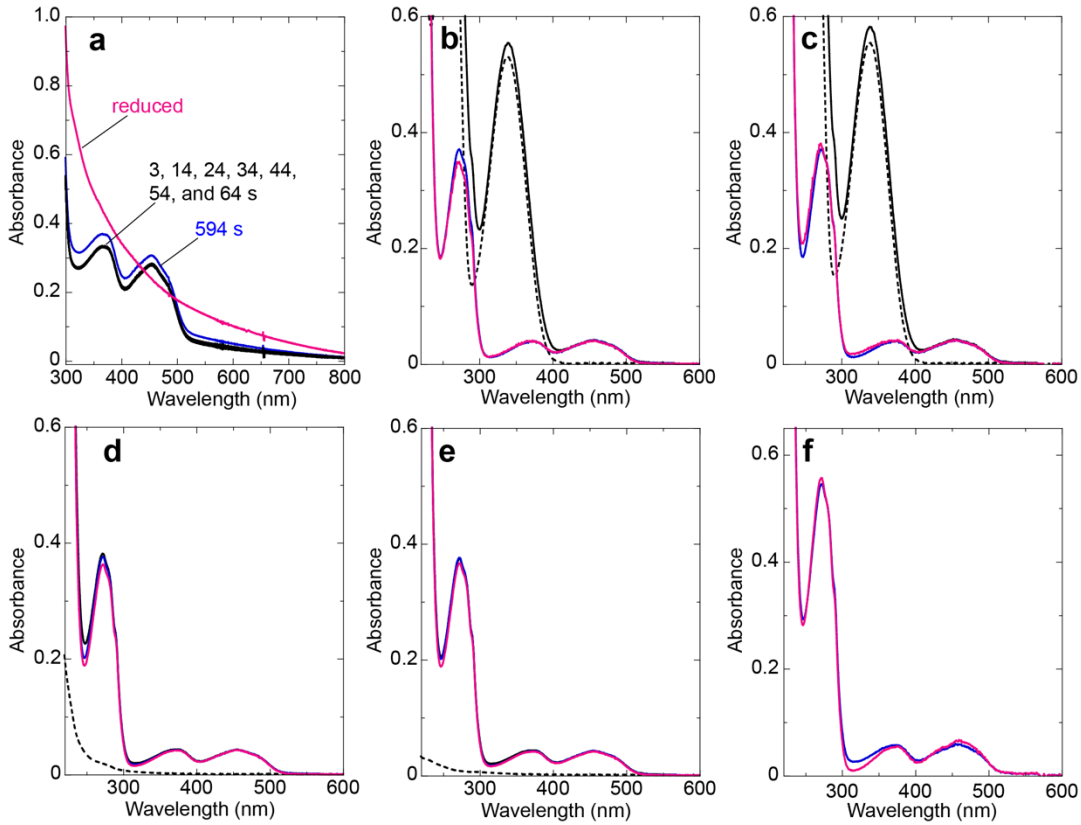

Fig. 4. Spectral changes of bound FAD. a, Re-oxidation of reduced FAD by O_2. QhpG (50 μM) was incubated with 250 μM dithionite in 25 mM Tris-HCl, pH 8.0, containing 150 mM NaCl and 10% (w/v) glycerol (buffer C) for 1 h under anaerobic conditions. The reduced QhpG was re-oxidized at 25 ºC by manually mixing with twice volumes of the O_2-satureated buffer C. UV-visible absorption spectra were monitored at indicated times after mixing (black and blue curves). The magenta curve represents the absorption spectrum of reduced QhpG mixed with twice volumes of O_2-depleted buffer C. **b**, **c**, **d**, and **e**, Spectral changes by addition of various reducing reagents. The oxidized form of QhpG (5 μM, blue curve) was incubated with 100 μM NADPH (**b**), NADH (**c**), reduced glutathione (**d**), or dihydrolipoate (**e**) at room temperature for 30 min under anaerobic conditions in buffer C (black curve in each panel). Black dotted and magenta curves represent spectra of the reducing reagent alone and those of QhpG,

from which the spectra of reducing reagents were subtracted, respectively. **f**, Spectral changes by addition of free $FADH_2$. A mixture of FAD and $FADH_2$ (about 1:9) was anaerobically prepared by spectral titration with sodium dithionite. QhpG (10 μM) was incubated with the FAD/$FADH_2$ mixture (100 μM) at room temperature for 30 min under anaerobic conditions in buffer C. After removing the free $FADH_2$ with desalting spin columns, the QhpG absorption spectrum was measured under anaerobic conditions (magenta). The absorption spectrum of the oxidative form of QhpG was also measured after an identical desalting treatment (blue).

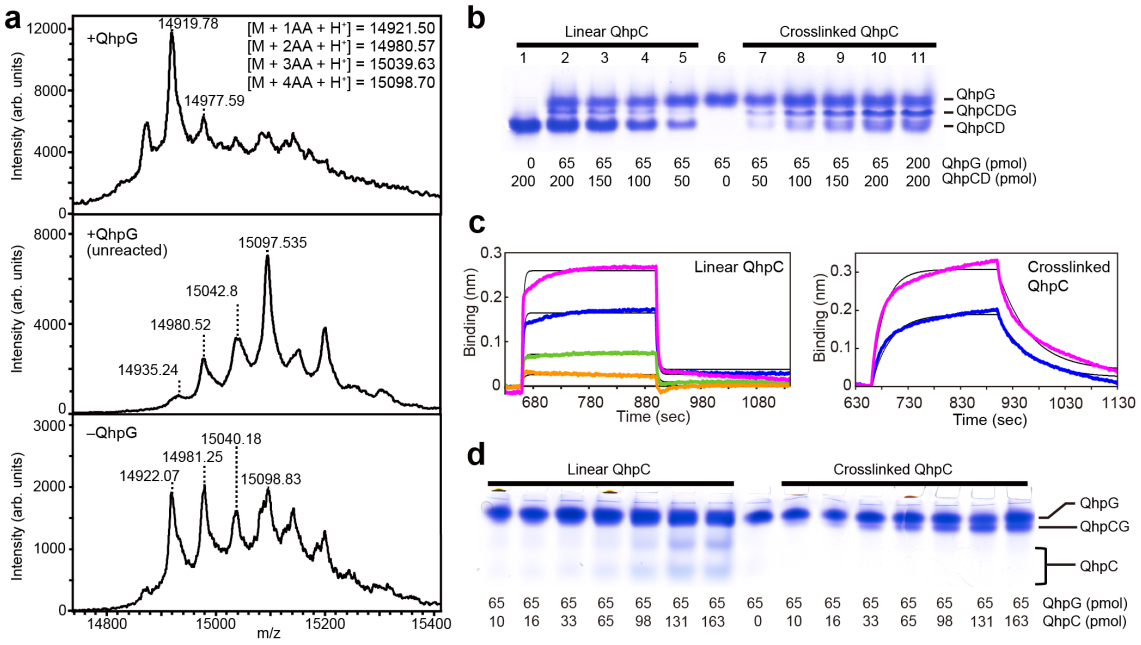

Fig. 5. Effect of QhpG on QhpD-catalyzed thioether bond formation in QhpC and inter-protein interactions among QhpCDG proteins. A, MALDI-TOF mass spectra are shown for IAA-treated products (crosslinked QhpC) of the QhpD-catalyzed thioether bond formation in the presence of an equimolar amount of QhpG (top panel) and in its absence before (middle) and after (bottom) the QhpD reaction. *Inset*: Calculated *m/z* values of 1–4 acetamidated (AA) peptides (monoprotonated form). Intensity is expressed in arbitrary units (arb. Units) for all mass spectra. Mobility shift assays for interactions between QhpG and the QhpCD binary complex (**b**) and between QhpG and QhpC (**d**). Indicated amounts (pmol) of respective proteins were applied in each lane. In **b** and **d**, the experiments repeated twice independently gave similar results. **C**, BLI assays for interactions between QhpG and linear (left) and crosslinked (right) QhpC immobilized on the biosensor tip. The analyte solution (4 µl) contained QhpG at 1.0 µM (magenta), 0.50 µM (blue), 0.25 µM (green), and 0.13 µM (orange) for linear QhpC (left) and at 62.5 nM (magenta) and 31.3 nM (blue) for crosslinked QhpC (right). Binding-induced changes in wavelength (nm) of the transmitted light were

recorded for measuring time (sec). Thin black curves represent theoretical fitting of the calculated data (Table 1).

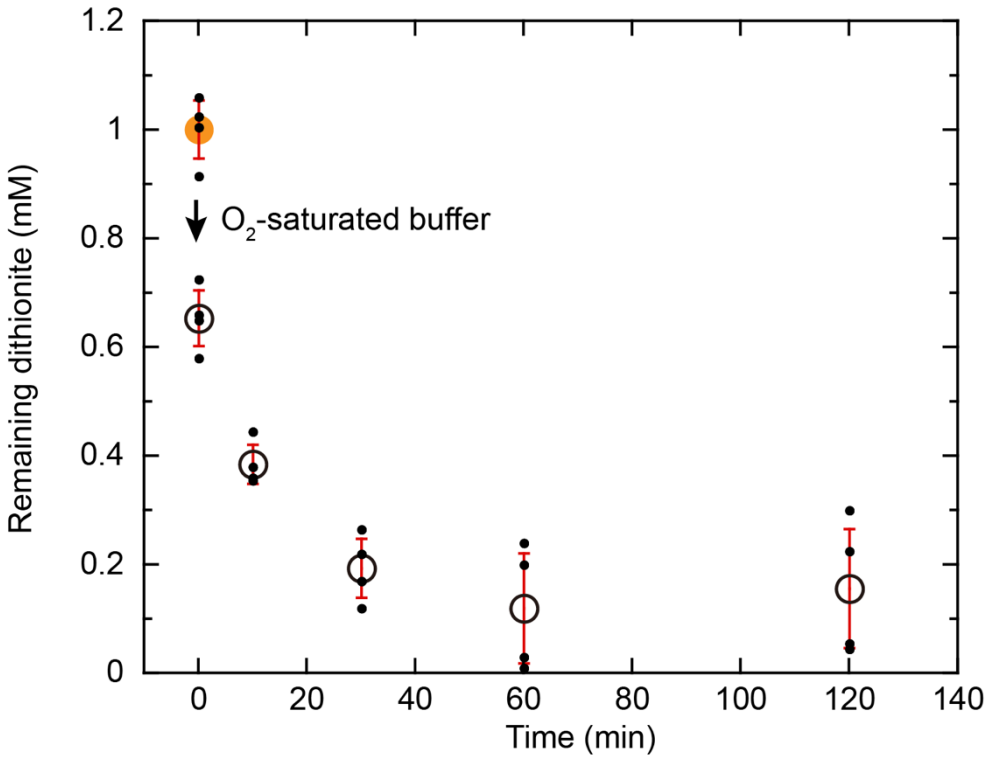

Fig. 6. Consumption of dithionite by addition of O_2-saturated buffer. The QhpG-reaction mixture containing 3 mM sodium dithionite (without proteins) was diluted with twice volumes of O_2-saturated buffer C and the remaining dithionite (open circles) was assayed by measuring spectral changes of an anaerobic solution of free FAD using an aliquot withdrawn at appropriate time intervals. Initial concentrations of dithionite (orange closed circle) were determined after addition of twice volumes of O_2-depleted buffer C. Data are presented as mean values (closed and open circles) ± s.d. (error bars) of n = 4 measurements (black dots) from two independent experiments.

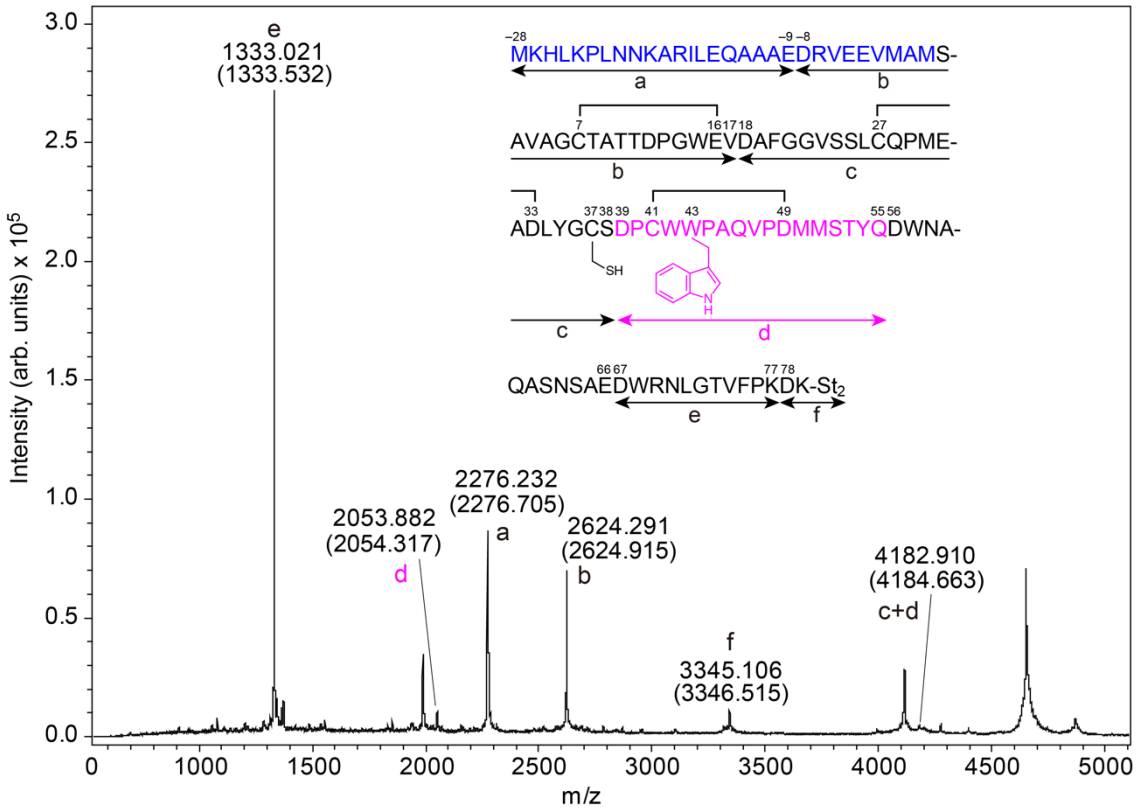

Fig. 7. MALDI-TOF mass spectrometric analysis of crosslinked QhpC digested with Asp-N. The observed and calculated (in parentheses) mass values (*m/z*) are indicated with an assigned fragment code. Fragment d (shown in magenta) contains the CTQ-precursor Trp43. Intensity is expressed in arbitrary units (arb. units). *Inset*: schematic representation of peptide fragments produced by Asp-N digestion. The leader peptide and fragment d are shown in blue and magenta, respectively.

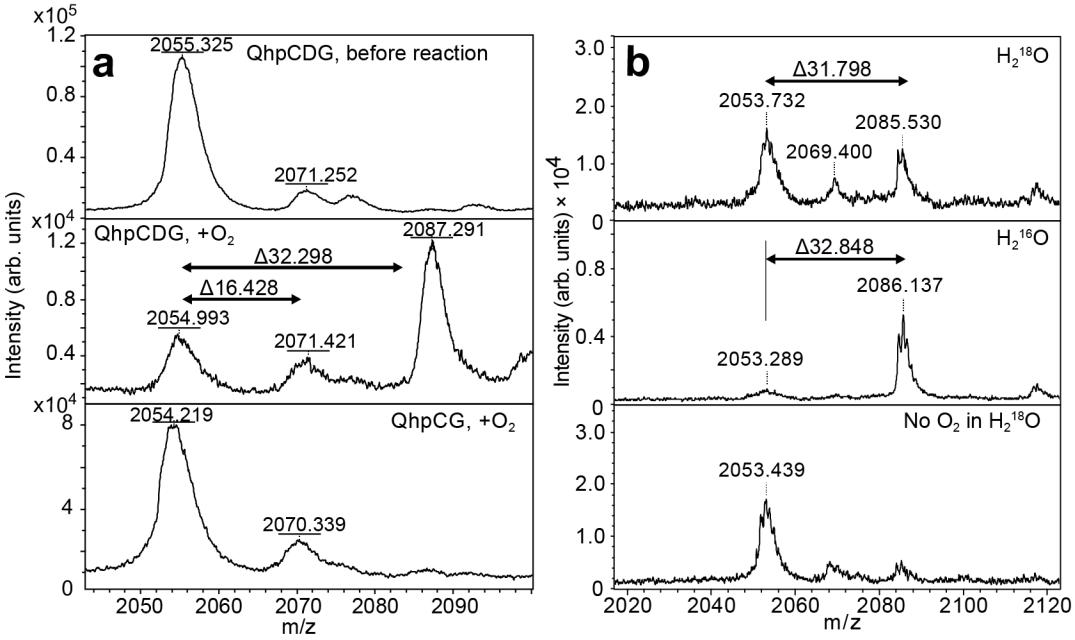

Fig. 8. Product analysis of QhpG reaction. a, MALDI-TOF mass spectrometric analysis of the QhpG reaction products in the QhpCDG ternary complex before (top panel) and after (middle) addition of O_2-saturated buffer and with the free crosslinked QhpC (bottom) (fragment d of Asp-N digestion). **b**, MALDI-TOF mass spectrometric product analysis for the QhpG reactions conducted in $H_2{}^{18}O$-buffer (top panel), $H_2{}^{16}O$-buffer (middle), and without O_2 addition in $H_2{}^{18}O$-buffer (bottom).

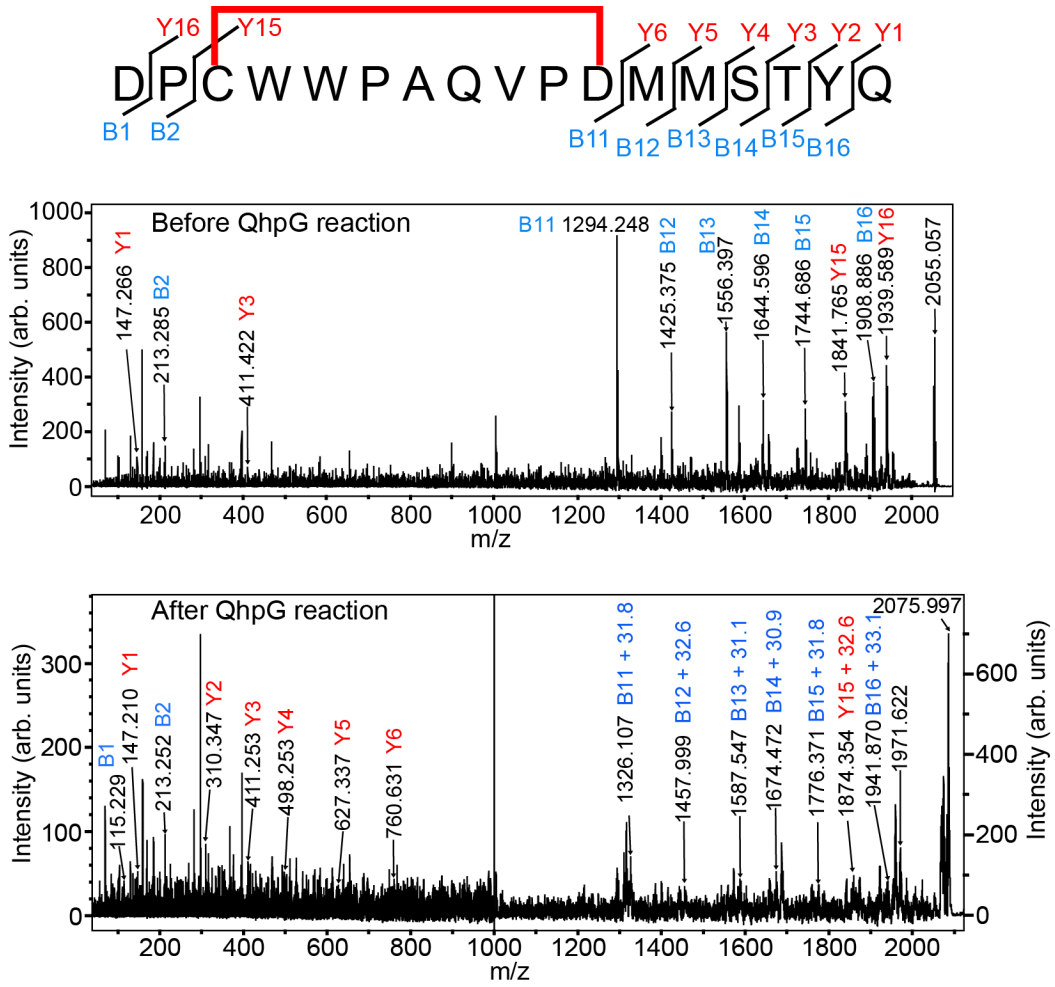

Fig. 9. MS/MS analysis of peptide fragment produced by QhpG reaction. Predicted fragmentation pattern of fragment d (Asp39–Gln55) is shown above. MS/MS spectra of the peptides of d and d+32 peaks obtained before and after the QhpG reaction are shown in upper and lower panels, respectively. Assigned fragments are indicated with *m/z* numbers.

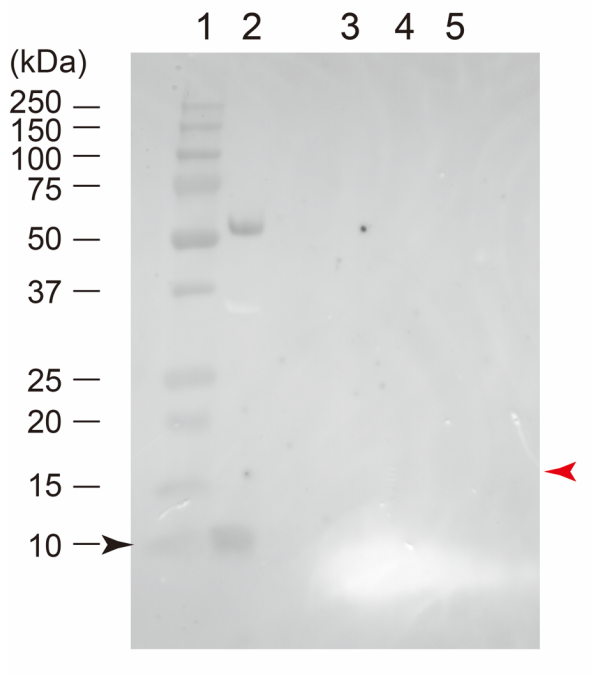

Fig. 10. Redox-cycling quinone staining of QhpG reaction product. The precipitated QhpG reaction product was subjected to sodium dodecyl sulfate PAGE and blotted onto a membrane for redox-cycling quinone staining. Lane 1, precision plus protein dual color standard (Bio-Rad); lane 2, purified QHNDH (0.5 μg); lanes 3–5, QhpG reaction products (total protein, ~20 μg) before (lane 3) and after the reaction in the presence of 1 mM sodium dithionite (lane 4) or 1 mM NADPH (lane 5). Black and red arrowheads indicate approximate positions of the γ-subunit (~9 kDa) (positive control) and crosslinked QhpC with the leader peptide (~15 kDa), respectively. A positive band of ~60 kDa in lane 2 is probably derived from hemes contained in the α-subunit of QHNDH. The experiments were repeated twice independently with similar results.

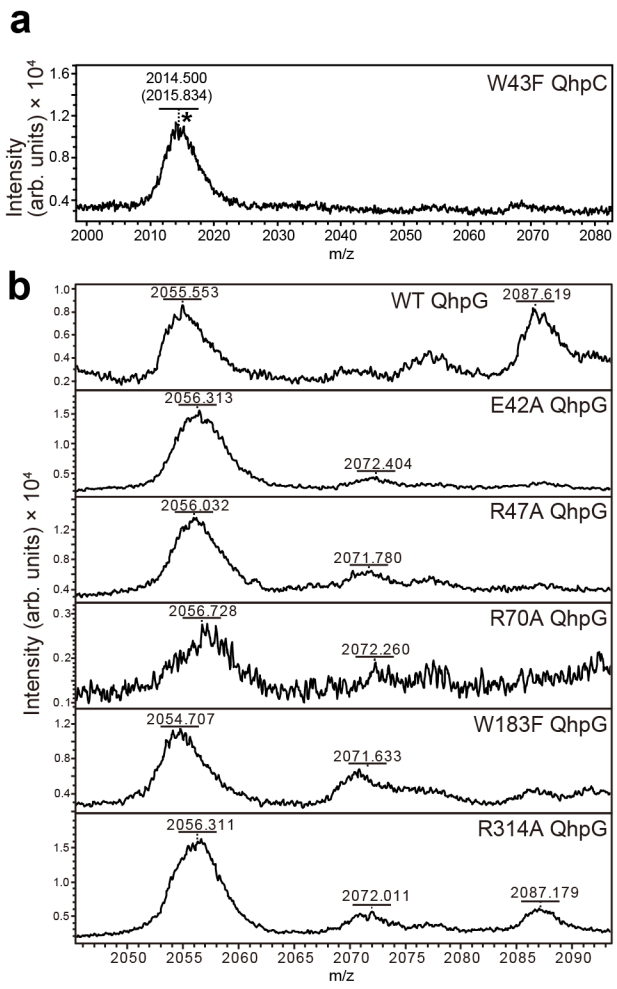

Fig. 11. MALDI-TOF MS analysis of QhpG-catalyzed reaction products. a, The reaction product with the W43F mutant of crosslinked QhpC as substrate for QhpG (*fragment d of Asp-N digestion). The calculated mass (*m/z*) is indicated in parentheses. **b**, The reaction product formed by the wild-type (WT) and various mutants (E42A, R47A, R70A, W183F, and R314A) of QhpG (fragment d of Asp-N digestion).

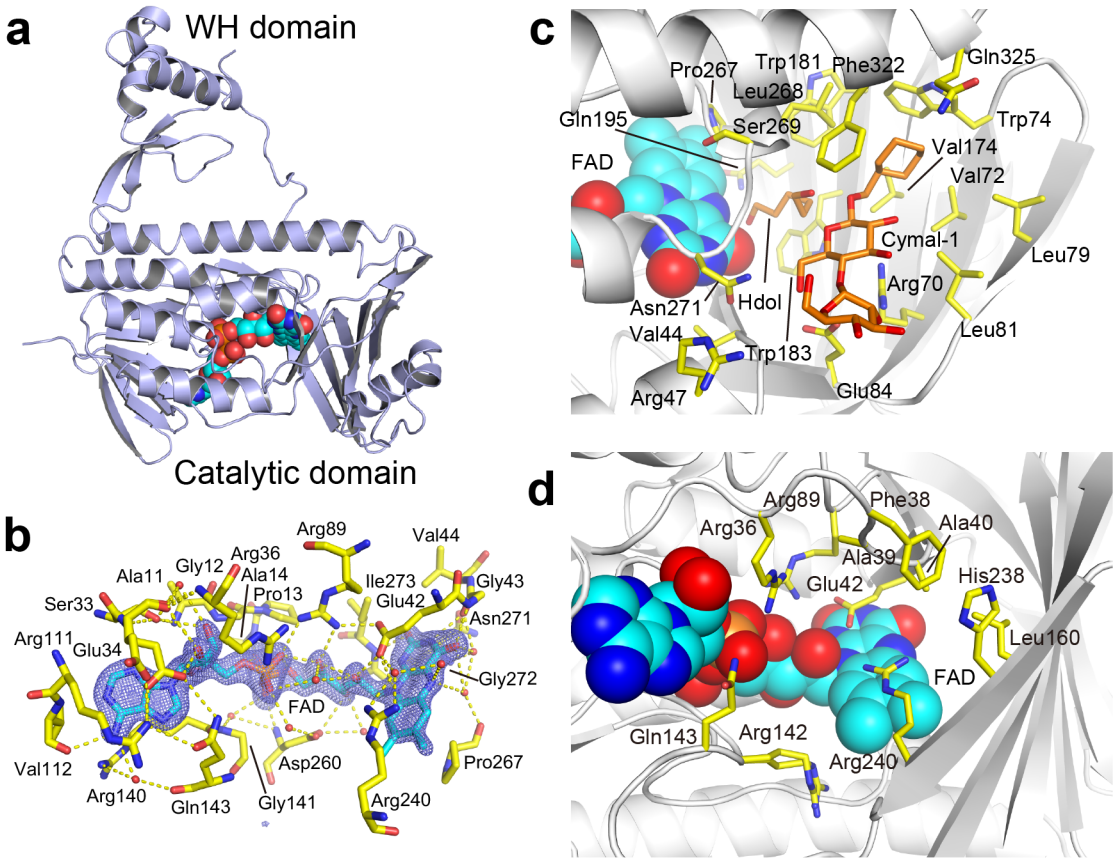

Fig. 12. X-ray crystal structure of QhpG. a, Overall structure of QhpG monomer. The monomer structure (chain A) is depicted by a cartoon model with a spherical model of the bound FAD. **b**, Structure of FAD-binding site. A stick model of the bound FAD is shown with the surrounding residues. An $F_o - F_c$ omit map for FAD, contoured at 5σ, is depicted by blue mesh. Hydrogen bonds and water molecules are shown by yellow dotted lines and red small spheres, respectively. **c**, **d**, Channels formed in the *re*-face (**c**) and *si*-face (**d**) sides of FAD (in chain B) is shown with stick models of the side chains (yellow) on the white cartoon model of QhpG. 1,6-Hexanediol (Hdol) and cyclohexyl-

methyl-β-D-maltoside (Cymal-1) (additives in crystallization buffer) bound to the *re*-face channel are indicated by orange stick models. FAD is indicated by a spherical model.

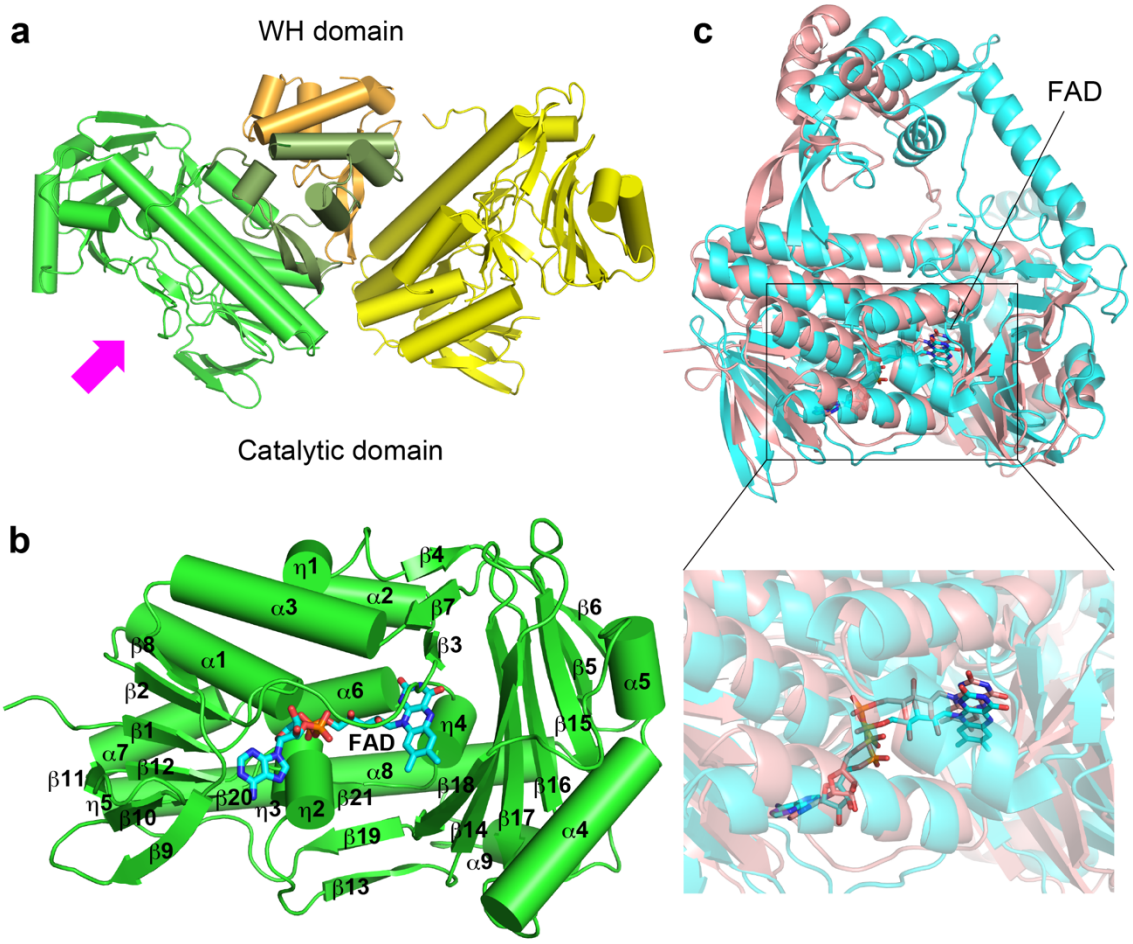

Fig. 13. Schematic drawings of the asymmetric unit in QhpG crystal and the FAD-binding region. a, An asymmetric unit showing inter-domain interactions between the two monomers, colored green and yellow for the catalytic domains and moss green and orange for respective WH domains. **b**, The FAD-binding region of the catalytic domain viewed form the direction of the magenta arrow shown in **a**. The secondary structural elements assigned to the main chain structure (*cf.* Fig. 14) are labeled. FAD is bound between two lobes; one consisting of the central 5-stranded parallel β-sheet (β1, β2, β8, β12, β20), three 3-stranded anti-parallel β-sheets (β3, β4, β7; β9–β11; β13, β19, β21), and 10 helices (α1–α3, α6–α8, η1–η3, η5; where η means a 3_{10}-helix) for the ADP moiety and the other consisting of a mixed 7-stranded β-sheet (β5, β6, β14–β18) in the core layer and 4 helices (α4, α5, α9, η4) in the surface layer for the isoalloxazine ring.

c, Structural comparison of QhpG (brown) with SvCmlS (cyan) with an enlarged view of the FAD-binding region. Proteins and the bound FAD were drawn by cartoon and stick models, respectively.

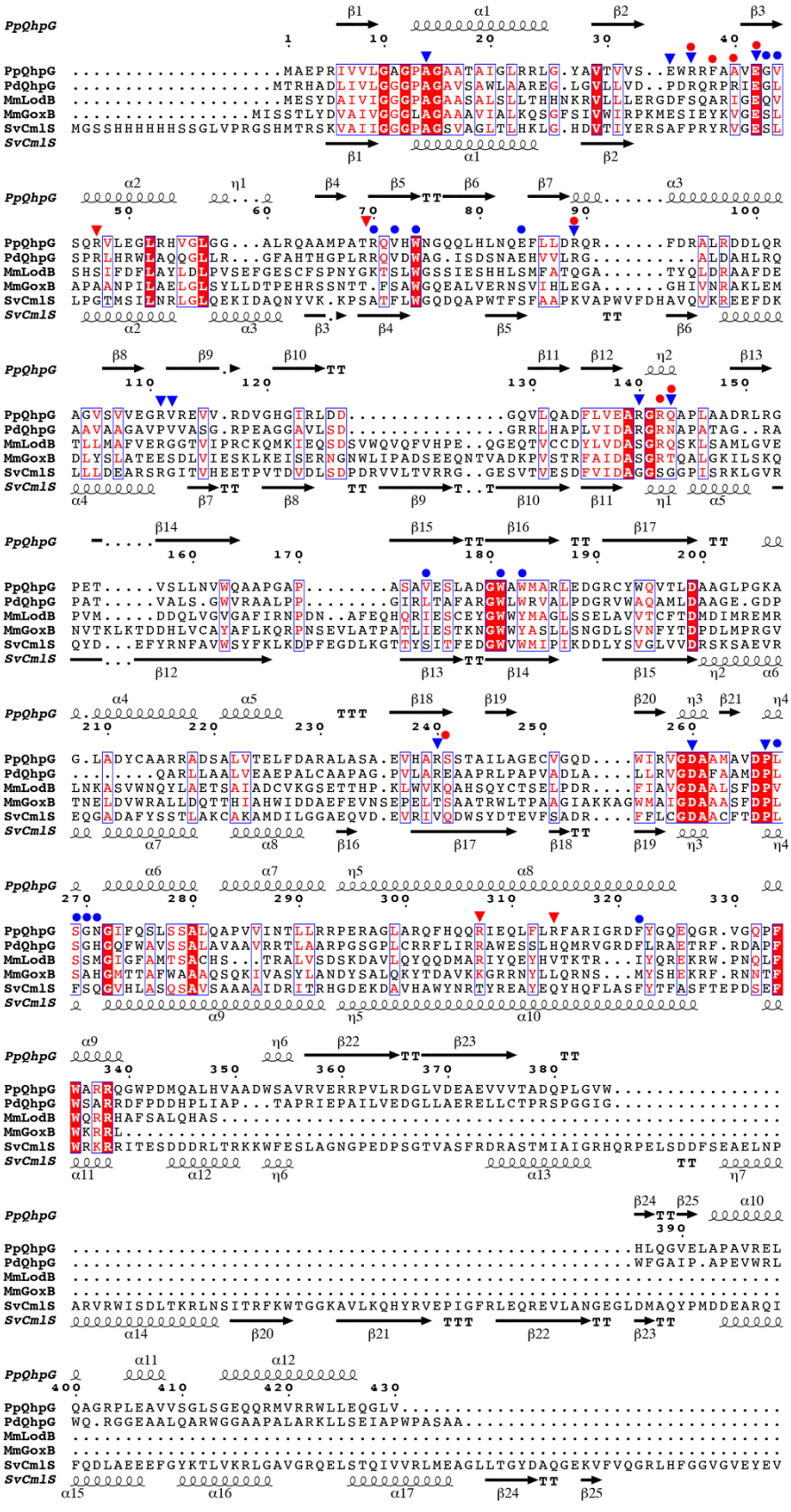
PpQhpG
PdQhpG
MmLodB
MmGoxB
SvCm1S
SvCm1S
β1 α1 β2 β3
1 10 20 30 40
MAEPRIVVLGAGPAGAATAIGLRRLG.YAVTVVS..EWRRFAAVEGV
MTRHADLIVLGGGPAGAVSAWLAAREG.LGVLLVD..PDRQRPRIEGL
MESYDAIVIGGGPAGAASALSLLTHHNKRVLLLERGDFSQARIGEQV
MISSTLYDVAIVGGGLAGAAAVIALKQSGFSIVWIRPKMESIEYKVGESL
MGSSHHHHHHSSGLVPRGSHMTRSKVAIIGGGPAGSVAGLTLHKLG.HDVTIYERSAFPRYRVGESL
β1 α1 β2
α2 η1 β4 β5 β6 β7 α3
50 60 70 80 90 100
SQRVLEGLRHVGLGG...ALRQAAMPATRQVHWNGQQLHLNQEFLLDRQR......FDRALRDDLQR
SPRLHRWLAQQGLLR...GFAHTHGPLRRQVDVAG.ISDSNAEHVVLRG..........ALDAHLRQ
SHSIFDFLAYLDIPVSEFGESCFSPNYGKTSLWGSSIESHHLSMFATQGA......TYQLDRAAFDE
APAANPILAELGLSYLLDTPEHRSSNTT.FSAWGQEALVERNSVIHLEGA......GHIVNRAKLEM
LPGTMSILNRLGLQEKIDAQNYVK.KPSATFLWGQDQAPWTFSFAAPKVAPWVFDHAVQVKREEFDK
α2 α3 β3 β4 β5 TT β6
β8 β9 β10 TT β11 β12 η2 β13
110 120 130 140 150
AGVSVVEGRVREVV.RDVGHGIRLDD..............GQVLQADFLVEARGRQAPLAADRLRG
AAVAAGAVPVVASG.RPEAGGAVLSD..............GRRLHAPLVIDARGRNAPATAG..RA
TLLMAFVERGGTVIPRCKQMKIEQSDSVWQVQFVHPE..QGEQTVCCDYLVDASGRQSKLSAMLGVE
DLYSLATEESDLVIESKLKEISERNGNWLIPADSEEQNTVADKPVSTRFAIDASGRTQALGKILSKQ
LLLDEARSRGITVHEETPVTDVDLSDPDRVVLTVRRG..GESVTVESDFVIDAGGSGGPLSRKLGVR
α4 β7 TT β8 TT β9 T..T β10 β11 η1 α5
β14 β15 β16 β17
160 170 180 190 200
PET.....VSLLNVWQAAPGAP.........ASAVESLADGWAWMARLEDGRCYWQVTLDAAGLPGKA
PAT.....VALS.GWVRAALPP.........GIRLTAFARGWLWRVALPDGRVWAQAMLDAAGE.GDP
PVM.....DDQLVGVGAFIRNPDN..AFEQHQRIESCEYGWWYMAGLSSELAVVTCFTDMDIMREMR
NVTKLKTDDHLVCAYAFLKQRPNSEVLATPATLIESTKNGWWYASLLSNGDLSVNFYTDPDLMPRGV
QYD...EFYRNFAVWSYFKLKDPFEGDLKGTTYSITFEDGWVWMIPIKDDLYSVGLVVDRSKSAEVR
β12 β13 TT β14 β15 η2 α6
α4 α5 TTT β18 β19 β20 η3 β21 η4
210 220 230 240 250 260
G.LADYCAARRADSALVTELFDARALASA.EVHARSSTAILAGECVGQD....WIRVGDAAMAVDPL
.....QARLLAALVEAEPALCAAPAG.PVLAREAAPRLPAPVADLA....LLRVGDAFAAMDPL
LNKASVWNQYLAETSAIADCVKGSETTHP.KLWVKQAHSQYCTSELPDR....FIAVGDAALSFDPV
TNELDVWRALLDQTTHIAHWIDDAEFEVNSEPELTSAATRWLTPAAGIAKKAGWMAIGDAAASFDPL
EQGADAFYSSTLAKCAKAMDILGGAEQVD.EVRIVQDWSYDTEVFSADR....FFLCGDAACFTDPL
α7 α8 β16 β17 β18 β19 η3 η4
α6 α7 η5 α8
270 280 290 300 310 320 330
SGNGIFQSLSSALQAPVVINTLLRRPERAGLARQFHQQRIEQLFLRFARIGRDFYGQEQGR.VGQPF
SGHCQFWAVSSALAVAAVRRTLAARPGSGPLCRRFLIRRAWESSLHQMRVGRDFLRAETRF.RDAPF
SSMGIGFAMTSACHS...TRALVSDSKDAVLQYQQDMARIYQEYHVTKTR...IYQREKRW.PNQLF
SAHGMTTAFWAAAQSQKIVASYLANDYSALQKYTDAVKKGRRNYLLQRNS...MYSHEKRF.RNNTF
FSQGVHLASQSAVSAAAAIDRITRHGDEKDAVHAWYNRTYREAYEQYHQFLASFYTFASFTEPDSEF
α9 η5 α10
α9 η6 β22 TT β23 TT
340 350 360 370 380
WARRQGWPDMQALHVAADWSAVRVERRPVLRDGLVDEAEVVVTADQPLGVW.....
WSARRDFPDDHPLIAP...TAPRIEPAILVEDGLLAERELLCTPRSPGGIG.....
WQRRHAFSALQHAS.....
WKRRL.....
WRKRRITESDDDRLTRKKWFESLAGNGPEDPSGTVASFRDRASTMIAIGRHQRPELSDDFSEAELNP
α11 α12 η6 α13 TT η7
β24 TT β25 α10
390
HLQGVELAPAVREL
WFGAIP.APEVWRL
ARVRWISDLTKRLNSITRFKWTGGKAVLKQHYRVEPIGFRLEQREVLANGEGLDMAQYPMDDEARQI
α14 β20 β21 TTT β22 TT β23 TT
α11 α12
400 410 420 430
QAGRPLEAVVSGLSGEQQRMVRRWLLEQGLV.....
WQ.RGGEAALQARWGGAAPALARKLLSEIAPWPASAA.....
FQDLAEEEFGYKTLVKRLGAVGRQELSTQIVVRLMEAGLLTGYDAQGEKVFVQGRLHFGGVGVEYEV
α15 α16 α17 β24 TT β25

Fig. 14. Multiple sequence alignment and secondary structure assignment of QhpG orthologs and homologs. Amino acid sequences of QhpG orthologs from *Ps. putida* IFO 15366 (PpQhpG, NCBI RefSeq: LC575123 [https://www.ncbi.nlm.nih.gov/nuccore/LC575123.1/]) and *Pa. denitrificans* Pd1222 (PdQhpG, WP_011747997 [https://www.ncbi.nlm.nih.gov/protein/WP_011747997.1]) and homologs; LodB from *Marinomonas mediterranea* MMB-1 (MmLodB, WP_013661795 [https://www.ncbi.nlm.nih.gov/protein/WP_013661795.1]), GoxB from *Marinomonas mediterranea* (MmGoxB, WP_013660822 [https://www.ncbi.nlm.nih.gov/protein/WP_013660822.1]), and CmlS from *Streptomyces venezuelae* (SvCmlS, AAK08979 [https://www.ebi.ac.uk/ena/browser/view/AAK08979]) were aligned using the program Clustal W[1]. Secondary structural elements in the crystal structure of QhpG and SvCmlS were assigned using the program DSSP[2], and are shown above and below each sequence, respectively. Residues, involved in binding of FAD or found in its vicinity, are shown in inverted blue triangles. Residues forming *re*-face and *si*-face channels are shown in blue and red circles, respectively. Positively charged residues locating near the *re*-face channel entrance are shown in inverted red triangles. The figure was drawn using the program ESPript[3].

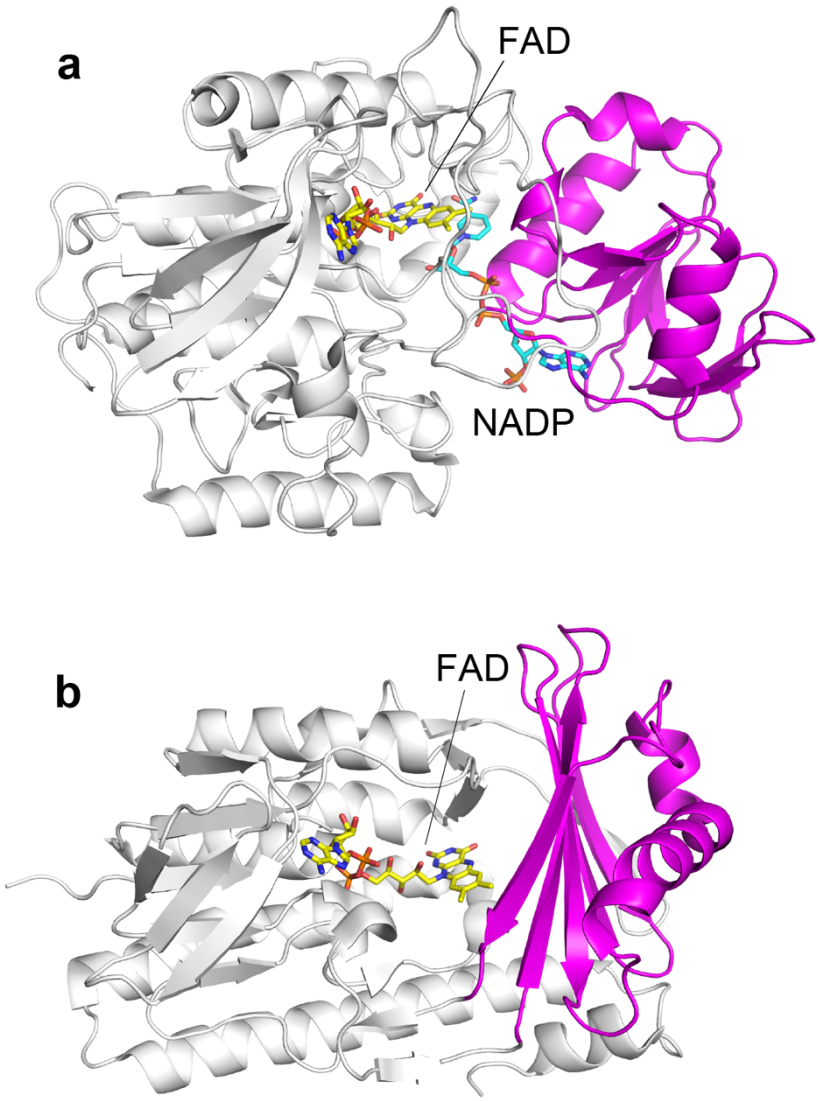

Fig. 15. Structural comparison of QhpG and an FAD-dependent monooxygenase requiring NADPH. a, X-ray crystal structure of the flavoprotein monooxygenase from *Schizosaccharomyces pombe* (PDB ID: 2GV8)[4] is shown by a cartoon model with the NADPH-binding domain (Tyr180–Gly289) colored magenta and the bound FAD (yellow) and NADPH (cyan) shown by stick models. **b**, The crystal structure of QhpG (this study) is shown by a cartoon model colored magenta for the region (Glu155–Thr243) besides the FAD-binding domain and the bound FAD shown by a stick model.

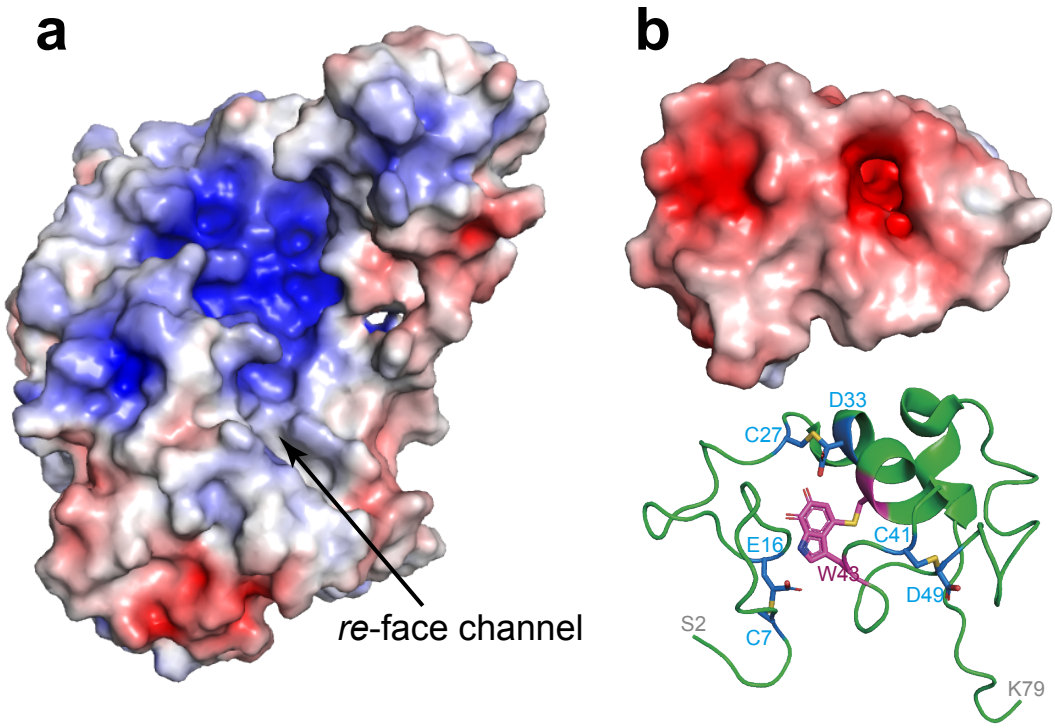

Fig. 16. Electrostatic surface potentials of QhpG and γ-subunit of QHNDH. Electrostatic potentials mapped onto the molecular surfaces of QhpG (**a**) and γ-subunit of QHNDH (**b**), colored in gradation from red (−5 *kT*) to blue (+5 *kT*), where *k* is the Boltzmann constant, and *T* is the absolute temperature, based on the calculation by PyMOL (Schrödinger Inc. New York, USA) and APBS[5]. In panel **b**, the γ-subunit structure (cartoon model, cyan) extracted from the *Ps. putida* QHNDH structure (1JMX) is also shown with surface Asp/Glu residues (magenta) and CTQ in stick models.

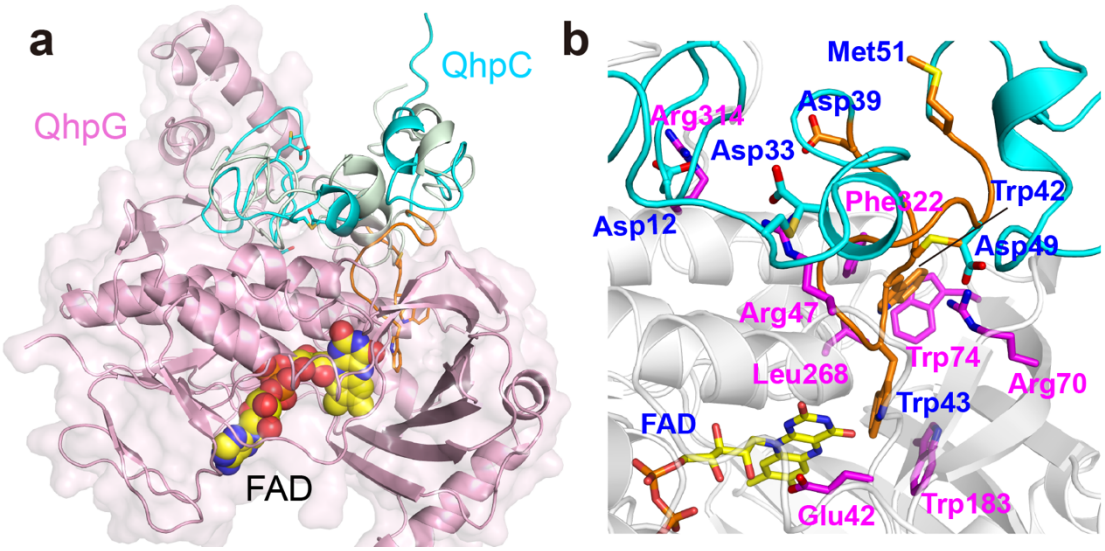

Fig. 17. Crosslinked QhpC-QhpG docking model. a, Overall structure of the docking model. A cartoon model of QhpG is colored light magenta with a spherical model of bound FAD and transparent molecular surfaces. The initial docking model of γ-subunit obtained with ZDOCK[6] is shown by pale green. The crosslinked QhpC (without the leader peptide) obtained by Coot[7]-based manual building followed by energy minimization is shown by orange for the Asp39–Met51 loop with the side chains of Trp42 and Trp43 and by cyan for the other region. The thioether bonds between Cys and Asp/Glu residues are shown in stick models. **b**, an enlarged view of the crosslinked QhpC-QhpG docking model. QhpG is depicted by a transparent white cartoon model with the side chains (magenta stick models) that are involved in the interactions with the crosslinked QhpC. FAD is also shown as a stick model. The bound QhpC is presented by the same colors used in panel **a** with the side chains involved in the interaction with QhpG and that of the CTQ precursor Trp43 (orange stick models).

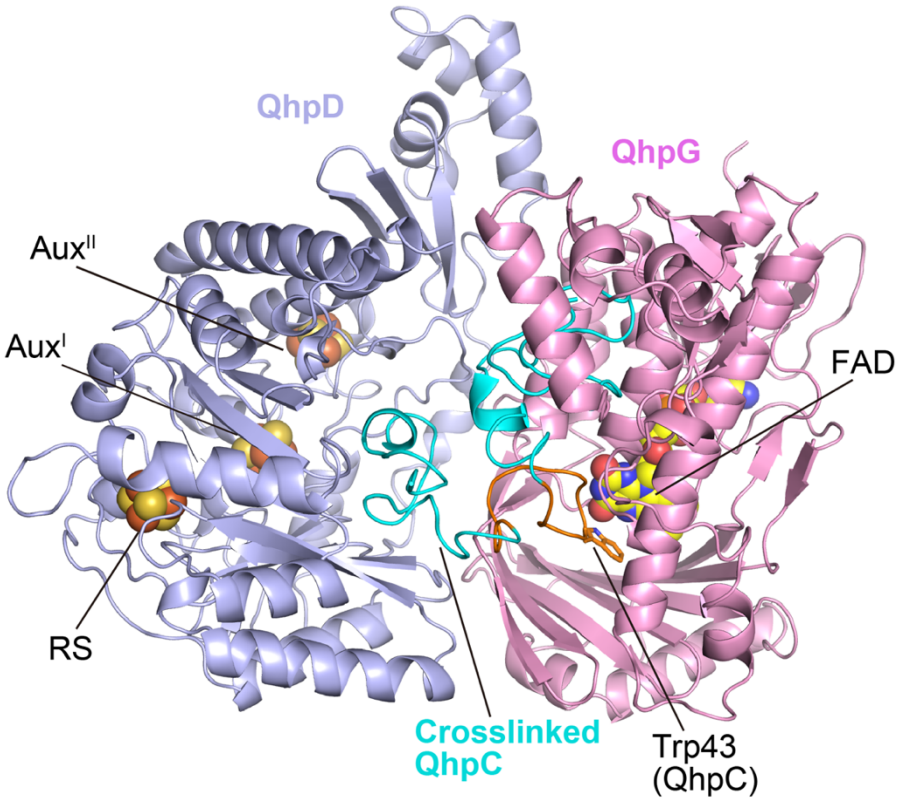

Fig. 18. Docking model of the QhpCDG ternary complex. A homology model of QhpD from *Ps. putida* (light blue) was docked onto the model of the QhpCG binary complex (Fig. 17) using ZDOCK[6]. Cartoon models of QhpD (light blue), QhpG (light magenta), and crosslinked QhpC (cyan; the Asp39–Met51 loop and the side chain of Trp43, orange) are depicted with FAD in QhpG and three [Fe_4S_4] clusters (RS, Aux^I, and Aux^{II}) in QhpD[8] shown by spherical models.

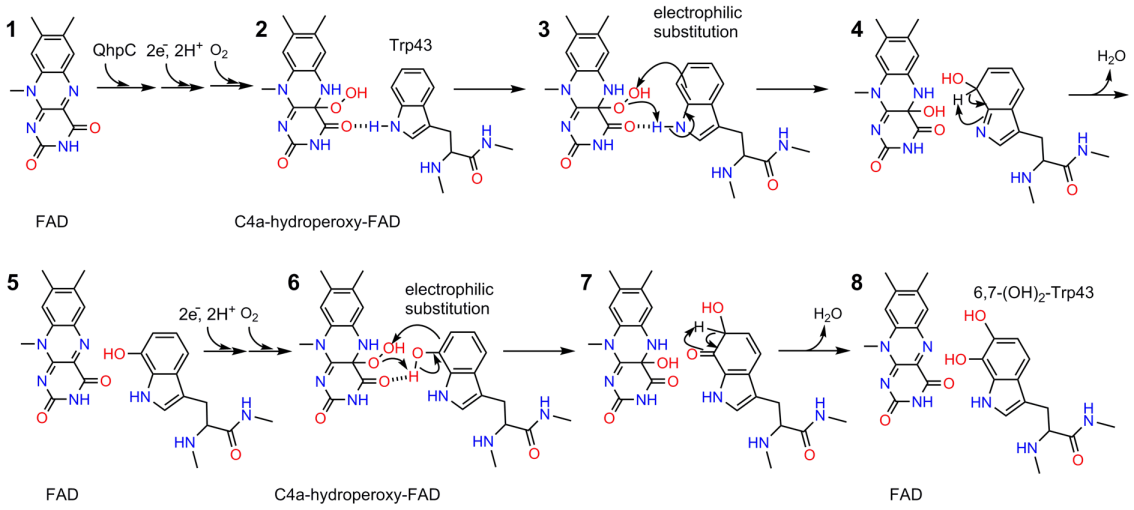

Fig. 19. Predicted reaction mechanism of QhpG.

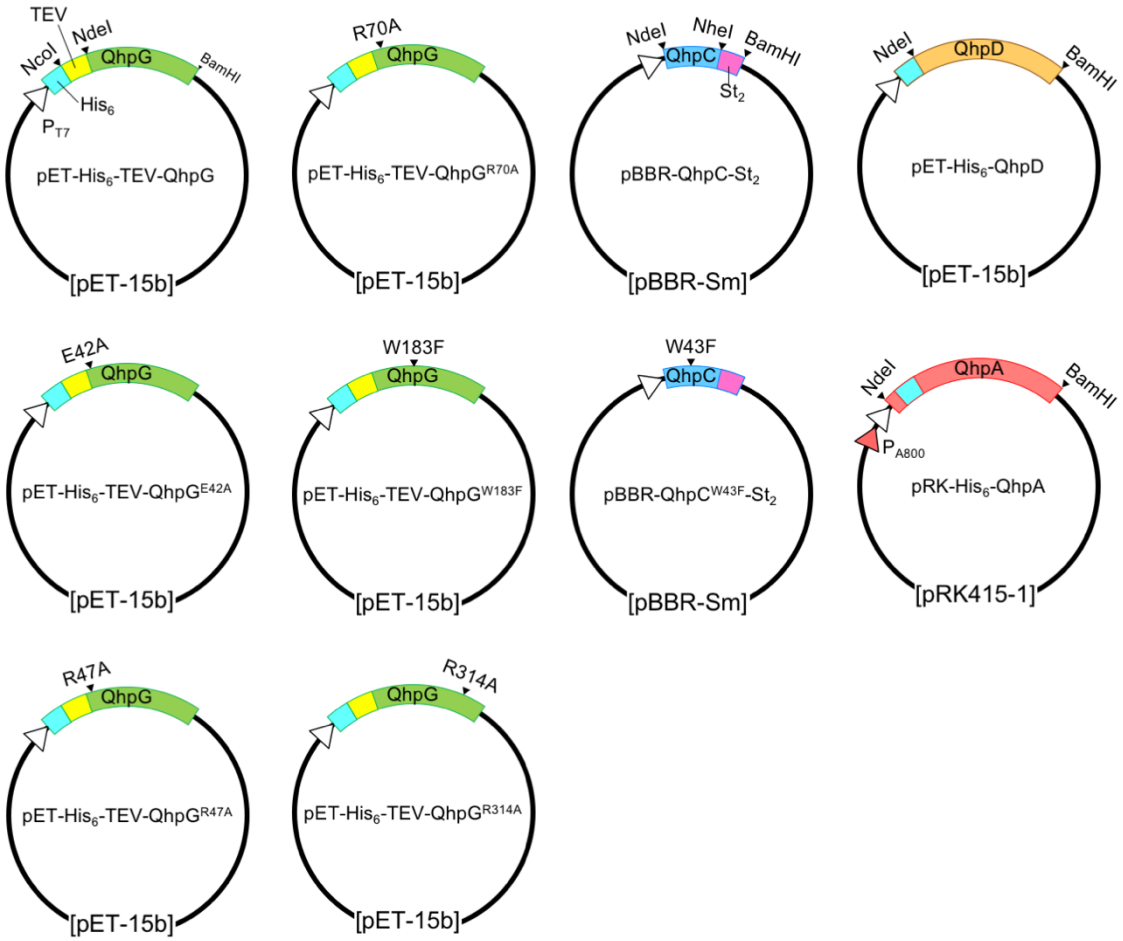

Fig. 20. Schematic structures of the plasmids used in this study. In all plasmids, only the restriction sites used for plasmid construction are indicated. His_6-tag, TEV cleavage site (TEV), and St_2-tag are shown by cyan, yellow, and pink bars, respectively. A T7 promoter (P_{T7}) and a promoter region of the *qhp* operon (P_{A800})[9] are depicted by white and red triangles, respectively. Coding regions for QhpA from *Pa. denitrificans*, QhpC (wild-type and W43F), QhpD, and QhpG (wild-type, E42A, R47A, R70A, W183F, and R314A) are colored red, sky blue, orange, and green, respectively, with vectors used for construction (pRK415-1, pET-15b, or pBBR1).

Table 1. **Dissociation constants and association and dissociation rate constants for interactions of wild-type and mutant QhpG with QhpC**

QhpG/QhpC	K_d (nM)	Association rate constant (k_a) (M^{-1} s^{-1})	Dissociation rate constant (k_d) (s^{-1})
Wild-type/linear	2800 ± 22	$(5.9 \pm 1.7) \times 10^4$	$(1.6 \pm 0.46) \times 10^{-1}$
Wild-type/crosslinked	28 ± 2.3	$(4.9 \pm 0.44) \times 10^5$	$(1.4 \pm 0.0090) \times 10^{-2}$
E42A/crosslinked	65 ± 8.1	$(1.7 \pm 0.16) \times 10^5$	$(1.1 \pm 0.29) \times 10^{-2}$
R47A/crosslinked	1500 ± 490	$(1.5 \pm 0.13) \times 10^4$	$(2.3 \pm 0.52) \times 10^{-2}$
R70A/crosslinked	48 ± 3.6	$(4.7 \pm 0.45) \times 10^5$	$(2.2 \pm 0.04) \times 10^{-2}$
W183F/crosslinked	37 ± 19	$(3.6 \pm 0.68) \times 10^5$	$(1.3 \pm 0.41) \times 10^{-2}$
R314A/crosslinked	78 ± 28	$(1.4 \pm 0.18) \times 10^5$	$(1.1 \pm 0.24) \times 10^{-2}$

Table 2. Data collection and crystallographic refinement statistics

Crystal (PDB entry ID)	Hg derivative	Native (7CTQ)
Data collection		
Wavelength (Å)	1.0070	0.9
Space group	$P2_1$	$P2_1$
Cell dimensions		
a, *b*, *c* (Å),	90.07, 52.20, 101.76,	88.61, 51.56, 101.79,
α, β, γ (°)	90, 99.50, 90	90, 99.77, 90
Resolution (Å)	100 – 2.79 (2.84 – 2.79)[a]	50 – 1.98 (2.10 – 1.98)
$I/\sigma(I)$	13.7 (2.1)	12.7 (2.2)
Redundancy	2.0 (1.9)	3.6 (3.6)
Overall completeness (%)	99.3 (99.8)	98.7 (97.2)
Overall R_{merge} (%)	8.7 (49.4)	6.8 (62.5)
SIRAS phasing		
Hg atom sites	2	
Resolution range of data used (Å)	40 – 2.79 (2.81 – 2.79)	
No. reflections	45360	
Figure of merit	0.201 (0.034)	
Phasing power (isomorphous)	0.374 (0.209)	
Phasing power (anomalous)	0.419 (0.112)	
Refinement		
Resolution (Å)		50 – 1.98 (2.05 – 1.98)
No. reflections		63142
R_{work} / R_{free} (%)		18.2 (26.8) / 22.2 (34.8)
No. atoms		
Protein		6800
Ligand		192
Water		421
Average temperature factors		
Protein		44.9
Ligand		50.1
Water		44.7
R.m.s. deviation from ideal values		
Bond lengths (Å)		0.0072
Bond angles (°)		0.91
Ramachandran plot statistics (%)		
Residues in favored regions		97.3
Residues in allowed regions		2.5
Outliers		0.2[b]

[a]Values in parentheses refer to the data for the highest resolution shells.

[b]The outlier residues are only Val119 in chains A and B (2/858). Val119 is contained in a short turn (Asp118–Gly120), in which the main chain carbonyl group of Asp118 is hydrogen-bonded to the main chain amide group of Gly120, stabilizing the turn structure with relatively high thermal factors.

Table 3. **Oligonucleotides used in this study**

Primer for plasmid construction[a]	Nucleotide sequence[b]	Introduced restriction site or mutation
QhpC (+)	tatacatatgaaacacttgaagcccct	NdeI
QhpC (–)	atatgctagccttgtctttcgggaacacgg	NheI
QhpD (+)	catatgggcgcgctactgaacctggtcgaacgc	NdeI
QhpD (–)	ggatcctcagtgcgccttccgcggggtgatgtagcg	BamHI
QhpG (+)	atatcatatggctgaaccgcgcattgtggtgttgggg	NdeI
QhpG (–)	atatggatcctcaa**a**ccaagccctgctccaacaaccaccg	BamHI
His_6-TEV (+)	catgggcagcagccatcatcatcatcacgattacgatatcccaa cgaccgaaaacctttacttccagggcca	NcoI/NdeI
His_6-TEV (–)	tatggccctggaagtaaaggttttcggtcgttgggatatcgtaatcgt gatgatgatgatgatggctgctgcc	NcoI/NdeI
QhpG-E42A (+)	cggtttgcggcggtc**gca**ggggtttcgcagcgg	E42A QhpG
QhpG-E42A (–)	ccgctgcgaaaccccc**cgt**gaccgccgcaaaccg	E42A QhpG
QhpG-R47A (+)	cggtcgaaggggtttcgcag**gcg**gtgctggaggggctgcgccac	R47A QhpG
QhpG-R47A (–)	tggcgcagcccctccagcac**cgc**ctgcgaaaccccttcgaccg	R47A QhpG
QhpG-R70A (+)	gcgtgacgaccttcagcgtg**gcg**gtgtgagcgtggtcgagggg	R70A QhpG
QhpG-R70A (–)	cccctcgaccacgctcacac**cgc**cacgctgaaggtcgtcacgc	R70A QhpG
QhpG-W183F (+)	gcctggcggatggctgggcg**ttc**atggcgcgcctggaagacgg	W183A QhpG
QhpG-W183F (–)	ccgtcttccaggcgcgccat**gaa**cgcccagccatccgccaggc	W183A QhpG
QhpG-R314A (+)	ggatcgaacagctgtttttg**gcc**tttgcccggatcgggcggg	R314A QhpG
QhpG-R314A (–)	cccgcccgatccgggcaaa**ggc**caaaaacagctgttcgatcc	R314A QhpG
QhpC-W43F (+)	tccgacccttgctgg**ttc**ccggcccaggtgccg	W43F QhpC
QhpC-W43F (–)	cggcacctgggccgg**gaa**ccagcaagggtcgga	W43F QhpC
pdQhpA[c] (+)	atatcatatgaagccattcacccgaaccgcgc	NdeI
pdQhpA[c] (–)	acatggatcctcaccggatcggcgcatcgacgaa	BamHI
His_6-pdQhpA[c] (+)	ggctcgagccatcaccatcaccatcactcgagcggcgtgacgggc gaggaggtg	His_6-pdQhpA[c]
His_6-pdQhpA[c] (–)	gccgctcgagtgatggtgatggtgatggctcgagcccgcaaggac cggcgcggc	His_6-pdQhpA[c]

[a]Plus and minus signs in parentheses denote sense and antisense strands, respectively.
[b]Restriction sites are underlined. Mismatching nucleotides at the mutated sites are shown in bold.
[c]QhpA of *Pa. denitrificans*.

2.5. References

1. Davidson, V. L. Generation of protein-derived redox cofactors by posttranslational modification. *Mol. Biosyst.* **7**, 29–37 (2011).

2. Yukl, E. T. & Wilmot, C. M. Cofactor biosynthesis through protein post-translational modification. *Curr. Opin. Chem. Biol.* **16**, 54–59 (2012).

3. Davidson, V. L. Protein-derived cofactors revisited: empowering amino acid residues with new functions. *Biochemistry* **57**, 3115–3125 (2018).

4. Davidson, V. L. & Liu, A. Tryptophan tryptophylquinone biosynthesis: a radical approach to posttranslational modification. *Biochim. Biophys. Acta.* **1824**, 1299–1305 (2012).

5. Klinman, J. P. & Bonnot, F. Intrigues and intricacies of the biosynthetic pathways for the enzymatic quinocofactors: PQQ, TTQ, CTQ, TPQ, and LTQ. *Chem. Rev.* **114**, 4343–4365 (2014).

6. Yukl, E. T. & Davidson, V. L. Diversity of structures, catalytic mechanisms and processes of cofactor biosynthesis of tryptophylquinone-bearing enzymes. *Arch. Biochem. Biophys.* **654**, 40–46 (2018).

7. Adachi, O. et al. Characterization of quinohemoprotein amine dehydrogenase from *Pseudomonas putida*. *Biosci. Biotechnol. Biochem.* **62**, 469–478 (1998).

8. Takagi, K., Yamamoto, K., Kano, K. & Ikeda, T. New pathway of amine oxidation respiratory chain of *Paracoccus denitrificans* IFO 12442. *Eur. J. Biochem.* **268**, 470–476 (2001).

9. Datta, S. et al. Structure of a quinohemoprotein amine dehydrogenase with an uncommon redox cofactor and highly unusual crosslinking. *Proc. Natl. Acad. Sci. U. S. A.* **98**, 14268–14273 (2001).

10. Satoh, A. et al. Crystal structure of quinohemoprotein amine dehydrogenase from *Pseudomonas putida*. Identification of a novel quinone cofactor encaged by multiple thioether cross-bridges. *J. Biol. Chem.* **277**, 2830–2834 (2002).

11. Nakai, T. et al. Identification of genes essential for the biogenesis of quinohemoprotein amine dehydrogenase. *Biochemistry* **53**, 895–907 (2014).

12. Altschul, S. F. et al. Gapped BLAST and PSI-BLAST: a new generation of protein database search programs. *Nucleic Acids Res.* **25**, 3389–3402 (1997).

13. Ono, K. et al. Involvement of a putative [Fe-S]-cluster-binding protein in the biogenesis of quinohemoprotein amine dehydrogenase. *J. Biol. Chem.* **281**, 13672–13684 (2006).

14. Nakai, T. et al. The *S*-adenosyl-L-methionine enzyme QhpD catalyzes sequential formation of intra-protein sulfur-to-methylene carbon thioether bonds. *J. Biol. Chem.* **290**, 11144–11166 (2015).

15. Nakai, T. et al. An unusual subtilisin-like serine protease is essential for biogenesis of quinohemoprotein amine dehydrogenase. *J. Biol. Chem.* **287**, 6530–6538 (2012).

16. Kapust, R. B. et al. Tobacco etch virus protease: mechanism of autolysis and rational design of stable mutants with wild-type catalytic proficiency. *Protein Eng.* **14**, 993–1000 (2001).

17. Gasteiger, E. et al. Protein Identification and Analysis Tools on the ExPASy Server, pp. 571–607; (In) John M. Walker (ed): The Proteomics Protocols Handbook, Humana Press, Totowa, N. J. (2005).

18. Macheroux, P. UV-visible spectroscopy as a tool to study flavoproteins, pp. 1–7; (In) S. K. Chapman and G. A. Reid (ed): Flavoprotein protocols, Vol. 131. Humana Press, Totowa, N. J. (1999).

19. Kabsch, W. *XDS*. *Acta Crystallogr*. *Sect*. *D Biol*. *Crytallogr*. **D66**, 125–132 (2010).

20. Otwinowski, Z. & Minor, W. Processing of X-ray diffraction data collected in oscillation mode. *Methods Enzymol*. **276**, 307–326 (1997).

21. Sheldrick, G. M. Experimental phasing with *SHELXC/D/E*: combining chain tracing with density modification. *Acta Crystallogr*. *Sect*. *D Biol*. *Crytallogr*. **D66**, 479–485 (2010).

22. Pearson, A. R. et al. Isotope labeling studies reveal the order of oxygen incorporation into the tryptophan tryptophylquinone cofactor of methylamine dehydrogenase. *J*. *Am*. *Chem*. *Soc*. **128**, 12416–12417 (2006).

23. de La Fortelle, E. & Bricogne, G. Maximum-likelihood heavy-atom parameter refinement for the multiple isomorphous replacement and multiwavelength anomalous diffraction methods. *Methods Enzymol*. **276**, 472–494 (1997).

24. Adams, P. D. et al. *PHENIX*: a comprehensive Python-based system for macromolecular structure solution. *Acta Crystallogr*. *Sect*. *D Biol*. *Crytallogr*. **D66**, 213–221 (2010).

25. Emsley, P., Lohkamp, B., Scott, W. G. & Cowtan, K. Features and development of *Coot*. *Acta Crystallogr*. *Sect*. *D Biol*. *Crytallogr*. **D66**, 486–501 (2010).

26. Pierce, B. G. et al. ZDOCK server: interactive docking prediction of protein-protein complexes and symmetric multimers. *Bioinformatics* **30**, 1771–1773 (2014).

27. Amaral, M. et al. Structural basis of kynurenine 3-monooxygenase inhibition. *Nature* **496**, 382–385 (2013).

28. Waterhouse, A. et al. SWISS-MODEL: homology modelling of protein structures and complexes. *Nucleic Acids Res*. **46**, W296–W303 (2018).

29. Camacho, C. et al. BLAST+: architecture and applications. *BMC Bioinformatics* **10**, 421 (2009).

30. Steinegger, M. et al. HH-suite3 for fast remote homology detection and deep protein annotation. *BMC Bioinformatics* **20**, 473 (2019).

31. Pierce, B. G. et al. ZDOCK server: interactive docking prediction of protein-protein complexes and symmetric multimers. *Bioinformatics* **30**, 1771–1773 (2014).

32. Vandenberghe, I. et al. The covalent structure of the small subunit from *Pseudomonas putida* amine dehydrogenase reveals the presence of three novel types of internal cross-linkages, all involving cysteine in a thioether bond. *J*. *Biol*. *Chem*. **276**, 42923–42931 (2001).

33. Krissinel, E. & Henrick, K. Inference of macromolecular assemblies from crystalline state. *J*. *Mol*. *Biol*. **372**, 774–797 (2007).

34. Yeh, E. et al. Chlorination by a long-lived intermediate in the mechanism of flavin-dependent halogenases. *Biochemistry* **46**, 1284–1292 (2007).

35. Buedenbender, S., Rachid, S., Müller, R. & Schulz, G. E. Structure and action of the myxobacterial chondrochloren halogenase CndH: a new variant of FAD-dependent halogenases. *J. Mol. Biol.* **385**, 520–530 (2009).

36. Podzelinska, K. et al. Chloramphenicol biosynthesis: the structure of CmlS, a flavin-dependent halogenase showing a covalent flavin-aspartate bond. *J. Mol. Biol.* **397**, 316–331 (2010).

37. Eppink, M. H., Bunthol, C., Schreuder, H. A. & van Berkel, W. J. Phe161 and Arg166 variants of *p*-hydroxybenzoate hydroxylase. Implications for NADPH recognition and structural stability. *FEBS Lett.* **443**, 251–255 (1999).

38. Amaral, M. et al. Structural basis of kynurenine 3-monooxygenase inhibition. *Nature* **496**, 382–385 (2013).

39. Holm, L. & Rosenstrom, P. Dali server: conservation mapping in 3D. *Nucleic Acids Res.* **38**, W545–W549 (2010).

40. Eswaramoorthy, S., Bonanno, J. B., Burley, S. K. & Swaminathan, S. Mechanism of action of a flavin-containing monooxygenase. *Proc. Natl Acad. Sci. U. S. A.* **103**, 9832–9837 (2006).

41. Teichmann, M., Dumay-Odelot, H. & Fribourg, S. Structural and functional aspects of winged-helix domains at the core of transcription initiation complexes. *Transcription* **3**, 2–7 (2012).

42. Pierce, B. G. et al. ZDOCK server: interactive docking prediction of protein-protein complexes and symmetric multimers. *Bioinformatics* **30**, 1771–1773 (2014).

43. Waterhouse, A. et al. SWISS-MODEL: homology modelling of protein structures and complexes. *Nucleic Acids Res*. **46**, W296–W303 (2018).

44. Grove, T. L. et al. Structural insights into thioether bond formation in the biosynthesis of sactipeptides. *J. Am. Chem. Soc*. **139**,11734–11744 (2017).

45. Greule, A., Stok, J. E., De Voss, J. J. & Cryle, M. J. Unrivalled diversity: the many roles and reactions of bacterial cytochromes P450 in secondary metabolism. *Nat. Prod. Rep*. **35**, 757–791 (2018).

46. Takahashi, S. et al. Kinetic and molecular analysis of 5-epiaristolochene 1,3-dihydroxylase, a cytochrome P450 enzyme catalyzing successive hydroxylations of sesquiterpenes. *J. Biol. Chem*. **280**, 3686–3696 (2005).

47. Pohle, S. et al. Biosynthetic gene cluster of the non-ribosomally synthesized cyclodepsipeptide skyllamycin: deciphering unprecedented ways of unusual hydroxylation reactions. *J. Am. Chem. Soc*. **133**, 6194–6205 (2011).

48. Chang, C. Y. et al. Biosynthesis of streptolidine involved two unexpected intermediates produced by a dihydroxylase and a cyclase through unusual mechanisms. *Angew. Chem. Int. Ed. Engl*. **53**, 1943–1948 (2014).

49. Agarwal, V. et al. Biosynthesis of polybrominated aromatic organic compounds by marine bacteria. *Nat. Chem. Biol*. **10**, 640–647 (2014).

50. Huijbers, M. M. et al. Flavin dependent monooxygenases. *Arch. Biochem. Biophys*. **544**, 2–17 (2014).

51. Visitsatthawong, S., Chenprakhon, P., Chaiyen, P. & Surawatanawong, P. Mechanism of oxygen activation in a flavin-dependent monooxygenase: a nearly

barrierless formation of C4a-hydroperoxyflavin via proton-coupled electron transfer. *J. Am. Chem. Soc.* **137**, 9363–9374 (2015).

52. Wang, Y. et al. MauG-dependent in vitro biosynthesis of tryptophan tryptophylquinone in methylamine dehydrogenase. *J. Am. Chem. Soc.* **127**, 8258–8259 (2005).

53. Shin, S. & Davidson, V. L. MauG, a diheme enzyme that catalyzes tryptophan tryptophylquinone biosynthesis by remote catalysis. *Arch. Biochem. Biophys.* **544**, 112–118 (2014).

54. McIntire, W. S., Wemmer, D. E., Chistoserdov, A. & Lidstrom, M. E. A new cofactor in a prokaryotic enzyme: tryptophan tryptophylquinone as the redox prosthetic group in methylamine dehydrogenase. *Science* **252**, 817–824 (1991).

55. Chacón-Verdú, M. D. et al. LodB is required for the recombinant synthesis of the quinoprotein L-lysine-□-oxidase from *Marinomonas mediterranea*. *Appl. Microbiol. Biotechnol.* **98**, 2981–2989 (2014).

56. Chacón-Verdú, M.D. et al. Characterization of recombinant biosynthetic precursors of the cysteine tryptophylquinone cofactors of L-lysine-epsilon-oxidase and glycine oxidase from *Marinomonas mediterranea*. *Biochim. Biophys. Acta*. **1854**, 1123–1131 (2015).

57. Sehanobish, E. et al. Interaction of GoxA with its modifying enzyme and its subunit assembly are dependent on the extent of cysteine tryptophylquinone biosynthesis. *Biochemistry* **55**, 2305–2308 (2016).

58. Mamounis, K. J., Ma, Z., Sánchez-Amat, A. & Davidson, V. L. Characterization of PlGoxB, a flavoprotein required for cysteine tryptophylquinone biosynthesis in

glycine oxidase from *Pseudoalteromonas luteoviolacea*. *Arch. Biochem. Biophys.* **74**, 108–110 (2019).

59. Okazaki, S. et al. X-ray crystallographic evidence for the presence of the cysteine tryptophylquinone cofactor in L-lysine ε-oxidase from *Marinomonas mediterranea*. *J. Biochem.* **154**, 233–236 (2013).

60. Andreo-Vidal, A. et al. Structure and enzymatic properties of an unusual cysteine tryptophylquinone-dependent glycine oxidase from *Pseudoalteromonas luteoviolacea*. *Biochemistry* **57**, 1155–1165 (2018).

61. Williamson, H. R. et al. Roles of copper and a conserved aspartic acid in the autocatalytic hydroxylation of a specific tryptophan residue during cysteine tryptophylquinone biogenesis. *Biochemistry* **56**, 997–1004 (2017).

62. Sehanobish, E., Williamson, H. R. & Davidson, V. L. Roles of conserved residues of the glycine oxidase GoxA in controlling activity, cooperativity, subunit composition, and cysteine tryptophylquinone biosynthesis. *J. Biol. Chem.* **291**, 23199–23207 (2016).

63. Jones, L. H. et al. Active site aspartate residues are critical for tryptophan tryptophylquinone biogenesis in methylamine dehydrogenase. *J. Biol. Chem.* **280**, 17392–17396 (2005).

64. Arnison, P. G. et al. Ribosomally synthesized and post-translationally modified peptide natural products: overview and recommendations for a universal nomenclature. *Nat. Prod. Rep.* **30**, 108–160 (2013).

Chapter 3

Biochemical and structural analysis of serine proteinase involved in biosynthesis of active-site subunit of quinohemoprotein amine dehydrogenase

3.1. Introduction

As described in Chapter 1, previous studies of my group have demonstrated that QhpD of *Pa. denitrificans* plays an essential role in the posttranslational processing of the QhpC, by participating in intrapeptidyl thioether crosslink formation via an [Fe-S] cluster- and AdoMet-dependent mechanism. Further, in the cytoplasmic nascent form, the QhpC has a 28-residue N-terminal leader peptide that is necessary for the production of active QHNDH but must be removed during the subsequent maturation process. This leader peptide is atypical as a signal peptide for the periplasmic translocation of the QhpC and instead seems to participate in the cytoplasmic processing of the QhpC. In addition, it was revealed that the dihydroxylation reaction of the Trp residue required for CTQ formation is catalyzed by QhpG in the QhpCDG complex. The interaction of QhpC with the enzymes involved in these two post-translational modifications also requires interaction with the leader peptide.

The preceding study has elucidated the role of the subtilisin-like serine protease (belonging to the subfamily S8A) QhpE encoded as the fifth ORF of *n*-butylamine utilizing operon in QHNDH biosynthesis of *Pa. denitrificans*[1-2]. Destruction of *qhpE* inhibited the growth of bacterial cells in *n*-butylamine-containing medium, producing

no active QHNDH. In the depleted mutant strain, QhpC was accumulated in cytoplasm, in which the leader peptide was not removed and CTQ was not generated. A catalytic triad variant of QhpE expressed in *E. coli* was unable to cleave a synthetic peptide that substitutes for the subunit leader peptide. Interestingly the cleaved leader peptide remained bound to QhpE, probably as an acyl enzyme intermediate that is covalently connected to the Ser residue of the active site. These results indicate that QhpE is essential for QHNDH biosynthesis and functions as a processing protease that cleaves the leader peptide in a nearly disposable manner. However, the reactivity of QhpE to QhpC in the ternary complex, QhpCDG, is unknown. In Chapter 2, it was demonstrated that formation of the ternary complex is essential to undergo efficient and successive Cys–Asp/Glu crosslinking and Trp-dihydroxylation reactions. In addition, it is necessary to elucidate how the multi-step QhpC biosynthesis reaction by such multiple modifying enzymes is regulated in the ternary complex.

QhpE from *Ps. putida* encodes a 22.5 kDa subtilisin-like protein and is comprised of 221 residues without a preprosequence. The Asp/His/Ser catalytic triads of serine proteinases are completely conserved as Asp11, His47, and Ser179 in QhpE. Biochemical and structural analyzes were performed to elucidate the role of QhpE in *Ps. putida*. Chapter 3 reports the unique properties of the bacterial processing protease and the X-ray crystal structure of QhpE.

Recently, various cyclic peptides are known to have unique physiological activities[3]. Natural or artificial cyclic peptides are applied to develop drugs. The posttranslational modification systems of QhpC generates four thioether crosslinks including three Cys-Asp/Glu and Cys-Trp (CTQ). Each crosslink structure has a 6-11-residues loop and is

regarded as a cyclic peptide. The preceding study of our laboratory[8] showed that short version of QhpC from *Pa. denitrificans* (sQhpC) that contains the leader peptide, single crosslink region (Cys7-Glu16), and C-terminal flanking region. It was demonstrated that the loop sequence can be genetically changed on a sQhpC plasmid construct and that the thioether crosslink within various sequences can be formed by QhpD. To evaluate the bioactivity of the cyclic region of sQhpC, the corresponding region should be cut out from the sQhpC by proteases. Chapter 3 showed that QhpE is available to remove the leader peptide from *Ps. putida* sQhpC. In addition, the biological activity of cyclic peptides containing a poly Ala loop is examined using animal cells.

3.2. Materials and methods

3.2.1. Plasmid construction

An expression plasmid for QhpE from *Ps. putida* IFO 15366 (NBRC 15366) was constructed using an *E. coli* expression vector pET-15b, mostly according to standard molecular genetic protocols. The coding region of the protein was amplified by PCR using a sense primer containing an *Nde*I site at the 5′-terminus and an antisense primer containing a *BamH*I or *Nhe*I site at the 3′-terminus, with *Ps. putida* genome DNA as template. In addition, a hexa-His (H_6)-tag and Tobacco Etch virus protease (TEV protease) digestion site were appended on the N-terminus of QhpE. Site-specific mutants of QhpE were obtained by the PCR-based site-directed mutagenesis. PCR primers used in construction of the plasmids as well as those for site-specific mutants of QhpE are summarized in (Table 1). Absence of PCR-derived errors, if any, were confirmed by sequencing the entire coding regions. The expression plasmids for QhpD,

QhpC and QhpG from *Ps. putida* IFO 15366 (pET-H_6-QhpD, pET-H_6-QhpC, pET-H_6-QhpG) were described in the previous Chapter.

Expression plasmids for mutant sQhpC, in which the connected loops between Cys and Asp/Glu residues comprise of poly Ala, were constructed with the sQhpC (from *Ps. putida*) expression plasmid (pBBR-11a-sQhpC-TEV-St_2) according to standard molecular genetic protocols as follows. The mutant plasmids were constructed in which the crosslinked loop was replaced by Ala residues of various lengths (sequence of Ala 4 residues in the crosslinked loop: (4 Ala residues: (Ala)×4, 5 Ala residues: (Ala)×5, 6 Ala residues: (Ala)×6). The region encoding sQhpC mutant ((Ala)×4, (Ala)×5, or (Ala)×6)) flanked by *Nde* I and *Nhe* I cleavage sites was synthesized by forward and reverse primers. At this time, two separate regions were designed, one to be complementary and the other to be modified (Table 1). The primers were mixed with KOD-plus (TOYOBO) and denatured at 94°C for 2 min, followed by annealing at 55°C for 30 sec and elongation at 68°C for 1 min. The elongated products were separated by 2% agarose gel electrophoresis, and gel extraction (Fast Gene Gel/PCR Extraction Kit, NIPPON genetics) was performed. The DNA fragments obtained by the PCR amplification were digested with *Nde*I/*Sal*I-HF (NEW ENGLAND BioLabs) and inserted into the pBBR-11a-TEV-St_2 vector. The plasmids (pBBR-11a-sQhpC-(Ala)×4-TEV-st_2, pBBR-11a-sQhpC-(Ala)×5-TEV-st_2, and pBBR-11a-sQhpC-(Ala)×6-TEV-st_2) were then prepared from the transformants of *E. coli* strain DH5α, and the presence of the introduced sequence and the absence of mutations in other parts of the plasmid were confirmed by DNA sequencing.

3.2.2. Expression and purification of QhpE

To prepare a recombinant QhpE, *E. coli* C41 (DE3) cells carrying the expression plasmid for QhpE were grown at 37 °C for 3 hr by reciprocal shaking at 160 rpm and subsequently at 25 °C for 20 hr by shaking at 180 rpm in Overnight Express™ Instant TB Medium (Novagen) supplemented with 100 μg/ml ampicillin. The cells were harvested by centrifugation at 5,000 × *g* for 10 min and stored at –80 °C until use. For purification of QhpE, frozen cells were resuspended in 20 mM Tris-HCl (pH 8.0), 0.5 M NaCl (buffer A) containing 50 mM imidazole. After ultrasonic disruption and of the cells, the cell extract was collected by centrifugation at 20,000 × *g* for 60 min, and was applied to a HisTrap FF crude column (5 ml, GE Healthcare) preequilibrated with buffer A. After washing the column with 20 column volumes of buffer A containing 50 mM imidazole, QhpE was eluted with a linear gradient of 50–150 mM imidazole. Fractions containing His_6-tagged QhpE were pooled, and dialyzed against buffer C. The obtained sample was further applied to HisTrap HP column (5 ml, GE Healthcare) preequilibrated with buffer A. After sufficiently washing the column with 20 column volumes of buffer A, QhpE was eluted with a linear gradient of 5–100 mM imidazole in buffer C. Fractions containing QhpE were dialyzed against buffer A. To remove N-terminal His_6-tag of QhpE, the dialyzed protein was digested with His_6-tagged TEV protease (weight ratio 1/100 amount) for 24 hr at 4 °C. TEV protease and released H_6-tag were removed by repeating HisTrap purification, and non-tagged QhpE was collected from fractions containing 40–50 mM imidazole because of its weak affinity toward the column. Thus, the obtained protein was dialyzed against buffer A, concentrated to 40 mg/ml, and stored at –80 °C until use.

3.2.3. Expression and purification of crosslinked QhpC in the QhpCDG ternary complex

The QhpCD complex and QhpG were prepared as described in Chapter 2. QhpD in the as-purified complex was reconstituted essentially according to the published method[8]. To conduct the crosslink reaction, the reconstituted QhpCD complex (~180 μM) in 25 mM Tris-HCl, pH 8.0, containing 150 mM NaCl and 10% (w/v) glycerol was incubated with 1 mM DT and 1 mM SAM. For crosslinking with QhpD, QhpG (~180 μM) was added to the reaction mixture. The crosslinked QhpC in the ternary complex was used for the QhpE reaction analysis (see below). Triply crosslinked QhpC was prepared as described previously using the QhpCDG complex. After crosslink reaction, QhpD was removed by heat denaturation (70 ºC and 20 min) and centrifugation.

3.2.4. Preparation of cyclic peptides with QhpD

The QhpD/sQhpC complex was expressed in *E. coli* C41(DE3) cells carrying the expression plasmids pET-His_6-QhpD (*Ps. putida*) and one of the sQhpC expression plasmids (pBBR-11a-sQhpC-(Ala)×4-TEV-st_2, pBBR-11a-sQhpC-(Ala)×5-TEV-st_2, or pBBR-11a-sQhpC-(Ala)×6-TEV-st_2) and purified as described above. After chemical reconstitution of the [Fe-S] cluster of QhpD, the QhpD/sQhpC complex was anaerobically incubated with 1 mM sodium dithionite and 1 mM SAM for ~15 h at ~20 °C for intrapeptidyl thioether bond formation. Crosslinked sQhpC was prepared by heat denaturing the QhpD protein at 60 °C for 20 min and removing QhpD by centrifugation. 100 μM sQhpC including poly Ala isolated as described above was incubated with 100 μM QhpE and 100 μM TEV protease in a buffer containing 25 mM Tris-HCl, pH 8.0, and 150 mM NaCl for ~15 h at room temperature. The products were desalted using a C_{18}ZipTip pipette tip and then analyzed by MALDI-TOF mass spectrometry using 2,5-dihydroxybenzoic acid dissolved in 90% acetonitrile and 0.01%

trifluoroacetic acid. The cyclic peptides were isolated by heat denaturing QhpE and TEV protease at 60°C for 20 min and centrifugation.

3.2.5. Bio-layer interferometry analysis

Binding affinity of QhpE-H47A and toward triply crosslinked and linear QhpC was measured by bio-layer interferometry using a BLItz system (Molecular Devices, LLC., CA) in 10 mM TBS, pH 7.4, 0.1% (w/v) BSA, and 0.02% (v/v) Tween 20 (kinetics buffer) at 25 °C. Streptavidin-coated biosensors (SA sensors) were hydrolyzed for 30 min in 250 μL kinetics buffer. A baseline was measured for the sensor in kinetics buffer for 30 s prior to the immobilization step. 4 μL of 0.5 μM crosslinked or linear QhpC tagged with St_2 was immobilized to SA biosensors for 4 min, and the baseline was measured for the sensors in kinetics buffer for 6.5 min. An association step was monitored by applying 1.5 - 12.5 μM QhpE-H47A, analyte solution, to the crosslinked or linear QhpC immobilized to SA biosensors for 20 sec. A dissociation step was monitored by running 250 μL kinetics buffer for 20 sec. To eliminate errors from non-specific binding of the analyte (QhpE) on the SA biosensor chips, the reference data with the same concentrations of the analyte were also measured with a ligand-free sensor. The obtained data sets were analyzed using global analysis mode, in which corrections for the association and dissociation steps were applied, by BLItz Pro1.2 software (Molecular Devices, LLC., CA) to determine a dissociation constant K_D.

3.2.6. Mass spectrometry analysis of QhpE for cleavage activity with QhpC

QhpE was assayed with the triply crosslinked premature QhpC, in which CTQ was not generated and the leader peptide was not removed, as a substrate. For the isolated

QhpC, 50 μM QhpE and 50 μM crosslinked QhpC (1: 1 in molar ratio) were mixed and further incubated at room temperature for overnight. Thus, the obtained reactant were desalted with a C_{18} ZipTip pipette tip, and subjected to MALDI-TOF MS analysis using sinapic acid dissolved in 90% acetonitrile and 0.01% TFA as matrix (see the next section). For the crosslinked QhpC complexed with QhpD and QhpG, after completion of the crosslink reaction, 50 μM QhpE were added to the crosslink reaction mixture (50 μM QhpCDEG mixture in buffer A) and incubated at room temperature for overnight. After the cleavage step, the same sample preparation protocol for the mass analysis was used as described above.

3.2.7. MALDI-TOF mass analysis

The mixture was acidified with 2% (v/v) formic acid, desalted with a C_{18} ZipTip pipette tip (Millipore) and eluted with 10 μl of 50% (v/v) acetonitrile in 0.1% (v/v) TFA. The eluate (1 μl) was subjected to mass analysis using a Bruker Ultraflex III MALDI-TOF mass spectrometer and 1 mg/ml sinapic acid (Bruker) dissolved in 90% (v/v) acetonitrile, containing 0.1% (v/v) TFA, as a matrix, which was co-crystallized with the protein by the drying-droplet method. Before every MS analysis, mass calibration was done using Protein Calibration Standard I (Bruker).

3.2.8. HPLC assay of QhpE protease with QhpC

The crosslinked or linear QhpC (3.25 mM) was incubated with the purified QhpE protein (0.065 and 3.25 mM) at 30 °C in 20 mM HEPES (pH 7.0) containing 5 mM DTT. After 15 h, a 100 μl aliquot of the reaction mixture was applied to the HPLC system equipped with a C4 reverse phase column (5C18-AR-II, 4.6 mm x 150 mm,

Nacalai Tesque). Separation was performed using a 35 min linear gradient of 0–80% CH_3CN containing 0.1% TFA at a flow rate of 0.5 ml/min, monitored with absorbance at 215 nm.

3.2.9. Evaluation of cleavage activity of QhpE using peptide substrates

Reactivity of QhpE was measured with a synthetic substrate peptide (6-FAM)-EEVMAMS-NH_2 (N-Flc substrate), in which N-terminal was labeled with 6-Carboxyfluorecein (6-FAM) and the C-terminus was treated with amide ($CONH_2$), as follows. The N-Flc substrate (0.2 μM) was incubated with QhpE (0.2 μM) for 15 h at 24 °C. A 5 μl aliquot of the reaction mixture containing 200 μg of the QhpE was subjected to SDS-PAGE. The SDS-PAGE was performed on Any kD™ Mini-PROTEAN® TGX™ Precast Protein Gels (Biorad) at 40 mA, 35 min in the presence of a buffer of 25 mM Tris, 192 mM Glycine, 0.1% (w/v) SDS, pH8.3. The gels were measured by excitation with a blue light at 472 nm and exposure time 30 sec (LuminoGraphII, ATTO) (Fig. 3a). After the fluorescence measurement, the gels were stained with Coomassie Brilliant Blue (CBB)

3.2.10. Crystallization and data collection

The buffer of stocked QhpE was exchanged with a PD-10 column (GE Healthcare) to 10 mM Tris-HCl, pH 8.0, 0.1 M NaCl, and 0.1 mM DTT and concentrated. After filtration with 0.22 μm of centrifugal filter (Millipore), 12.5 mg/ml QhpE was used for crystallization screening. The crystallization conditions were screened with commercially available screening kits by the sitting-drop vapor diffusion method. After optimization, the crystals used for data collection were obtained by the sitting-drop

method at 4 ºC in the reservoir solution consisting of 100 mM Bicine-HCl (pH 9.0), 18% (v/v) 2-propanol, 36% (v/v) Polyethylene glycol 1500. Small plate shape of crystals (ca. 0.1-0.2 mm size) appeared within 1 months. The crystals were mounted on thin nylon loops (ϕ, 0.1–0.2 mm) and frozen by flash cooling at 100 K in a cold N_2 gas stream or in liquid nitrogen. Diffraction data sets were collected with a synchrotron X-radiation at SPring-8 (Hyogo, Japan) at 100 K in the beam-line station BL44XU using a CCD detector EIGER X 16M (Dectris) at λ = 0.900 Å. The collected data were processed, merged, and scaled using the program XDS[4]. The space group was *P*1 with the unit cell dimensions of *a* = 35.4 Å, *b* = 50.6 Å, and *c* = 53.2 Å, α = 88.1°, *β* = 85.9°, γ = 70.2° in the crystal. The cell content analysis suggested that two molecules are in the asymmetric unit. The details and statistics of the data collection are summarized in Table 2.

3.2.11. Structure determination and refinement

Phase determination was performed using molecular replacement with Phaser. The remaining model was built manually into the map using the program Coot[5]. Refinement using the programs PHENIX[6], and manual model rebuilding cycles produced the final model. The refinement statistics are summarized in Table 2.

3.2.12. Evaluation of cytotoxic activity for cyclic peptides

Cytotoxic activity was evaluated for the cyclic peptides (CAAAAE, CAAAAAE, CAAAAAAE; underlined residues are crosslinked) that were prepared with the sQhpC constructs. A459 cells were cultured in Dulvecco's modified Eagl's medium (DMEM, Nacalai) supplemented with 10% (v/v) FBS (fetal bovine serum) at 37 °C in a 5% (v/v)

FBS under 5% (v/v) CO_2 humidified atmosphere. A549 (5 x 10^3 cells/well) were subcultured in a 96-well plate (Thermoficher scientific), on the next day, added 50 mM peptide. After incubated at 37°C in a 5% (v/v) CO_2 humidified atmosphere for 3 days, cell viability was measured using a WST-8 assay kit (Dojindo) according to manufactural protocols.

3.2.13. Construction of a docking model of QhpE/QhpC

The crystal structure of *Ps. putida* QHNDH (PDB entry ID: 1JMX) with γ-subunits was used to construct a docking model of the QhpCE complex using the ZDOCK software server[7] with the monomeric structure of QhpE (chain A) as the acceptor. The model structure of QhpC with the leader peptide used in the model construction consisted of the α-helix used in previous study[8].

3.3. Results

3.3.1. Purification of QhpE, and QhpE substrates

QhpE was cloned from *Ps. putida* IFO 15366 (NBRC 15366). N-terminal His_6-tagged QhpE was expressed in recombinant *E. coli* cells and purified by Ni affinity chromatography. The N-terminal His6 tag of QhpE was removed using TEV protease. Purity of the purified protein was checked by SDS-PAGE, and QhpE contains almost no impurities. Similarly, we also purified Ala mutants of residues His47, and Asp179 (respectively H47A and D179A), which are predicted to be a highly conserved catalytic triad with other serine proteases. Crosslinked QhpC was expressed as a stable QhpCD binary complex in *E. coli* cells for analysis of the QhpE reaction in vitro, as described in Chapter 2.

3.3.2. Determination of catalytic activity of QhpE

To investigate the reactivity of the serine protease QhpE to QhpC, crosslinked or linear QhpC reacted with QhpE at 25 °C overnight, and then the products were subjected to MALDI-TOF mass spectroscopic analysis. Mass peaks (*m/z*: 3336.36 and 11603.33) corresponding to the leader peptide (Met-28-Met1 calculated mass: 3336.93) and QhpC (Ser2-Lys79, calculated mass: 11608.51) without the leader peptide were observed in both cases of crosslinked or linear QhpC (Fig. 2a). It was shown that QhpE cleaves the leader peptide of QhpC with or without the interpeptidyl crosslinks. There were no digested mass peak in the Ala-substituted mutants (H47A and D179A) of the catalytic 3 residues.

Previous studies have shown that crosslink formation and hydroxylation of the CTQ precursor Trp43 residue occurs in the QhpCDG ternary complex. Therefore, I examined whether QhpE is also active for cleaving the leader peptide of QhpC in the QhpCDG ternary complex. Most of them were cleaved in an overnight reaction mixture of the crosslinked QhpC in the ternary complex and QhpE (Fig. 2b). In contrast, no cleavage was observed in the linear QhpC in the ternary complex, and a mass peak of QhpC, in which the leader peptide remained undigested, was observed (Fig. 2b). In summary, QhpE was identified as a serine protease that can specifically cleave the leader peptide of either crosslinked or linear QhpC. It was also found that QhpE can cleave only crosslinked QhpC in the QhpCDG complex.

3.3.3. The time course of the leader peptide digestion from QhpC

To investigate the reactivity of QhpE with QhpC in more detail, time course of digestion of the leader peptide was determined by reversed phase HPLC analysis on a C18 reverse phase column (Fig. 3a). When the linear QhpC was reacted with QhpE in a molar ratio of 1:1, it takes 450 min that most of the leader peptides of QhpC were cleaved (Fig. 3b). For the crosslinked QhpC, most of the leader peptides were cleaved at only 10 min when the molar ratio of QhpE was 1: 1. To more quantitatively evaluate the reactivity of QhpE to the crosslinked and linear QhpC, the 1/50 molar amount of QhpE was added to QhpC. As a result, the kinetic data showed that the initial reaction rates of QhpE toward the linear and crosslinked QhpC were 7.5 and 150 μM/min, respectively, indicating that the leader peptides of the crosslinked QhpC was cleaved by about 20-fold faster than that of the linear QhpC. The initial QhpC concentration 3.25 mM is excess in comparison with K_D values determined with BLItz analyses (see below). Under the conditions, the binding site of QhpE is occupied with QhpC, indicating that the above reaction rates are approximate values of the maximum velocities. These results are consistent with the MALDI-TOF mass experiments, where the crosslinked QhpC was found to cleave more quickly.

3.3.4. Analysis of QhpE-QhpC interactions

To evaluate the difference of the reactivity of QhpE toward linear or crosslinked, the interaction between QhpE and linear or crosslinked QhpC was quantitatively analyzed by bio-layer interferometry (BLI) assay; QhpC was immobilized on the surface of the SA biosensor and the binding of QhpE was measured (Fig. 2b). The inactive mutants of QhpE (H47A, D179A), in which one of the catalytic triad residues are mutated to Ala, were used in the experiments to prevent the leader peptide cleavage of QhpC. Estimated K_D

values from global analysis of the dissociation curves (Fig. 2b) showed that the affinity of crosslinked QhpC was 2.5-fold higher than that of linear QhpC. The association rate constant (k_a) and dissociation rate constant (k_d) were compared, and k_a were no significant difference between the crosslinked ($(3.1 \pm 0.06) \times 10^4$) and linear ($(1.2 \pm 0.28) \times 10^4$) QhpC. However, dissociation was slower in the crosslinked QhpC as shown in k_d values ($(9.0 \pm 0.87) \times 10^{-1}$) than in the liner QhpC ($(6.0 \pm 6.0) \times 10^2$). Similar results were also obtained in the native-PAGE mobility shift assay (Fig. 2a). The interaction of linear QhpC with QhpE formed a binary complex of QhpCE (Fig. 2a). In contrast, there was no binary complex band between QhpE and crosslinked QhpC. This result was thought to be due to the rapid cleavage of the leader peptide of QhpC by QhpE. Similarly, QhpCDE complex band were not observed for the QhpE and crosslinked QhpC in the binary complex. Therefore, to prevent leader peptide cleavage by QhpE, I performed the same experiment using the inactive mutant QhpE-S179A. The formation of binary complex was more pronounced for the crosslinked QhpC (lanes 7-11) than for the linear QhpC (lanes 1-5). In the QhpCD binary complex, the formation of ternary complexes was also more pronounced in the crosslinked QhpC (lanes 8-12). These results indicate that QhpE binds preferentially to the QhpCD complex via crosslinked QhpC than the linear one without thioether bonds. In summary, it is conclude that QhpE is a substrate for crosslinked QhpC and recognizes the crosslinked structure of QhpC.

3.3.5. Cleavage of synthetic peptides

In a previous study of *Pa. denitrificans* QhpE[2], the experiments using synthetic peptides as a substrate showed that they were not hydrolyzed and remained bound to Ser179 as the acyl intermediate in the active center. To investigate whether *Ps. putida*

QhpE forms the similar acyl intermediate with a substrate synthetic peptide, N-Flc substrate was used for the QhpE assay. The reaction products were subjected to SDS-PAGE (Fig. 3). After the fluorescence measurement of the gel, the gels were stained with Coomassie Brilliant Blue (CBB) (Fig. 3b). As a result, fluorescent bands were observed in *Ps. putida* QhpE and *Pa. denitrificans* QhpE. Quantification of the bands showed that the fluorescence band in *Ps. putida* QhpE was only about 4.5% compared to *Pa. denitrificans* QhpE. Because the fluorescence bands correspond to the acyl intermediate in which a digested N-terminal region, (6-FAM)-EEVMAM, is covalently connected to the side chain of Ser179 as shown in previous work, the formation of the intermediate in *Ps. putida* QhpE was marginal in comparison with that in *Pa. denitrificans* QhpE. In *Pa. denitirificans* QhpE, it was found that the covalent intermediate of QhpE with the cleaved peptide was stable under weakly acidic to neutral pH conditions[2]. The amount of the intermediate decreased with increasing pH. In *Ps. putida* QhpE, the intermediate formation was examined under various pH conditions using the crosslinked QhpC. The mass peak before the QhpE reaction (m/z, 2820.52) matched well with the calculated molecular weight (m/z, 2821.49) of the peptide fragment containing the active center Ser179 residue (Fig. 4c, top panel). When the leader peptide of QhpC binds to this peptide fragment, the acyl-enzyme intermediate is cleaved by MALDI-induced cleavage, resulting in a decrease in molecular weight (calculated mass, 2803.49) during mass spectrometry. All the mass peaks after the QhpE reaction under various pH conditions were consistent with the mass peaks before the QhpE reaction, and the mass peaks indicating the cleaved acylase intermediates were not observed (Fig. 4C). Although *Ps. putida* QhpE is homologous to *Pa*

denitrificans QhpE (sequence identity 41.9 %) and catalyzes the same enzymatic reaction, this difference may be due to difference in bacterial species.

3.3.6. Crystal structure of QhpE

To shed light on the substrate recognition mechanism of QhpE, QhpE was crystallized as a needle-like crystal in 100 mM Bicine-HCl (pH 9.0), 18% (v/v) 2-propanol, 36% (v/v) polyethylene glycol 1500 and at 4 °C. The space group was *P*1 with the unit cell dimensions of a = 35.4 Å, b = 50.6 Å, and c = 53.2 Å, $\alpha = 88.1°$, $\beta = 85.9°$, $\gamma = 70.2°$ in the crystal. The X-ray crystal structure was determined at 2.0 Å resolution by molecular replacement. In the crystal, each asymmetric unit contained two monomers that are related by a non-crystallographic two-fold axis. The model was finally refined to R_{work} and R_{free} values of 16.6% and 21.1%, respectively. The overall structure of QhpE are composed of five α-helices and eight β-strands, forming a subtilisin-like α/β domains, as shown in Figure 5. QhpE is similar to other subtilisin-like serine proteases, such as Tk-subtilisin from *Thermococcus kodakarensis* (PDB entry ID, 3WIV; root mean squared deviation, 2.0 Å over 198 superposed residues; sequence identity, 23.1%; Z-score, 21.1)[8], Alkaline serine protease from *Pseudoalteromonas sp*. AS-11 (PDB entry ID, 1V6C; root mean squared deviation, 2.3 Å over 198 superposed residues; sequence identity, 24%; Z-score, 20.8)[9], subtilisin-like serine protease from *Fervidobacterium pennivorans* (PDB entry ID, 1R6V; root mean squared deviation, 2.4 Å over 198 superposed residues; sequence identity, 23%; Z-score, 20.3, in Dali server search23)[10] with a structure similar to that of QhpE. Sequence alignment of QhpE with other subtilases showed that the active site of QbpE, like all members of the subtilase family, consisted of three conserved residues, a catalytic triad of Asp11, His47, and Ser179 (Fig. 5b). Asp11 was located at

β1 on the C-terminal side. His47 and Ser179 were located at α3 and α4 on the C-terminal side, respectively; the O-δ1 atom of Ser179 is 2.7 Å from the His47 N-δ1 atom, and the His47 N-δ1 atom is 2.4 Å from the O-δ2 atom of Asp11 (Fig. 5b). Hydrogen bonds were formed between the three residues that probably contribute to the stabilization of the active site.

3.3.7. QhpE and TEV protease-catalyzed cleavage of leader peptide and St_2-Tag

My group were able to form crosslinks of sQhpC containing various peptide sequences (Kozakai, thesis for master degree). I constructed expression plasmids of mutant sQhpC (pBBR-11a-sQhpC-(Ala)×4-TEV-st_2, pBBR-11a-sQhpC-(Ala)×5-TEV-st_2, and pBBR-11a-sQhpC-(Ala)×6-TEV-st_2), in which the linkage loop between Cys residues and Asp/Glu residues consists of polyAla (Ala×4, Ala×5, Ala×6) of various lengths. On the C-terminal side, a TEV protease cleavage sequence was introduced between sQhpC and the gene encoding the St_2-tag (Fig. 9a). The mass peak of sQhpC (*m/z*, 9555.28) was in good agreement with the calculated molecular weight (*m/z*, 9564.48) (Fig. 9b). The sQhpC treated with QhpE showed a peak of reduced mass (*m/z,* 6246.81) and a mass peak on the low molecular side (*m/z,* 3335.41), which were assigned to the leader cleaved sQhpC (calculated mass, 6247.76) and peptide (calculated mass, 3336.93), respectively (Fig. 9b and c). When sQhpC was treated with TEV protease, two similar peaks (*m/z*, 6467.44, and 3116.54) were observed, which were assigned to the cleaved sQhpC (calculated mass, 6466.11) and the St_2-tag (calculated mass, 3116.38), respectively. In addition, sQhpC was treated with both QhpE and TEV protease. As a result, the mass peaks of leader peptide (*m/z*, 3337.56), st2 tag (*m/z*, 3118.55), and sQhpC (no leader peptide and st2 tag) (*m/z*, 3149.00) were

observed. These results indicate that QhpE and TEV protease can be used to isolate peptide fragments containing crosslinking sites in sQhpC with various sequences.

3.3.8. Evaluation of cytotoxicity of cyclic peptides with Ala loops of various lengths (Ala4, Ala5, Ala6)

The bioactivity of the cyclic peptides was measured using A549 cells. The cyclic peptides used for the measurements were sQhpC ((Ala)×4, (Ala)×5, and (Ala)×6) substituted with Ala residues of various lengths. These cyclic peptides substituted with Ala residues were expected to bind to metal ions and adopt an ionophore type structure (Kozakai, thesis for master degree). Therefore, Zn^{2+} and Fe^{2+}, which are predicted to have the lowest potential energy, were mixed with the peptides and added to the cells. The results showed that the cell viability of (Ala)×4 was 70% (Fig. 10). Compared to Mock, (Ala)×4 showed 30% cytotoxicity. However, the cytotoxicity was abolished by mixing with Zn^{2+}, and the cell viability was comparable to that of Mock. Interestingly, when Fe^{2+} and (Ala)×4 were added simultaneously, cell viability decreased by 40%. In contrast, (Ala)×5 and (Ala)×6) did not have a significant effect on cell viability under all conditions. These results suggest that (Ala)×4 disrupts the cell membrane due to its higher hydrophobicity and smaller molecule than (Ala)×5 and (Ala)×6. In addition, the cytotoxicity of (Ala)×4 was abolished by binding Zn^{2+}, which predicted that the binding of metal ions would result in the loss of invasiveness of the cell membrane.

3.4. Discussion

In a previous study[2], QhpE was expressed in the cytoplasmic fraction of *Pa. denitrificans* pd1222 cells cultured in medium containing n-butylamine. In *qhpE*

destruction cells, QhpC accumulated in the cytoplasm while retaining its N-terminal leader peptide; QhpE was thought to recognize the QhpC precursor and cleave the leader peptide after the formation of a thioether crosslinks by QhpD. To investigate the mechanism of the reaction in detail, I examined the reactivity of *Ps. putida* QhpE with the purified QhpC, and especially evaluate the difference of reactivity between the crosslinked or linear form. At the cellular level, only crosslinked QhpC was transported into the periplasm and its leader peptide was cleaved. To investigate this difference between in vitro and in vivo, the time course of leader peptide dissociation was analyzed by reversed-phase HPLC analysis on a C18 column. The results showed that the reaction rate to QhpE was significantly increased in the crosslinked QhpC compared to the linear QhpC. For the dissociation constant K_D value using BLItz, there was almost no significant difference between the crosslinked and linear QhpC, indicating that the thioether crosslinks of QhpC has little effect on the interaction with QhpE. However, when the maximum reaction rate was calculated based on the data obtained from HPLC, a large difference was observed between the crosslinked and linear QhpC. The reactivity of QhpE to crosslinked or linear QhpC was found to be largely related to the reaction rate. This suggests that the crosslinks structure influences the reaction rate. The in vivo results may be driven by this difference in reactivity.

In previous studies, analysis of QhpE isolated from *Pa. denitrificans* pd1222 cells has shown that the leader peptide binds to the active center Ser residue of QhpE. This result suggests that the leader peptide is likely to be an unstable acyltransferase intermediate that is bound to the active site Ser residue without being hydrolyzed after cleavage. Thus, it was concluded that QhpE from *Pa. denitrificans* functions as an almost disposable enzyme in the leader peptide cleavage process of QhpC. However, the results obtained

by the experiments performed in this study with *Ps. putida* QhpE showed that most of the leader peptidases were hydrolyzed (Fig 4c). To gain insight into this difference, a structural comparison was performed using a homology model of *Pa. denitrificans* QhpE. There was no significant difference in the presumed substrate pockets in and around the active center. However, it is found that *Pa. denitrificans* QhpE has a loop structure that is five residues longer than that of *Ps. putida* QhpE (Fig 6a). I constructed a model of the QhpCE complex and obtained a structure, in which QhpC binds to a highly conserved region of QhpE (Fig. 7). The above loop structure was also suggested to be involved in the binding of QhpC. Therefore, this loop is located at a close distance to the active center Ser179 and may be involved in the retention of the substrate by the enzyme. However, it was unable to predict how the crosslinked structure is recognized on the basis of the available structural information. In the future, more detailed substrate recognition mechanism should be investigated by crystallographic analysis of the QhpCE complex.

A recent study revealed that the hydroxylation of Trp residues in the formation of CTQ of QhpC is catalyzed by QhpG. I also found that QhpCDG forms a triple complex, in which thioether crosslink formation and hydroxylation of the CTQ precursor Trp residue proceed in the complex state. Therefore, the protease activity of QhpE in the QhpCDG complex was measured using mass spectrometry. The results showed that the leader peptide was cleaved for the crosslinked QhpC even in the QhpCDG complex. However, for the linear QhpC in the QhpCDG complex, the leader peptide remained intact even after overnight reaction. These results suggest that after two post-translational modifications proceed in the QhpCDG complex, the leader peptide of QhpC is cleaved and only QhpC is released for transport to the periplasm. The different reactivity of QhpE to QhpC may also regulate the cleavage of the newly translated QhpC leader peptide.

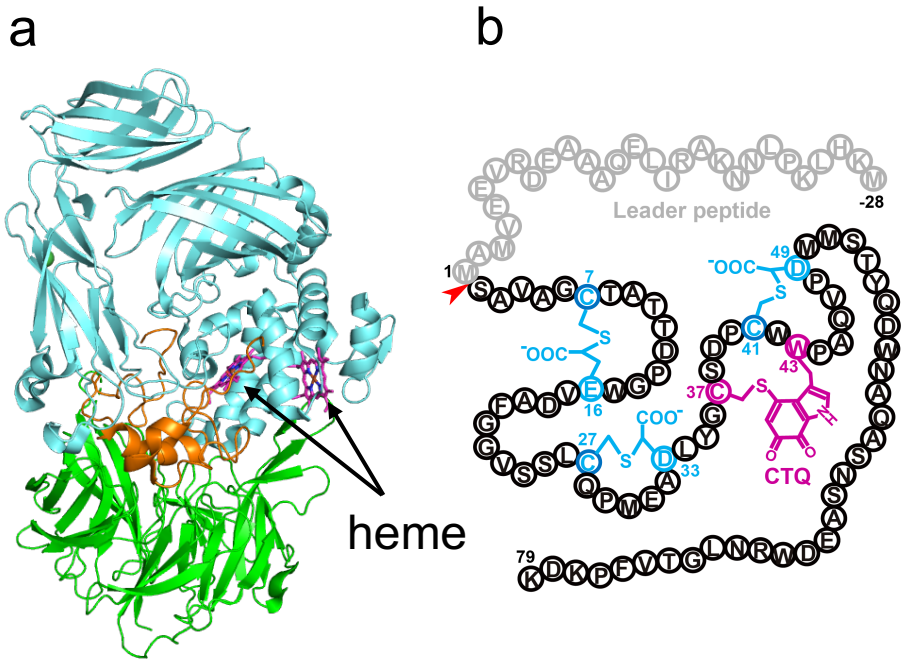

Fig. 1. Structure of QHNDH and schematic drawing of the γ-subunit. a, Cartoon model of QHNDH from *Ps. putida* (PDB code 1JMX). The α, β, and γ-subunits colored cyan, green, and orange, respectively. Two hemes and CTQ shown in green stick model. **b**, Schematic structure of γ-subunit polypeptide with a 28-residue leader peptide.

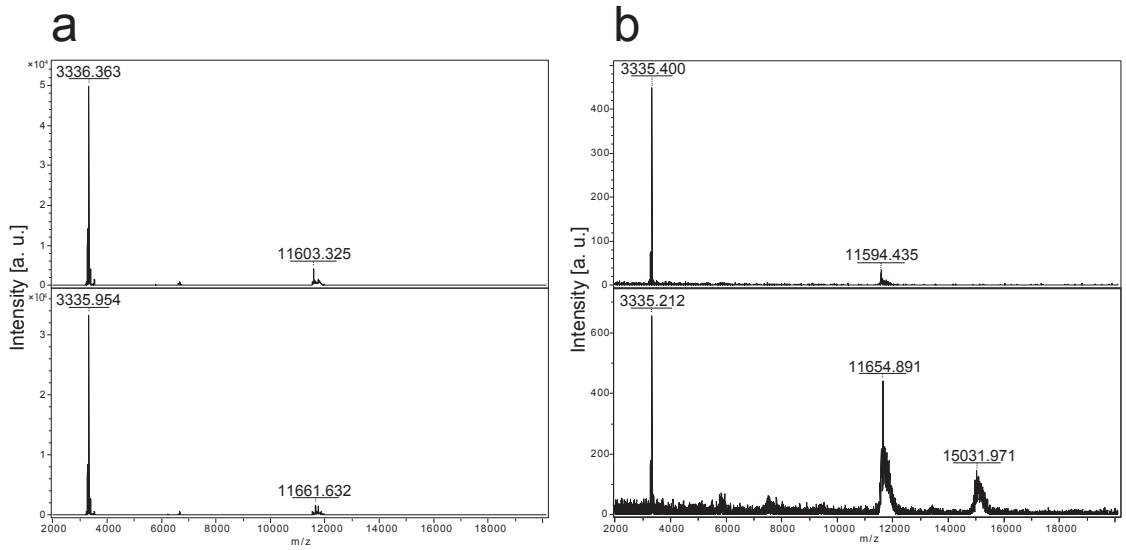

Fig. 2. MALDI-TOF MS analysis of QhpE-catalyzed products. a, MALDI-TOF mass spectrometric analysis of the QhpE reaction products with crosslinked (*top panel)* and linear *(bottom)* QhpC. **b**, MALDI-TOF mass spectrometric product analysis for the QhpG reaction products in the crosslinked (*top panel)* and liner *(bottom)* QhpC in the QhpD/QhpG ternary complexes.

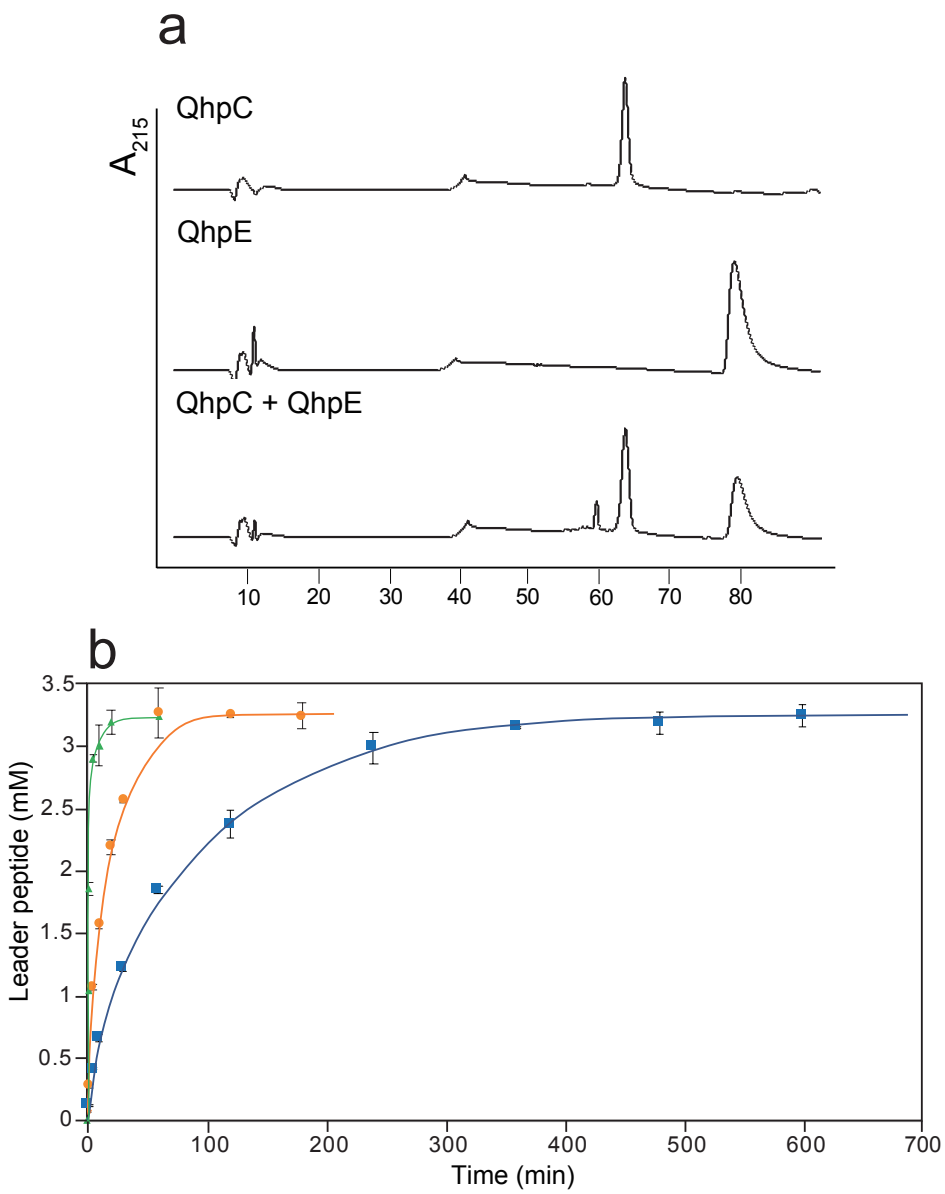

Fig. 3. HPLC analysis of the proteinase activity of QhpE. Purified QhpE (0.065 or 3.25 mM) was incubated with 3.25 mM crosslinked and liner QhpC for 0 - 10 h at 24°C. A 100 µl aliquot of the reaction mixture was analyzed by HPLC as described in the Experimental Procedures. Absorbance at 220 nm was monitored. **a**, HPLC assay of QhpC *(top)*, QhpE *(middle)*, and reaction products of QhpCE *(bottom)*. **b**, Time-course measurement of the leader peptide dissociation by reversed-phase HPLC analysis. The leader peptides were quantified and plotted when QhpE and crosslinked QhpC were

reacted at a molecular ratio of 1: 1 for 0 - 1 hour (green) and 1 : 0.5 for 0 – 3 hour (orange). QhpE and linear QhpC were reacted at a molecular ratio of 1: 1 for 0 - 10 hour (blue).

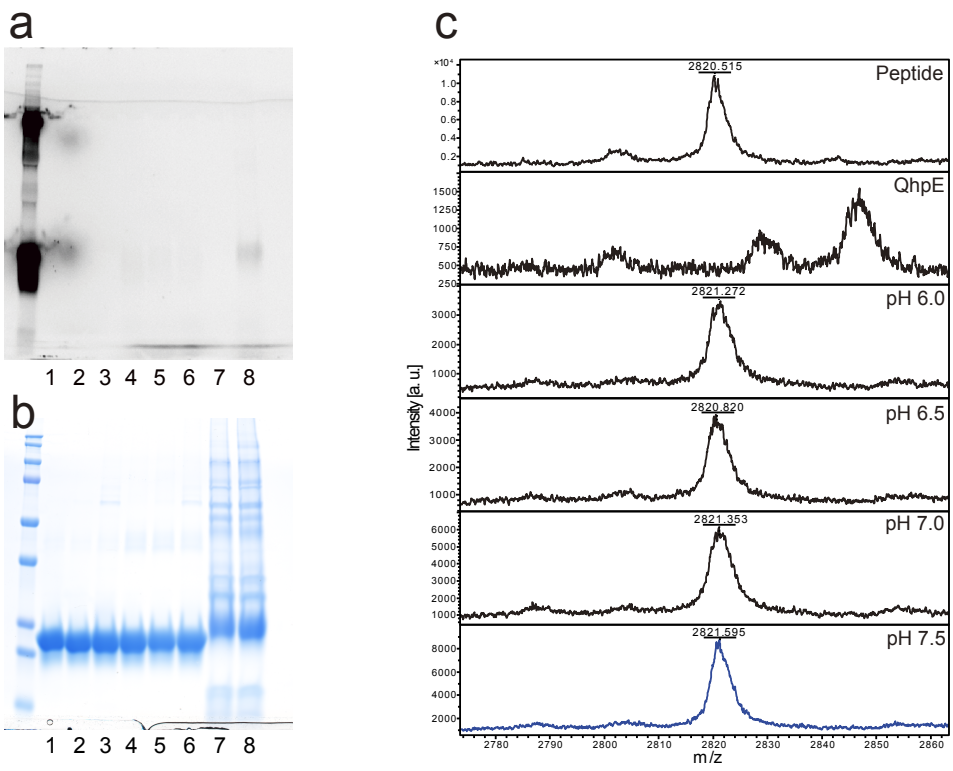

Fig. 4. Products analysis of QhpC and peptide bound to QhpE. 0.2 μM N-Flc substrate was incubated with 0.2 μM QhpE for 15 h at 24°C. A 5 μl aliquot of the reaction mixture containing 200 μg of the QhpE was subjected to SDS-PAGE (15% polyacrylamide gel) and analyzed by fluorescence scan (**a**) and Coomassie Brilliant Blue staining (**b**). **a** and **b**, lane 1, *Ps. putida* QhpE alone; lane 2, H47A (mutant) alone; lane 3, S179A (mutant) alone; lane 4, *Ps. putida* QhpE and N-Flc substrate; lane 5, H47A and N-Flc substrate; lane 6, S179A and N-Flc substrate; lane 7, *Pa. denitrificans* QhpE alone; and lane 8, QhpE reacted with N-Flc substrate. **c**, *Ps. putida* QhpE (50 μM) and crosslinked QhpC (50 μM) were incubated in 100 mM buffer with the indicated pH values for 15 h at 24°C. The reaction products were analyzed by MADLI-TOF mass spectrometry.

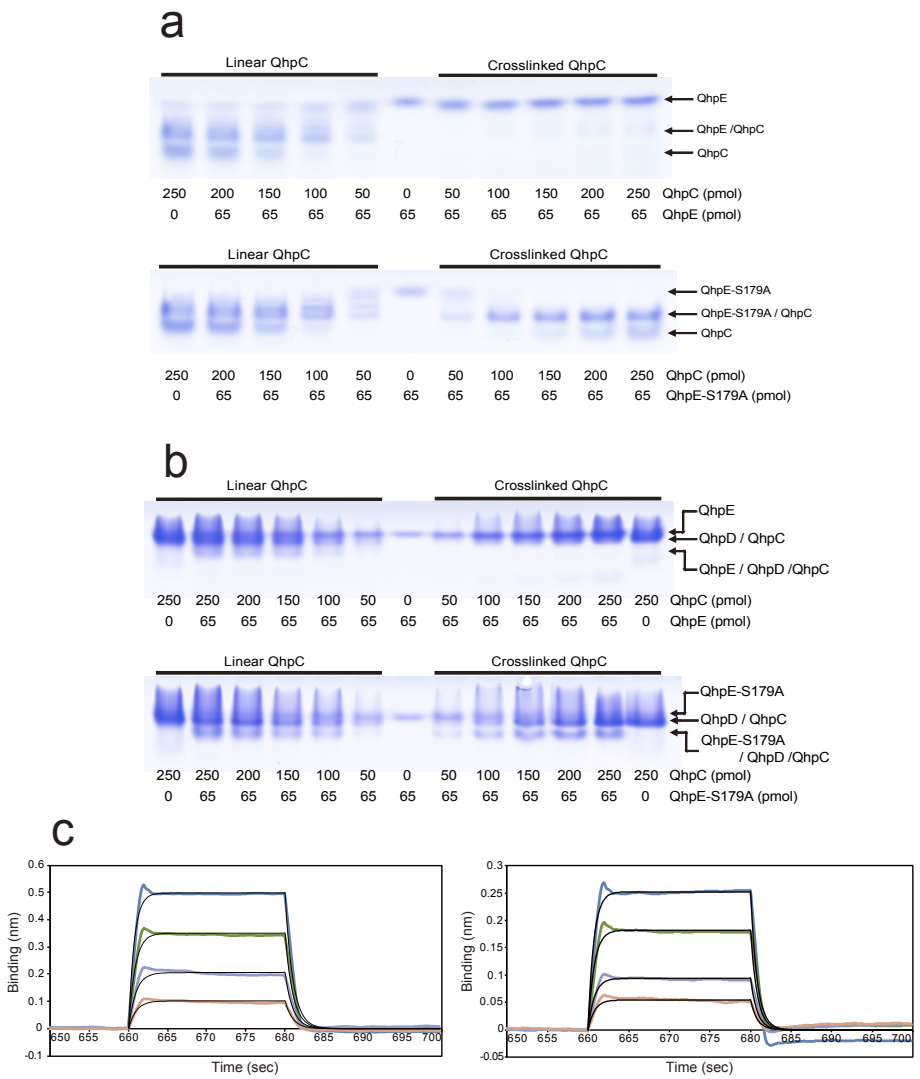

Fig. 5. Protein-protein interaction among QhpCDE proteins. Mobility shift assay for the interaction between QhpE (WT or S179A) and QhpCD binary complexes (**a**) and between QhpE (WT or S179A) and QhpC (**b**). **c**, BLI assay of the interaction between linear (left) and crosslinked (right) QhpC and QhpE-H47A mutant immobilized on a biosensor chip. The analyte solution (4 ml) contained 0.5 mM of QhpE-H47A mutant, 12.5 mM (blue), 6.3 mM (green), 3.2 mM (light blue), and 1.6 mM (orange) of linear QhpC and 12.5 mM (blue), 6.3 mM (green), 3.2 mM (light blue), and 1.6 mM (orange) of crosslinked QhpC. The binding-induced change in wavelength (nm) of transmitted

light were recorded to measure time (sec). The thin black curve shows the theoretical fitting of the calculated data (Table 3).

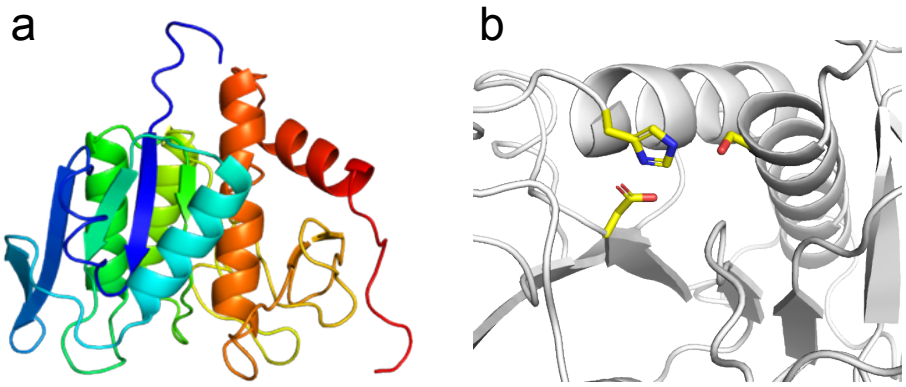

Fig. 6. Crystal structure of QhpE. a, Overall structure of QhpE monomer. The monomer structure (chain A) is depicted by a cartoon model. **b**, A stick model of catalytic triad (Asp11, His47, Ser179).

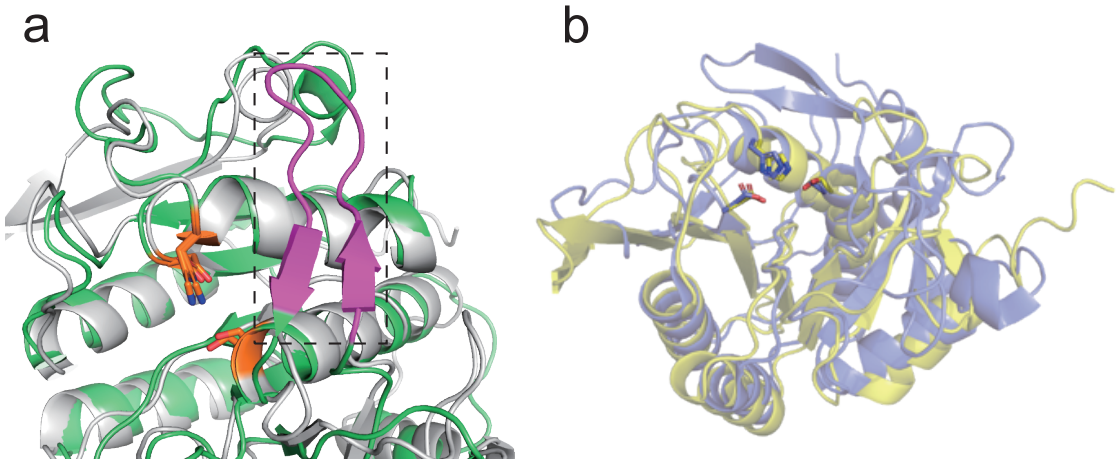

Fig. 7. Structural comparison of QhpE, QhpE from *Pa. denitrificans* and Tk-subtilisin. a, structural superposition of QhpE from *Pa. denitrificans* by homology modeling (green) and QhpE from *Ps. putida* (gray). **b**, Structural comparison of QhpE (yellow) and Tk-subtilisin (purple); root mean squared deviation, 2.3 Å over 198 superposed residues; sequence identity, 24%; Z- score, 20.8.

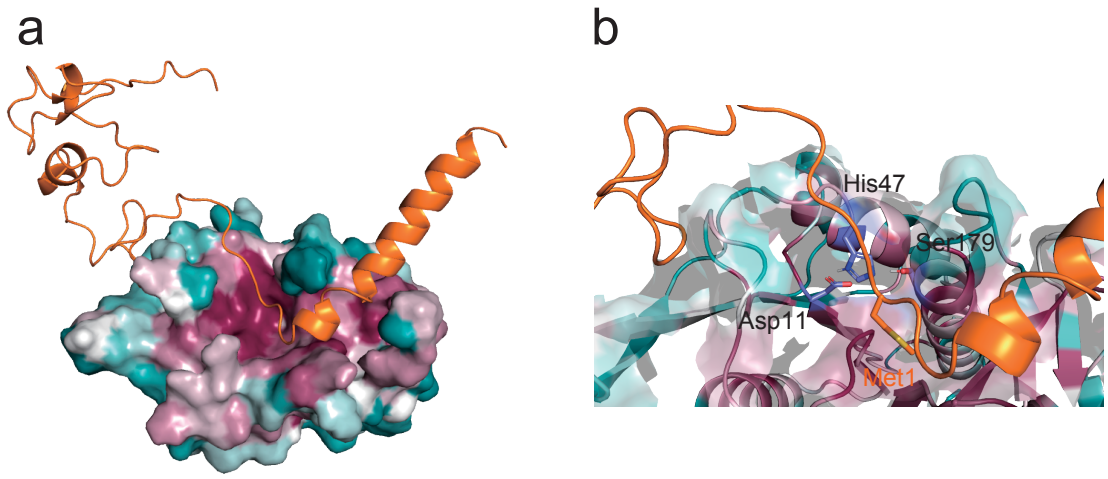

Fig. 8. Crosslinked QhpC-QhpE docking model. a, Overall structure of QhpCE complex model. QhpE is colored according to conservation (red: high, cyan: low). **b**, Enlarged view of **a**. The catalytic triad of the active center (purple) and the cleavage site Met1 (orange) of QhpC are shown as stick models.

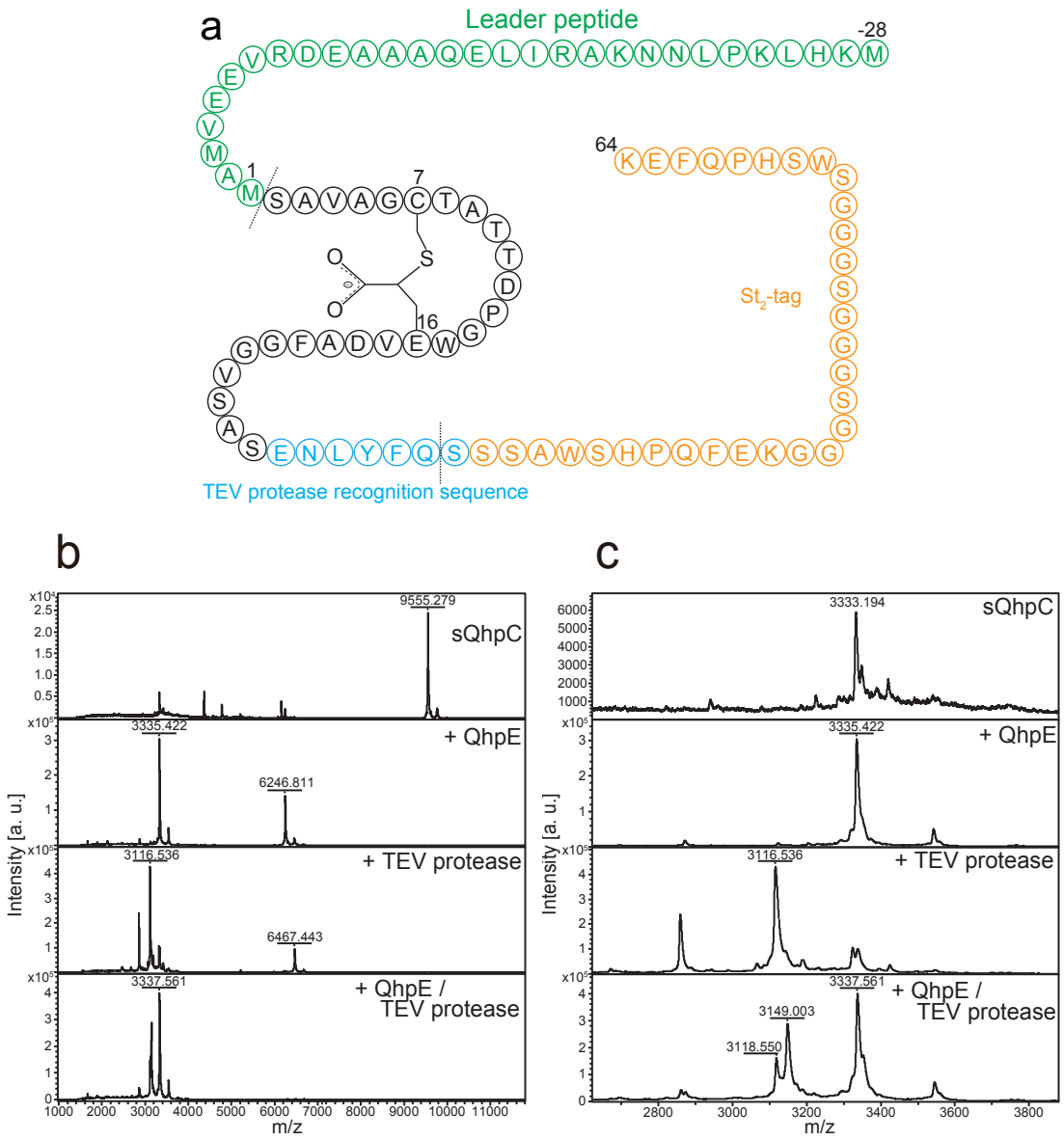

Fig. 9. Products analysis of sQhpC digested by QhpE. a, Schematic diagram of sQhpC. Leader peptide, TEV protease recognition sequence, and St_2-tag are shown in green, blue, and orange, respectively. **b** and **c**, MALDI-TOF mass spectrometric analysis of the sQhpC (first panel), sQhpC/QhpE reaction products (second), sQhpC/TEV protease reaction products (third), and sQhpC/QhpE/TEV protease reaction products.

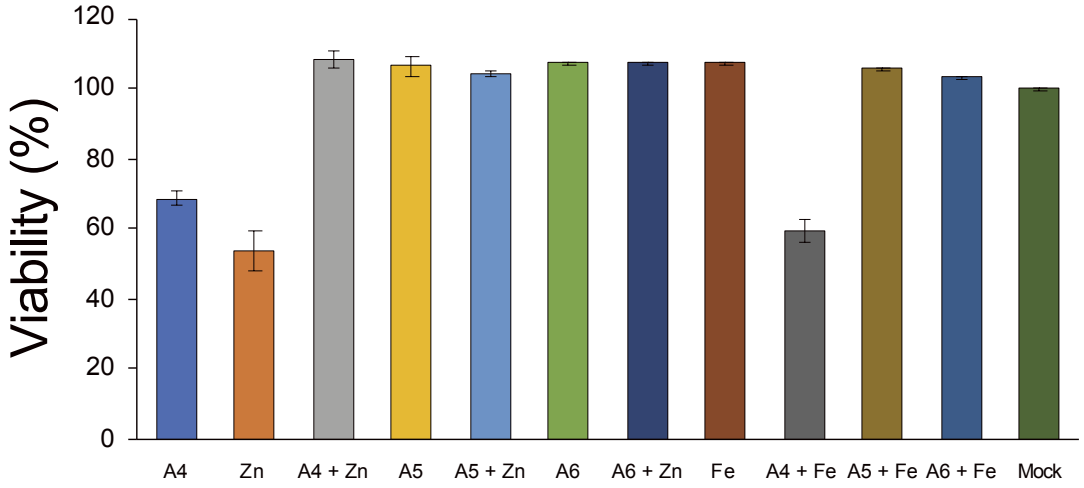

Fig. 10. Evaluation of crosslinked peptide functions. The bioactivity of peptides with Ala loops of various lengths (Ala × 4-6) was investigated in A549 cells. Standard errors are shown as error bars (n = 4).

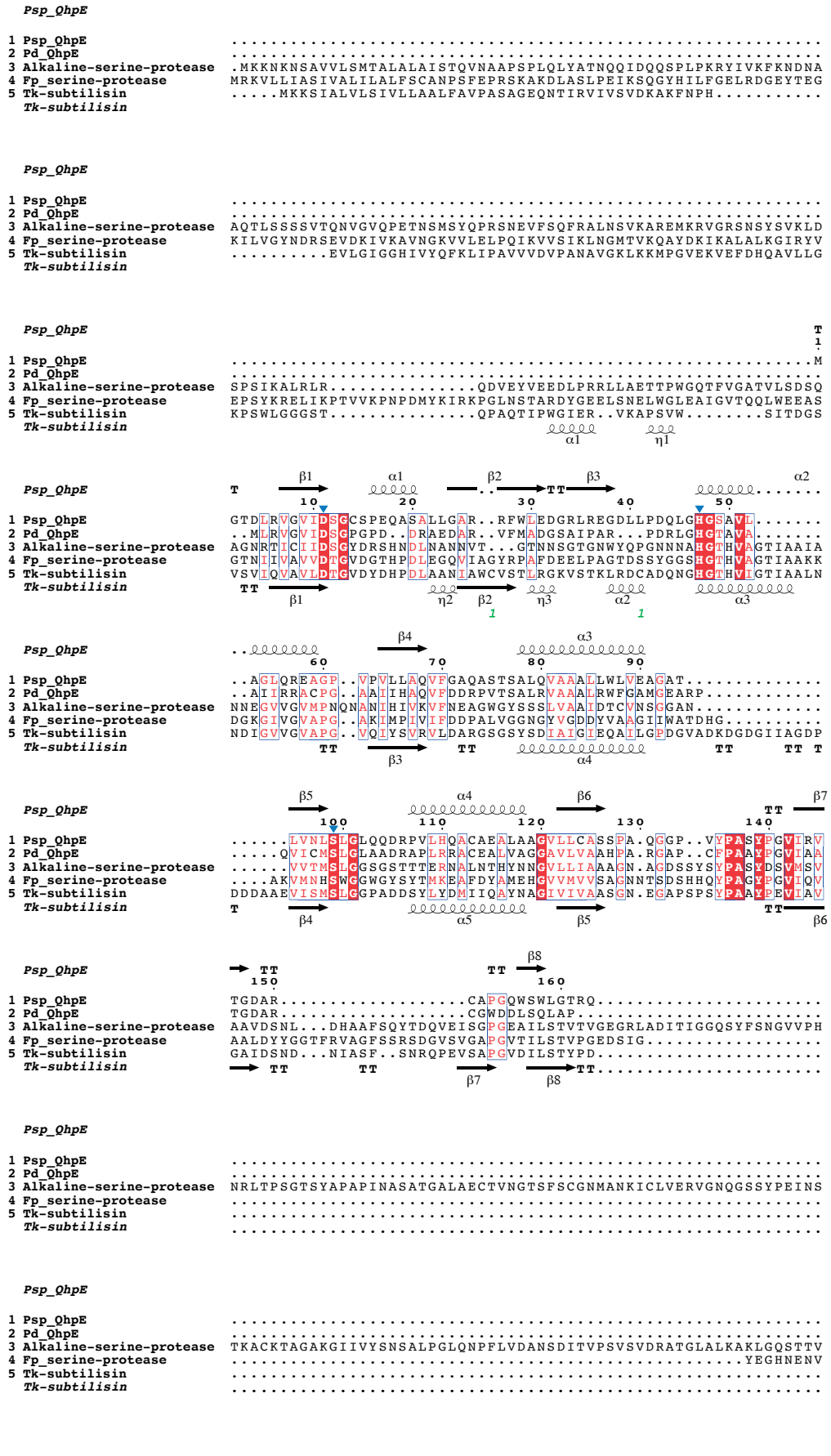
Psp_QhpE
1 Psp_QhpE
2 Pd_QhpE
3 Alkaline-serine-protease
4 Fp_serine-protease
5 Tk-subtilisin
Tk-subtilisin
.MKKNKNSAVVLSMTALALAISTQVNAAPSPLQLYATNQQIDQQSPLPKRYIVKFKNDNA
MRKVLLIASIVALILALFSCANPSFEPRSKAKDLASLPEIKSQGYHILFGELRDGEYTEG
.....MKKSIALVLSIVLLAALFAVPASAGEQNTIRVIVSVDKAKFNPH
AQTLSSSSVTQNVGVQPETNSMSYQPRSNEVFSQFRALNSVKAREMKRVGRSNSYSVKLD
KILVGYNDRSEVDKIVKAVNGKVVLELPQIKVVSIKLNGMTVKQAYDKIKALALKGIRYV
.....EVLGIGGHIVYQFKLIPAVVVDVPANAVGKLKKMPGVEKVEFDHQAVLLG
SPSIKALRLR.....QDVEYVEEDLPRRLLAETTPWGQTFVGATVLSDSQ
EPSYKRELIKPTVVKPNPDMYKIRKPGLNSTARDYGEELSNELWGLEAIGVTQQLWEEAS
KPSWLGGGST.....QPAQTIPWGIER..VKAPSVW.....SITDGS
GTDLRVGVIDSGCSPEQASALLGAR..RFWLEDGRLREGDLLPDQLGHGSAVL.....
..MLRVGVIDSGPGPD..DRAEDAR..VFMADGSAIPAR...PDRLGHGTAVA.....
AGNRTICIIDSGYDRSHNDLNANNVT...GTNNSGTGNWYQPGNNNAHGTHVAGTIAAIA
GTNIIVAVVDTGVDGTHPDLEGQVIAGYRPAFDEELPAGTDSSYGGSHGTHVAGTIAAKK
VSVIQVAVLDTGVDYDHPDLAANIAWCVSTLRGKVSTKLRDCADQNGHGTHVIGTIAALN
..AGLQREAGP..VPVLLAQVFGAQASTSALQVAAALLWLVEAGAT.....
..AIIRRACPG..AAIIHAQVFDDRPVTSALRVAAALRWFGAMGEARP.....
NNEGVVGVMPNQNANIHIVKVFNEAGWGYSSSLVAAIDTCVNSGGAN.....
DGKGIVGVAPG..AKIMPIVIFDDPALVGGNGYVGDDYVAAGIIWATDHG.....
NDIGVVGVAPG..VQIYSVRVLDARGSGSYSDIAIGIEQAILGPDGVADKDGDGIIAGDP
.....LVNLSLGLQQDRPVLHQACAEALAAGVLLCASSPA.QGGP..VYPASYPGVIRV
.....QVICMSLGLAADRAPLRRACEALVAGGAVLVAAHPA.RGAP..CFPAAYPGVIAA
.....VVTMSLGGSGSTTTERNALNTHYNNGVLLIAAAGN.AGDSSYSYPASYDSVMSV
....AKVMNHSWGGWGYSYTMKEAFDYAMEHGVVMVVSAGNNTSDSHHQYPAGYPGVIQV
DDDAAEVISMSLGGPADDSYLYDMIIQAYNAGIVIVAASGN.EGAPSPSYPAAYPEVIAV
TGDAR.....CAPGQWSWLGTRQ.....
TGDAR.....CGWDDLSQLAP.....
AAVDSNL...DHAAFSQYTDQVEISGPGEAILSTVTVGEGRLADITIGGQSYFSNGVVPH
AALDYYGGTFRVAGFSSRSDGVSVGAPGVTILSTVPGEDSIG.....
GAIDSND...NIASF..SNRQPEVSAPGVDILSTYPD.....
NRLTPSGTSYAPAPINASATGALAECTVNGTSFSCGNMANKICLVERVGNQGSSYPEINS
TKACKTAGAKGIIVYSNSALPGLQNPFLVDANSDITVPSVSVDRATGLALKAKLGQSTTV
.....YEGHNENV

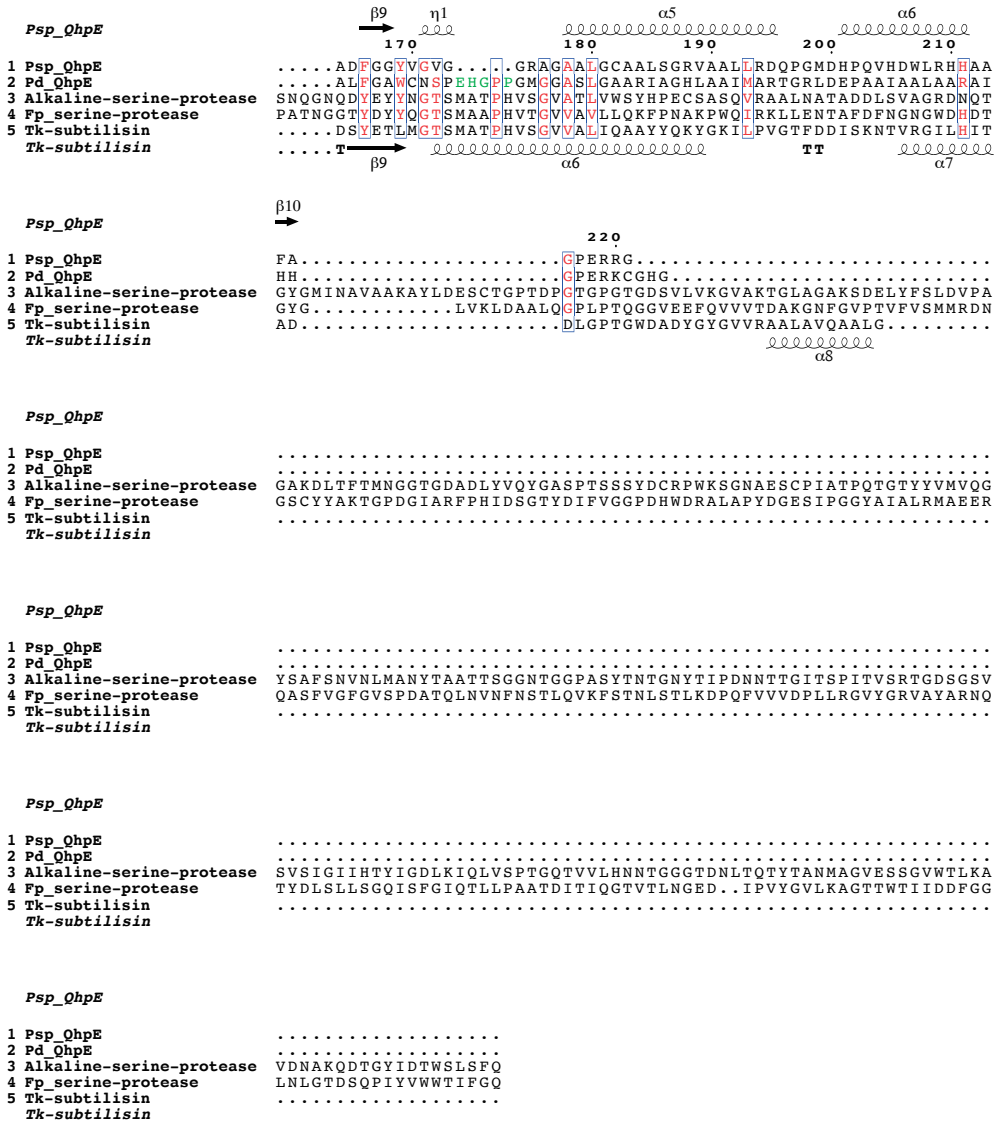

Fig. 11. Multiple sequence alignment of QhpE homologs. Amino acid sequences of QhpE orthologs from *Ps. putida* IFO 15366 (Pp_QhpE) and *Pa. denitrificans* Pd1222 (Pd_QhpE, WP_011748002.1 [https://www.ncbi.nlm.nih.gov/protein/WP_011748002.1]) and homologs; Tk-subtilisin from *Thermococcus kodakarensis* (Tk-subtilisin, WP_011250626,1 [https://www.ncbi.nlm.nih.gov/protein/WP_011250626.1]), Alkaline serine protease from *Pseudoalteromonas sp*. AS-11 (Alkaline-serine-protease, BAD51450.1 [https://www.ncbi.nlm.nih.gov/protein/BAD51450.1]), and Subtilisin-like serine

protease from *Fervidobacterium pennivorans* (Fp_serine-protease, WP_014451857.1 [https://www.ncbi.nlm.nih.gov/protein/WP_014451857.1]) were aligned using the program Clustal W1. Secondary structural elements in the crystal structure of QhpE and Tk-subtilisin were assigned using the program DSSP, and are shown above and below each sequence, respectively. Residues forming catalytic triad are shown in inverted blue triangles. The figure was drawn using the program ESPript.

Table 1. Oligonucleotides used in this study.

Primer for plasmid construction[a]	Nucleotide sequence[b]	Introduced restriction site or mutation
QhpC (+)	tatacatatgaaacacttgaagcccct	NdeI
QhpC (–)	atatgctagccttgtctttcgggaacacgg	NheI
QhpD (+)	catatgggcgcgctactgaacctggtcgaacgc	NdeI
QhpD (–)	ggatcctcagtgcgccttccgcggggtgatgtagcg	BamHI
QhpG (+)	atatcatatggctgaaccgcgcattgtggtgttgggg	NdeI
QhpG (–)	atatggatcctcaaaccaagccctgctccaacaaccaccg	BamHI
QhpE (+)	ccgaggaggtgatcacatatgggcactgacttg	NdeI
QhpE (–)	cgcgggaattcgattcaccacaatgggatcctcagccatgg	BamHI
H_6-TEV (+)	catgggcagcagccatcatcatcatcacgattacgatatcccaacg accgaaaaccttttacttccagggcca	NcoI/NdeI
H_6-TEV (–)	tatggccctggaagtaaaggttttcggtcgttgggatatcgtaatcgtgat gatgatgatgatggctgctgcc	NcoI/NdeI
QhpE-D11A (+)	cgcgttggcgtcatcgccagtggttgctcgccg	QhpE (D11A)
QhpE-D11A (–)	cggcgagcaaccactggcgatgacgccaacgcg	QhpE (D11A)
QhpE-H47A (+)	ctgctgcccgaccagcttggggccggtagcgccgtgctc	QhpE (H47A)
QhpE-H47A (–)	gagcacggcgctaccggccccaagctggtcgggcagcag	QhpE (H47A)
QhpE-S179A (+)	gtgggcggcagggcgggcgcggccctgggctgtgcggcc	QhpE (S179A)
QhpE-S179A (–)	ggccgcacagcccagggccgcgcccgccctgccgcccac	QhpE (S179A)

[a]Plus and minus signs in parentheses denote sense and antisense strands, respectively.
[b]Restriction sites are underlined. Mismatching nucleotides at the mutated sites are shown in bold.

Table 2. Data collection and crystallographic refinement statistics.

Crystal	QhpE
Data collection	
Wavelength (Å)	0.9
Space group	*P1*
Unit-cell dimensions	
a, *b*, *c* (Å),	35.46, 50.67, 53.38,
α, β, γ (°)	88.10, 85.86, 70.15
Resolution (Å)	50.00 – 2.1 (2.22 – 2.09)
No. of observations	66121
No. of unique reflections	37037
$I/\sigma(I)$ [a]	4.63 (1.49)
Redundancy [a]	1.8 (1.7)
Overall completeness (%)[a]	89.6 (86.0)
Overall R_{merge} (%)[a,b]	14.3 (55.3)
Refinement statistics	
Resolution (Å)	50 – 1.80 (2.15 – 2.08)
No. of atoms per asymmetric unit	3571
No. of solvent atoms	320
Average temperature factors	
Protein[e]	16.3 (442)
Ligand[e]	0 (0)
Solvent[e]	25.3 (320)
R.m.s. deviation from ideal values	
Bond lengths (Å) [a]	0.0023
Bond angles (deg) [a]	0.57
R_{work} (%)[a,c]	16.6 (17.8)
R_{free} (%)[a,d]	21.1 (27.3)
Ramachandran plot statistics (%)	
Residues in favored regions	97.0
Residues in allowed regions	2.9
Outliers	0.0

[a]Values in parentheses refer to data for the highest resolution shells.
[b]$R_{merge} = \Sigma_h \Sigma_i |I_{h,i} - \langle I_h \rangle| / \Sigma_h \Sigma i\, I_{h,i}$, where $I_{h,i}$ is the intensity value of the i^{th} measurement of h and $\langle I_h \rangle$ is the corresponding mean value of I_h for all i measurements.
[c]$R_{work} = \Sigma||F_o| - |F_c|| / \Sigma|F_o|$.
[d]R_{free} is an R factor of the refinement evaluated for 5% of reflections that were excluded from the refinement.
[e]Values in parentheses correspond to number of residues or molecules.

Table 3. Dissociation and equilibrium constants for interactions of mutant QhpE with QhpC.

QhpE/QhpC	K_D (μM)	Association rate constant (k_a) ($M^{-1}•s^{-1}$)	Dissociation rate constant (k_d) (s^{-1})
H47A/crosslinked	29.1 ± 2.3	(3.1 ± 0.06) × 10^4	(9.0 ± 0.87) × 10^{-1}
H47A/uncrosslinked	97.8 ± 17.9	(1.2 ± 0.28) × 10^4	(6.0 ± 6.0) × 10^2
S180A/crosslinked	14.5 ± 1.6	(4.2 ± 0.28) × 10^4	(6.0 ± 0.28) × 10^{-1}
S180A/uncrosslinked	19.4 ± 0.85	(3.8 ± 0.02) × 10^4	(7.4 ± 0.37) × 10^{-1}

2.5. References

1. Nakai, T. et al. Identification of genes essential for the biogenesis of quinohemoprotein amine dehydrogenase. *Biochemistry* **53**, 895–907 (2014).
2. Nakai, T. et al. An unusual subtilisin-like serine protease is essential for biogenesis of quinohemoprotein amine dehydrogenase. *J. Biol. Chem.* **287**, 6530–6538 (2012).
3. Timony, A. H. et al Constraining cyclic peptides to mimin protein structure motifs. *Angew. Chem. Int. Ed.* **53**, 13020-13041 (2014)
4. Nakai, T. et al. The *S*-adenosyl-L-methionine enzyme QhpD catalyzes sequential formation of intra-protein sulfur-to-methylene carbon thioether bonds. *J. Biol. Chem.* **290**, 11144–11166 (2015).
5. Kabsch, W. *XDS*. *Acta Crystallogr. Sect. D Biol. Crytallogr.* **D66,** 125–132 (2010).
6. Emsley, P., Lohkamp, B., Scott, W. G. & Cowtan, K. Features and development of *Coot*. *Acta Crystallogr. Sect. D Biol. Crytallogr.* **D66**, 486–501 (2010).
7. Adams, P. D. et al. PHENIX: a comprehensive Python-based system for macromolecular structure solution. *Acta Crystallogr. Sect. D Biol. Crytallogr.* **D66**, 213–221 (2010).
8. Pierce, B. G. et al. ZDOCK server: interactive docking prediction of protein-protein complexes and symmetric multimers. *Bioinformatics* **30**, 1771–1773 (2014).
9. Uehara, R. et al. Requirement of the insertion sequence for activation of Tk-subtilisin. *Extremophiles* **16**, 841-851 (2012).
10. Dong, D. Crystal Structure of Psychrophilic Subtilisin-like Protease Apa1 from Antarctic Psychrotroph Pseudoalteromonas sp. AS-11. *Acta Crystallogr. Sect. F Struct. Biol. Cryst. Commun.* **F61**, 308-311 (2005)

11. Kim, J. S. et al. Crystal Structure of Fervidolysin from Fervidobacterium pennivorans, a Keratinolytic Enzyme Related to Subtilisin. *J. Mol. Biol.* **3**, 787-797 (2004)

Chapter IV

Comprehensive Discussion

Formation mechanism of CTQ

The multistep TTQ biogenesis in MADH occurs after the TTQ-less β-subunit is translocated into the periplasm that is under aerobic conditions. On the other hand, to complete the CTQ biogenesis, all the single-turnover reactions by QhpD, QhpG, and QhpE on QhpC occur within the less aerobic cytoplasm. By analogy with TTQ biogenesis in MADH, the final oxidation to CTQ of 6,7-dihydroxy-Trp in the crosslinked QhpC (pre-γ-subunit) produced by the QhpG reaction may be catalyzed by the two *c*-type hemes that are contained within the α-subunit, presumably after the periplasmic translocation of both of the pre-γ- and α-subunits.

Altogether, it is now evident that markedly divergent strategies have evolved to convergently generate the tryptophylquinone cofactor in different proteins. It was concluded that the oxidation of βTrp57 in MADH proceeds by the involvement of two heme irons and hydrogen peroxide that is catalyzed MauG[1,2,3]. The crosslinking of βTrp57 and βTrp108 has also been found to occur in conjugation with this oxidation reaction. In fact, the MauG crystal structure in complex with a MADH intermediate containing βTrp57 hydroxylated at position 7 was determined, and the addition of hydrogen peroxide to this complex was shown to form TTQ in the complex crystal[4]. Furthermore, the mutation of Trp108 to Cys in MADH has been reported to produce CTQ instead of TTQ, strongly suggesting that the biosynthesis of TTQ and CTQ has a common mechanism that proceeds, at least in part, within the periplasm[5]. This strongly suggests that the biosynthesis of TTQ and CTQ proceeds, at least in part, within the periplasm. The 2 heme *c* is bound to the α-subunit of QHNDH as well as to MauG[6,7]. In

a previous study, it was found that CTQ was not formed by introducing an amino acid mutation into the *c*-type heme-binding site of the α-subunit to prevent heme-binding (Nakai, T. et al., unpublished). This suggests that 6,7-dihydroxy-Trp is oxidized by the *c*-type heme in the α-subunit. In addition, it was suggested that Trp43 and Cys37 form a crosslink in conjugation with this oxidation reaction. In order to clarify the mechanism of this hypothesis, much experimental evidence is needed. It is clear that it is necessary to reconstitute the oxidation and crosslinking of Trp43, the final reaction in QHNDH biosynthesis, in vitro by applying the previously successful in vitro reaction systems of QhpD, QhpG, and QhpE.

Biosynthetic mechanism of the mature QhpC in QHNDH

In conclusion, the data presented here showed that the FAD-dependent hydroxylase QhpG is essential for QHNDH biosynthesis and catalyzes the hydroxylation of Trp residues in CTQ formation. It was also shown that the QhpCDG ternary complex catalyzes the formation of thioether crosslinks and hydroxylation reaction. In addition, QhpE was shown to actively cleave the leader peptide of the crosslinked QhpC in the QhpCDG complex. Thus, multiple enzymes regulate the biosynthesis of mature QhpC by a complex formation. Compared with L-lysine oxidase (LodA)[8] and glycine oxidase (GoxA)[9] having CTQ as a cofactor, the active center γ subunit (QhpC) in QHNDH has a unique chemical structure with three thioether bridges and CTQ. These interpeptidyl crosslinks are very unique in that they are formed by the tight control of various modified enzymes. These efficient and rational mechanisms may be important for the rapid production of the active form of QHNDH and the rapid accumulation of primary amines under starvation conditions without carbon sources.

The present results are considered an important first step toward a complete understanding of the post-translational modifications of QhpC. It will also be an important step to understanding the formation mechanism in CTQ in other enzymes.

A Tool for the Preparation of Bioactive Cyclic Peptides

In a previous study, I have successfully formed crosslinks of shortened QhpC (sQhpC) with various sequences using the thioether crosslink-forming enzyme QhpD. In this paper, I have succeeded in isolating a crosslinked region including poly Ala loops by cleaving franking regions: N-terminal leader peptide and C-terminal St_2 tag of sQhpC using QhpE and TEV protease. When the Ala×4 peptide was added to A549 cells, it showed cytotoxicity. These results suggest that QhpD and QhpE can be applied to the development of new synthetic methods for cyclic peptides with various amino acid sequences and loop structures. In fact, a wide variety of functional cyclic peptides are known to exist in nature, such as conotoxin, an extremely potent calcium channel inhibitor, and cyclosporine, an immunosuppressive agent, which are used in clinical practice[10]. As an artificial cyclic peptide, a cyclic N-methyl peptide inhibitor of the ubiquitin ligase E6AP has been created[11]. Although vigorous research is being conducted by pharmaceutical companies and universities, attempts to create artificial bioactive cyclic peptides have only just begun. Organic chemical cyclization methods include spontaneous cyclization within synthetic peptides containing Cys residues and chloroacetyl groups[12]. On the other hand, enzymatic methods using QhpD and QhpG have features not found in organic chemical methods, such as the ability to perform multiple cyclization. It is also noteworthy in the QhpD-catalyzed thioether crosslink formation that the asymmetric carbon atoms produced by the cyclization have a specific

steric configuration, and that ease of screening system with a bacterial expression system can be constructed for antibacterial properties. In addition, the introduction of multiple cyclic regions within the same peptide is possible, and the creation of novel heterocyclic peptides is expected. It is also possible to give individual functionality to each cyclic region, or to repeat the same sequence to enhance the function. Further structural analysis of QhpD and understanding of the substrate recognition mechanism will enable us to modify the catalytic function.

References

1. Wang, Y. et al. MauG, a novel diheme protein required for tryptophan tryptophylquinone biogenesis. Biochemistry 42, 7318-7325 (2003)
2. Wang, Y. et al. MauG-Dependent in Vitro Biosynthesis of Tryptophan Tryptophylquinone in Methylamine Dehydrogenase. J. Am. Chem. Soc. 127, 8258-8259 (2005)
3. Li, X. et al. A catalytic di-heme bis-Fe(IV) intermediate, alternative to an Fe(IV)=O porphyrin radical. Proc. Natl. Acad. Sci. USA 105, 8597-8600 (2008)
4. Jansen, L. M. et al. In Crystallo Posttranslational Modification Within a MauG/Pre–Methylamine Dehydrogenase Complex. Science 327, 1392-1394
5. Person, A. R. et al. Understanding quinone cofactor biogenesis in methylamine dehydrogenase through novel cofactor generation. Biochemistry 42, 3224–3230 (2003)
6. Datta, S. et al. Structure of a quinohemoprotein amine dehydrogenase with an uncommon redox cofactor and highly unusual crosslinking. Proc. Natl. Acad. Sci. U.S.A. 98, 14268–14273 (2001).
7. Satoh, A. et al. Crystal Structure of Quinohemoprotein Amine Dehydrogenase from Pseudomonas putida. J. Biol. Chem. 277, 2830–2834 (2002).
8. Okazaki, S. et al. X-ray crystallographic evidence for the presence of the cysteine tryptophylquinone cofactor in L-lysine ε-oxidase from Marinomonas mediterranea. J. Biochem. 154, 233–236 (2013).
9. Andreo-Vidal, A. et al. Structure and enzymatic properties of an unusual cysteine

tryptophylquinone-dependent glycine oxidase from Pseudoalteromonas luteoviolacea. Biochemistry 57, 1155–1165 (2018).

10. Timony, A. H. et al Constraining cyclic peptides to mimin protein structure motifs. Angew. Chem. Int. Ed. 53, 13020-13041 (2014)

11. Yamagishi et al. Ribosomal Synthesis of Cyclic Peptides with a Fluorogenic Oxidative Coupling Reaction, ChemBioChem 10(9), 1469-1472 (2009).

12. Fairlie, A. P. et al. Review stapling peptides using cysteine crosslinking. Biopolymers 106(6), 843-852 (2016).

Acknowledgements

This study has been performed at the Institute of Scientific and Industrial Research, Osaka University from 2018 to 2021 under the direction of Prof. Shun'ichi Kuroda in the Department of Biomolecular Science and Reaction. During this study, I received financial assistance from Japan Society for the Promotion of Science as fellowships DC1.

The present work has been performed under the direction of Dr. Shun'ichi Kuroda, Professor of Institute of Scientific and Industrial Research, Osaka University. The author would like to express his sincere gratitude to Prof. Shun'ichi Kuroda for their valuable advices and encouragement throughout the course of this study.

I also indebted to Dr. Toshihide Okajima, Associate Professor of Institute of Scientific and Industrial Research, Osaka University, and Dr. Katsuyuki Tanizawa, honorary professor of Institute of Scientific and Industrial Research, Osaka University, for careful advices and guidance.

I also wish his sincere thanks to Dr. Tadashi Nakai, Associate Professor of Hiroshima Institute of Technology, for his fruitful discussion and advice.

I also thank the member of Department of Biomolecular Science and Reaction during this study.

List of Publications

Original papers

- Functional and structural characterization of a flavoprotein monooxygenase essential for biogenesis of tryptophylquinone cofactor Functional and structural characterization of a flavoprotein monooxygenase essential for biogenesis of tryptophylquinone cofactor.

  Toshinori Oozeki, Tadashi Nakai, Kazuki Kozakai, Kazuki Okamoto, Shun'ichi Kuroda, Kazuo Kobayashi, Katsuyuki Tanizawa and Toshihide Okajima.

  Nat. Commun., 2021, in press.

- Biochemical and Structural analysis of serine proteinase involved in biosynthesis of active-site subunit of quinohemoprotein amine dehydrogenase.

  Toshinori Oozeki, Tadashi Nakai, Shun'ichi Kuroda, Kazuo Kobayashi, Katsuyuki Tanizawa and Toshihide Okajima.

  in preparation

International and Domestic Meetings, and Awards

Presentation in international conference

1. Toshinori Oozeki, Tadashi Nakai, Katsuyuki Tanizawa, Toshihide Okajima. Characterization of FAD-dependent monooxygenase involved in quinone cofactor biosynthesis, The 20th SANKEN International, The 15th SANKEN Nanotechnology Symposium, Osaka, Japan, Dec. 12 - 13, 2016. Osaka, Japan （Poster）
2. Oozeki T, Nakai T, Tanizawa K, Okajima T., Role of flavin-containing enzyme in the post-translational modification of quinoheme protein amine dehydrogenase.The 21st SANKEN International Symposium, Jan. 16 - 17, 2018, Osaka, Japan (Poster)
3. Toshinori Oozeki, Tadashi Nakai, Katsuyuki Tanizawa, Toshihide Okajima, Functional analysis of serine proteinase involved in biosynthesis of active-site subunit of quinohemoprotein amine dehydrogenase, The 22nd SANKEN International Symposium, The 17th SANKEN Nanotechnology International Symposium, Jan. 15 - 16, 2019, Osaka, Japan (Poster)
4. Toshinori Oozeki, Kazuki Kozakai, Tadashi Nakai, Katsuyuki Tanizawa, Toshihide Okajima, Sequence Specificity for Peptide Substrates in Thioether Crosslinking Reaction Catalyzed by Radical SAM Enzyme QhpD, The 33rd Proteine Society Annual Symposium, Jun. 30 – Jul 3, 2019, Seattle, U. S. A (Poster)
5. Toshinori Oozeki, Tadashi Nakai, Katsuyuki Tanizawa, Toshihide Okajima, Biochemical and structural analysis of serine proteinase involved in biosynthesis of active-site subunit of quinohemoprotein amine dehydrogenase, The 23rd SANKEN International Symposium, The 18th SANKEN Nanotechnology International

Symposium, Scientific and Industrial Research for Space Age, Jan. 9 – 10, 2020, Hyogo, Japan (Poster)

Presentation in domestic meeting

1. 大関 俊範, 中井 忠志, 谷澤 克行, 岡島 俊英, キノン補酵素生合成に関わる FAD 依存性モノオキシゲナーゼ QhpG の精製と分光学的特性, 第 89 回日本生化学会大会, Sep. 25 - 27, 2016, Sendai, Japan (Poster)
2. 大関 俊範, 中井 忠志, 谷澤 克行, 岡島 俊英, キノン補酵素生合成に関わる FAD 依存性モノオキシゲナーゼ QhpG の分光学的特性と基質タンパク質 QhpC との相互作用, 日本農芸化学会 2017 年度大会, Mar. 17 – 20, 2017, Kyoto, Japan (Oral)
3. 大関 俊範, 中井 忠志, 谷澤 克行, 岡島 俊英, トリプトフィルキノン補酵素生合成に関与する FAD 依存性オキシゲナーゼの機能解明, 日本農芸化学会関西支部例会（第 499 回講演会）, Jun. 3, 2017, Kyoto, Japan (Oral)
4. 大関 俊範, 中井 忠志, 谷澤 克行, 岡島 俊英, キノヘムプロテイン・アミン脱水素酵素補酵素含有サブユニットの翻訳後修飾機構の解析, 2017 年酵素・補酵素研究会, Jun. 23 – 24, 2017, Sendai, Japan (Oral and Poster)
5. 大関 俊範, 中井 忠志, 谷澤 克行, 岡島 俊英, キノヘムプロテイン・アミン脱水素酵素のキノン補酵素含有サブユニットの翻訳後修飾機構, 第 69 回日本生物工学会大会, Sep. 11 – 14, 2017, Tokyo, Japan (Poster)
6. 大関 俊範, 中井 忠志, 谷澤 克行, 岡島 俊英, キノヘムプロテイン・アミン脱水素酵素の翻訳後修飾におけるフラビン含有酵素の役割, 2017 年度生

命科学系学会合同年次大会, Dec. 6 – 9, 2017, Kobe, Japan (Oral and Poster)

7. 岡島 俊英, 大関 俊範, 小酒井 一輝, 中井 忠志, 谷澤 克行, キノヘムプロテイン・アミン脱水素酵素補酵素含有サブユニットの多段階翻訳後修飾の分子機構, ワークショップ：多様な微生物に見出したユニークな細胞・酵素機能とその応用, 2017 年度生命科学系学会合同年次大会, Dec. 6 – 9, 2017, Kobe, Japan (Oral)
8. 大関 俊範, 中井 忠志, 谷澤 克行, 岡島 俊英, キノヘムプロテイン・アミン脱水素酵素の翻訳後修飾における修飾酵素複合体の機能解明, 日本農芸化学会 2018 年度大会, Mar. 15 – 18, 2018, Nagoya, Japan (Oral)
9. 小酒井 一輝, 大関 俊範, 中井 忠志, 谷澤 克行, 岡島 俊英, ペプチド・チオエーテル架橋形成酵素 QhpD による環状ペプチド形成機構の解明: 基質配列長および配列許容性の解析, 日本農芸化学会 2018 年度大会, Mar. 15 – 18, 2018, Nagoya, Japan (Oral)
10. 大関 俊範、小酒井 一輝、中井 忠志、谷澤 克行、岡島 俊英, ラジカル SAM 酵素 QhpD のペプチド・チオエーテル架橋形成反応における架橋ループ配列長依存性および架橋繰り返し能の解析, 第 18 回日本蛋白質科学会, Jun. 26 – 28, 2018, Niigata, Japan (Poster)
11. 大関 俊範、小酒井 一輝、中井 忠志、谷澤 克行、岡島 俊英, ペプチド鎖チオエーテル架橋形成酵素 QhpD による単一鎖内多重架橋形成と Ala 繰り返し配列の環状化,酵素・補酵素研究会 2018, Sep. 11 – 12, 2018, Chiba, Japan (Poster)
12. 大関 俊範、小酒井 一輝、中井 忠志、谷澤 克行、岡島 俊英, ラジカル SAM 酵素 QhpD のペプチドチオエーテル架橋形成反応による Ala 繰り返

し配列の環状化と複数架橋形成, 第 91 回日本生化学会大会, Sep. 24 – 26, 2018, Kyoto, Japan (Oral)

13. 大関 俊範、中井 忠志、谷澤 克行、岡島 俊英, キノヘムプロテイン・アミン脱水素酵素の活性中心サブユニット生合成に関与するセリンプロテアーゼの機能解析, 日本農芸化学会 2019 年度大会, Mar. 24 – 27, 2019, Tokyo, Japan (Oral)
14. 大関 俊範、中井 忠志、谷澤 克行、岡島 俊英, キノヘムプロテイン・アミン脱水素酵素の活性中心サブユニット生合成に関与するセリンプロテアーゼの機能解析, 第 19 回日本蛋白質科学会年会, 第 71 回日本細胞生物学会大会 合同大会, Jun. 24 – 26, 2019, Kobe, Japan (Poster)
15. 大関 俊範、中井 忠志、谷澤　克行、岡島　俊英, キノヘムプロテイン・アミン脱水素酵素の活性中心サブユニット生合成に関与するセリンプロテアーゼの生化学的・構造学的解析, 日本農芸化学会 2020 年度大会, Mar. 25 – 28, 2020, Fukuoka, Japan (Oral)
16. Toshinori Oozeki, Tadashi Nakai, Katsuyuki Tanizawa, Toshihide Okajima, Biochemical and structural analyses of serine proteinase involved in biosynthesis of active-site subunit of quinohemoprotein amine dehydrogenase, 第 10 回日本蛋白質科学会年会, Jul. 28, 2020, Web (Poster)
17. 大関 俊範、中井 忠志、谷澤　克行、岡島　俊英, キノヘムプロテイン・アミン脱水素酵素の活性中心サブユニット生合成に関与するセリンプロテアーゼの生化学的・構造学的機能解析, 第 93 回日本生化学会大会, Sep. 14 – 16, 2020, Web (Poster)

Awards

2017 年度酵素補酵素研究会　2017 年度酵素補酵素研究会最優秀ポスター賞, 2017, Japan